NASA Contract Report 159138

ANOPP Validation Study — Lockheed L-1011

Larry Godby

LOCKHEED-CALIFORNIA COMPANY
BURBANK, CALIFORNIA

CONTRACT NAS1-15651
October 31 [illegible]

NASA

Langley Research Center

NASA Contract Report 159138

ANOPP Validation Study – Lockheed L-1011

Larry Godby

LOCKHEED-CALIFORNIA COMPANY
BURBANK, CALIFORNIA

CONTRACT NAS1-15651
October 31, 1979

NASA
National Aeronautics and Space Administration

Langley Research Center
Hampton, Virginia 23665
AC 804 827-3966

PREFACE

Thanks are due to Dr. W. Zorumski of the Acoustic and Noise Reduction Division for his helpful guidance while monitoring this program.

A number of members of the Technical staff of the Lockheed-California Company contributed to the program. Special acknowledgement must be given to Wiley A. Guinn and Nathan Shapiro for their valuable assistance throughout the study. Cooperation of the personnel from Flight Sciences Acoustics Lab, James Hayward, Flight Sciences Propulsion, Bruce Flornes and L-1011 Flight Test, James Vogel to support this effort are much appreciated.

Thanks are addressed to Dr. K. Bushell and David Tomlinson of Rolls-Royce, Ltd. for their contributions of vital engine information.

TABLES OF CONTENTS

Section		Page
	PREFACE	iii
	LIST OF FIGURES	vii
	LIST OF TABLES	xii
	SUMMARY	1
	INTRODUCTION	2
	LIST OF SYMBOLS	2
1	FLYOVER NOISE DATA BASE	5
1.1	Aircraft Description	5
1.1.1	Aircraft Geometry	5
1.1.2	RB.211-524 turbofan engine	5
1.1.3	Acoustic liner	11
2.2	Test	14
2.2.1	Ambient conditions	14
2.2.2	Flight trajectory	15
2.2.3	Engine operating conditions	30
2.2.4	Noise Measurements	30
3	ANOPP VALIDATION	36
3.1	Program Requirements	36
3.1.1	Computer Facility	36
3.1.2	Functional Modules	36
3.1.3	Run deck description	38
3.2	Aircraft Noise Predictions and Measured Data	38
3.2.1	Perceived noise level field shapes	42
3.2.2	Third-octave band sound pressure level	42

TABLE OF CONTENTS (Continued)

Section		Page
4	COMPONENT ANALYSIS AND VALIDATION	
4.1	Source Separation of Predicted Data.	42
4.1.1	Perceived Noise Levels.	42
4.1.2	Third-octave band sound presssure levels.	84
4.2	Correction of Predicted Noise Levels to Measured Noise Levels	84
4.2.1	Perceived Noise Levels	84
4.2.2	Third-octave band sound pressure levels	84
5	CONCLUSIONS AND RECOMMENDATIONS	117

LIST OF FIGURES

Figure		Page
1	Three-View Drawing of L-1011-1-385	6
2	RB.211 cutaway	8
3	Aircraft position time history plots, condition no. 44.036.300.08	17
4	Aircraft position time history plots, condition no. 44.034.011.15	18
5	Aircraft position time history plots, condition no. 44.036.300.04	19
6	Aircraft position time history plots, condition no. 44.034.300.08	20
7	Aircraft position time history plots, condition no. 44.034.300.04	21
8	Aircraft position time history plots, condition no. 44.035.900.01	22
9	Aircraft velocity and lift coefficients condition no. 44.036.300.08	23
10	Aircraft velocity and lift coefficients, condition no. 44.034.011.15	24
11	Aircraft velocity and lift coefficients condition no. 44.036.300.04	25
12	Aircraft velocity and lift coefficients condition no. 44.034.300.08	26
13	Aircraft velocity and lift coefficients, condition no. 44.034.300.04	27
14	Aircraft velocity and lift coefficients condition no. 44.035.900.01	28
15	Angle of attack vs lift coefficient	29
16	Microphone location	35
17	Noise data acquisition equipment	37
18	ANOPP run deck schematic	39

LIST OF FIGURES (Continued)

Figure		Page
19	Field shape comparison, condition no. 44.036.300.08	43
20	Field shape comparison, condition no. 44.034.011.15	43
21	Field shape comparison, condition no. 44.036.300.04	44
22	Field shape comparison, condition no. 44.034.300.08	44
23	Field shape comparison, condition no. 44.034.300.04	45
24	Field shape comparison, condition no. 44.035.900.01	45
25	Noise comparison, forward quadrant (θ = 30° to 90°)	46
26	Noise comparison, aft quadrant (θ = 100 to 150°)	47
27	Comparison of component spectra, condition no. 44.036.300.08, θ = 30°	48
28	Comparison of component spectra, condition no. 44.036.300.08, θ = 60°	49
29	Comparison of component spectra, condition no. 44.036.300.08, θ = 91°	50
30	Comparison of component spectra, condition no. 44.036.300.08, θ = 121°	51
31	Comparison of component spectra, condition no. 44.036.300.08, θ = 152°	52
32	Comparison of component spectra, condition no. 44.034.011.15, θ = 30°	53
33	Comparison of component spectra, condition no. 44.034.011.15, θ = 61°	54
34	Comparison of component spectra, condition no. 44.034.011.15, θ = 91°	55
35	Comparison of component spectra, condition no. 44.034.011.15, θ = 122°	56
36	Comparison of component spectra, condition no. 44.034.011.15, θ = 152°	57
37	Comparison of component spectra, condition no. 44.036.300.04, θ = 30°	58
38	Comparison of component spectra, condition no. 44.036.300.04, θ = 60°	59
39	Comparison of component spectra, condition no. 44.036.300.04, θ = 91°	60

LIST OF FIGURES (Continued)

Figure		Page
40	Comparison of component spectra, condition no. 44.036.300.04, $\theta = 121^{o}$	61
41	Comparison of component spectra, condition no. 44.036.300.04, $\theta = 152^{o}$	62
42	Comparison of component spectra, condition no. 44.034.300.08, $\theta = 32^{o}$	63
43	Comparison of component spectra condition no. 44.034.300.08, $\theta = 62^{o}$	64
44	Comparison of component spectra, condition no. 44.034.300.08, $\theta = 92^{o}$	65
45	Comparison of component spectra, condition no. 44.034.300.08, $\theta = 122^{o}$	66
46	Comparison of component spectra, condition no. 44.034.300.08, $\theta = 152^{o}$	67
47	Comparison of component spectra, condition no. 44.034.300.04, $\theta = 30^{o}$	68
48	Comparison of component spectra, condition no. 44.036.300.08, $\theta = 60^{o}$	69
49	Comparison of component spectra, condition no. 44.034.300.04, $\theta = 90^{o}$	70
50	Comparison of component spectra, condition no. 44.034.300.04, $\theta = 121^{o}$	71
51	Comparison of component spectra, condition no. 44.034.300.04, $\theta = 151^{o}$	72
52	Comparison of component spectra, condition no. 44.035.900.01, $\theta = 31^{o}$	73
53	Comparison of component spectra, condition no. 44.035.900.01, $\theta = 61^{o}$	74
54	Comparison of component spectra, condition no. 44.035.900.01, $\theta = 91^{o}$	75
55	Comparison of component spectra, condition no. 44.035.900.01, $\theta = 122^{o}$	76
56	Comparison of component spectra, condition no. 44.035.900.01, $\theta = 152^{o}$	77

LIST OF FIGURES (Continued)

Figure		Page
57	Component field shape, condition no. 44.036.300.08, $N_1/\sqrt{\theta}$ = 60%	78
58	Component field shape, condition no. 44.034.011.15, $N_1/\sqrt{\theta}$ = 60%	79
59	Component field shape, condition no. 44.036.300.04, $N_1/\sqrt{\theta}$ = 70%	80
60	Component field shape, condition no. 44.034.300.08, $N_1/\sqrt{\theta}$ = 80%	81
61	Component field shape, condition no. 44.034.300.04, $N_1/\sqrt{\theta}$ = 90%	82
62	Component field shape, condition no. 44.035.900.01, $N_1/\sqrt{\theta}$ = 100%	83
63	Component spectra, condition no. 44.036.300.08, $\theta = 30^\circ$	85
64	Component spectra, condition no. 44.036.300.08, $\theta = 60^\circ$	86
65	Component spectra, condition no. 44.036.300.08, $\theta = 91^\circ$	87
66	Component spectra, condition no. 44.036.300.08, $\theta = 121^\circ$	88
67	Component spectra, condition no. 44.036.300.08, $\theta = 152^\circ$	89
68	Component spectra, condition no. 44.034.011.15, $\theta = 30^\circ$	90
69	Component spectra, condition no. 44.034.011.15, $\theta = 61^\circ$	91
70	Component spectra, condition no. 44.034.011.15, $\theta = 91^\circ$	92
71	Component spectra, condition no. 44.034.011.15, $\theta = 122^\circ$	93
72	Component spectra, condition no. 44.034.011.15, $\theta = 152^\circ$	94
73	Component spectra, condition no. 44.036.300.04, $\theta = 30^\circ$	95
74	Component spectra, condition no. 44.036.300.04, $\theta = 60^\circ$	96
75	Component spectra, condition no. 44.036.300.04, $\theta = 91^\circ$	97
76	Component spectra, condition no. 44.036.300.04, $\theta = 121^\circ$	98
77	Component spectra, condition no. 44.036.300.04, $\theta = 152^\circ$	99
78	Component spectra, condition no. 44.034.300.08, $\theta = 32^\circ$	100
79	Component spectra, condition no. 44.034.300.08, $\theta = 62^\circ$	101
80	Component spectra, condition no. 44.034.300.08, $\theta = 92^\circ$	102
81	Component spectra, condition no. 44.034.300.08, $\theta = 122^\circ$	103

LIST OF FIGURES (Continued)

Figure		Page
82	Component spectra, condition no. 44.034.300.08, $\theta = 152^{\circ}$ . . .	104
83	Component spectra, condition no. 44.034.300.04, $\theta = 30^{\circ}$ . . .	105
84	Component spectra, condition no. 44.034.300.04, $\theta = 60^{\circ}$ . . .	106
85	Component spectra, condition no. 44.034.300.04, $\theta = 90^{\circ}$ . . .	107
86	Component spectra, condition no. 44.034.300.04, $\theta = 121^{\circ}$ . . .	108
87	Component spectra, condition no. 44.034.300.04, $\theta = 151^{\circ}$ . . .	109
88	Component spectra, condition no. 44.035.900.01, $\theta = 31^{\circ}$ . . .	110
89	Component spectra, condition no. 44.035.900.01, $\theta = 61^{\circ}$ . . .	111
90	Component spectra, condition no. 44.035.900.01, $\theta = 91^{\circ}$ . . .	112
91	Component spectra, condition no. 44.035.900.01, $\theta = 122^{\circ}$ . . .	113
92	Component spectra, condition no. 44.035.900.02, $\theta = 152^{\circ}$ . . .	114
93	Average difference between predicted and measured tone corrected perceived noise levels, 60%, 66%, and 70%	115
94	Average difference between predicted and measured tone corrected perceived noise levels, 80%, 90%, and 100%	116

LIST OF TABLES

Table		Page
1	Aircraft Geometry	7
2	Air Induction System	9
3	LP System	9
4	Core Engine Design	10
5	Acoustic Liner Description	12
6	RB.211-524B Acoustic Liner Insertion Loss for Broadband Noise - ΔdB	13
7	RB.211-524B Acoustic Liner Insertion Loss for Tones and Buzz Saw Noise - ΔdB	13
8	RB.211-524B Acoustic Liner Attenuation Directory Exponent	14
9	Flight Conditions for Test Data Base	15
10	Weather Conditions	16
11	Engine Axis Orientation	31
12	L-1011-524 Flyover Engine Data	32
13	RB.211-524B - Average Engine Operating Parameters	33
14	Observer Locations	36
15	ANOPP Modules Executed	38
16	L-1011 Data Input for ANOPP*	40
17	Ranking of Noise Sources from Field Shapes	84
18	Frequency Range for ΔdB Corrections	117
19	ΔdB SPL Corrections Condition No. 44.036.300.08 $N_1\sqrt{\theta}$ = 60%	118
20	ΔdB SPL Corrections Condition No. 44.034.011.15 $N_1/\sqrt{\theta}$ = 66%	119
21	ΔdB SPL Corrections Condition No. 44.036.300.04 $N_1/\sqrt{\theta}$ = 70%	120
22	ΔdB SPL Corrections Condition NO. 44.036.300.08 $N_1/\sqrt{\theta}$ = 80%	121

LIST OF TABLES (Continued)

Table		Page
23	Δ dB SPL Corrections Conditions No. 44.034.300.04 $N_1/\sqrt{\theta}$ = 90%	122
24	Δ dB SPL Corrections Conditions No. 44.035.900.01 $N_1/\sqrt{\theta}$ = 100%	123

ANOPP VALIDATION STUDY
LOCKHEED L-1011

Larry Godby

Lockheed-California Company
Burbank, California

SUMMARY

This report describes the work completed by Lockheed to verify the Aircraft Noise Prediction Program developed by NASA Langley Research Center. In this study, ANOPP was used to predict the far-field noise characteristics of an L-1011 aircraft equipped with RB.211-524B engines.

A comparison was made with actual flight noise with noise predicted for the same operating and weather conditions. Correlation of predicted and measured results was very good in the aft quadrant of radiated noise. Predicted noise levels were significantly different from measured values in the forward quadrant because fan noise was predicted high.

Since the major noise sources were fan and core, corrections are supplied to adjust ANOPP fan and core noise components so that the total predicted noise matches the measured L-1011 noise levels.

INTRODUCTION

NASA has developed a modular computer program, Aircraft Noise Prediction Program (ANOPP), for calculating far-field engine and aircraft radiated noise. This program structure is based on a wide variety of functional modules that allow a user to select noise source components and propagation characteristics that are relevant to his particular problem. Since most of the ANOPP prediction methods are constructed from scale model test data and static engine data, it is important that noise predictions are verified with measured data for actual aircraft. Inclusion of the Lockheed L-1011 aircraft in this validation effort would serve this end.

The purpose of this validation study is to

- provide a quality flyover noise data base
- determine the accuracy of ANOPP with respect to this data base
- analyze the data for source and propagation effects.

Lockheed has conducted such an exercise with the L-1011-1-385, SN 1001 flight test aircraft as shown in this report.

LIST OF SYMBOLS

A1	Primary jet area, m^2 (ft^2)
A2	Secondary jet area, m^2 (ft^2)
AF	Trailing edge flap segments (1 or 2)
AH	Horizontal tail area, m^2 (ft^2)
AREA	Fan duct area, m^2 (ft^2)
AV	Vertical tail area, m^2 (ft^2)
AW	Wing area, m^2 (ft^2)
BH	Horizontal tail span, m (ft)
BPF	Blade passage frequency, Hz
BV	Vertical tail span, m (ft)
BW	Wing span, m (ft)
CF	Trailing edge flap total chord, m (ft)
CL	Local speed of sound at LP turbine, m/s (ft/sec)
C_L	Lift coefficient
CMG	Main landing gear strut length, m (ft)
CNG	Nose Landing gear strut length
D	Diameter, m (ft)
DELTA	Sum of $\alpha + \gamma$, deg
DELT	Stagnation temperature rise across fan, ^oR (^oF)
TDDELT	Temperature rise for fan design, ^oK (^oR)
DIAM	Fan diameter, m (ft)
DIS	Inlet flow distortion factor
DM	Fan blade tip mach number design value, dim.
DOTM	Mass flow rate, (kg/s) (slugs/s)

f	Frequency, Hz
GAMA	Trailing edge flap aft-segment deflection, deg
IGV	Inlet guide vanes, dim.
MLG	Main landing gear.
NB	Number of fan blades, dim.
NF	Number of trailing edge flap segments (1 or 2)
NLG	Nose landing gear.
NMG	Number of main landing gear wheels/unit
NNG	Number of nose landing gear wheels/unit
NV	Number of fan stator vanes, dim.
$N_1/\sqrt{\theta}$	Corrected low pressure compressor (fan) speed-% (ref=3900 RPM)
$N_2/\sqrt{\theta}$	Corrected intermediate pressure compressor speed-% (ref=7000 RPM)
$N_3/\sqrt{\theta}$	Corrected high pressure compressor speed-% (ref=10611 RPM)
OMEGA	Fan speed, revolution/sec
P	Pressure, N/m^2 (lb/ft^2)
P1	Primary jet total pressure, N/m^2 (lb/ft^2)
P2	Secondary jet total pressure, N/m^2 (lb/ft^2)
P3	Total pressure at combustor inlet, N/m^2 (lb/ft^2)
PWL	Sound power level, re 10^{-12} watts
RHO1	Density of primary jet kg/m^3 ($slugs/ft^3$)
RHO2	Density of secondary jet kg/m^3 ($slugs/ft^3$)
ROT	Sum of $\epsilon + \alpha + \vartheta$, deg
RSS	Fan sector spacing in blade chords, dim.
SPL	Sound pressure level, re 2×10^{-5} N/m^2
SRS	Stator/rotor spacing

Ti	Primary jet stagnation temperature, ^{o}K (^{o}R)
T2	Secondary jet stagnation temperature, ^{o}K (^{o}R)
T3	Total temperature at combustor inlet, ^{o}K (^{o}R)
T4	Total temperature at combustor exit, ^{o}K (^{o}R)
TDDELT	Design temperature rise across fan stage, ^{o}K (^{o}R)
TDMG	Diameter of main landing gear wheels, ft
TDNG	Diameter of nose landing gear wheels
V	Velocity m/s (ft/sec)
V1	Primary jet velocity, m/s (ft/s)
V2	Secondary jet velocity, m/s (ft/s)
VA	Aircraft velocity, m/s (ft/s)
VTR	Relative tip speed for turbine, m/s (ft/s)
x	Coordinate along runway centerline, m (ft)
XA	Aircraft position, x coordinate, m (ft)
y	Coordinate perpendicular to x-axis and in-ground plane m (ft)
YA	Aircraft lateral position, y coordinate, m (ft)
z	Coordinate perpendicular to ground plane, m (ft)
ZA	Aircraft position, z coordinate, m (ft)
α	Angle of attack, deg
δ	Flap angle, deg
ϵ	Engine angle, deg
γ	Climb angle, deg
θ	Noise radiation angle relative to engine inlet centerline, deg

1. FLYOVER NOISE DATA BASE

Six sets of test data have been selected for this study. Engine operating conditions range from 60 to 100 percent $N_1/\sqrt{\theta}$. Although the data have been extracted from special tests, instrumentation and test conditions comply with FAR Part 36 requirements in reference 1.

1.1 Aircraft Description

Aircraft geometry, engine description, data acquisition instrumentation, test procedures and data are presented in the following section.

1.1.1 Aircraft geometry. - Figure 1 shows a three-view drawing of the L-1011 aircraft, a widebody aircraft with two engines mounted under the wing and one engine mounted in the empennage. Leading edge slats are along the entire length of the wing. The trailing edge flaps are double-slotted Fowler flaps. There are two inboard and two outboard segments on each side of the wing. Geometrical parameters that will be used for input to the ANOPP program for making noise predictions are given in table 1.

Engine orientation relative to the fuselage reference plane is 3° up for fan axis, or 3° down for jet exhaust axis. This angle is an average of three engine orientations under low speed and low altitude flight conditions.

1.1.2 RB.211-524B turbofan engine. - The L-1011 is powered by three Rolls-Royce RB.211-524B engines, each developing 2.224×10^5 N (50 000 lb) of takeoff thrust flat rated to ISA + 13.9°C (25°F). However, since this rating is not needed at sea level and normal operating temperature, an operational rating of 2.135×10^5 N (48 000 pounds) has been selected. This rating extends the sea level flat rating to ISA + 19.6°C(35.3°F). The equivalent of the full 2.224×10^5 (50 000 lb) is used at airports above 610m (2000 ft).

The engine is a three-spool design. The low-pressure (LP) system consists of a single-stage fan driven by a three-stage uncooled power turbine. The core engine has an intermediate-pressure (IP) spool with a seven-stage compressor driven by a single-stage uncooled turbine, and a high-pressure (HP) spool with a six-stage compressor driven by a single air-cooled turbine. A cutaway of the engine is presented in figure 2.

The wing and S-duct inlet systems provide the engines with airflow at nearly free stream total pressure with only a negligible cruise drag penalty. Each of the inlets (both wings and center) incorporate acoustic liners. General characteristics of the wing and S-duct systems are provided in table 2.

The engine exhaust is equipped with a fixed convergent-divergent nozzle on the core stream and a convergent nozzle on the bypass stream. The fan bypass duct extends from the fan outlet guide vanes to approximately the LP

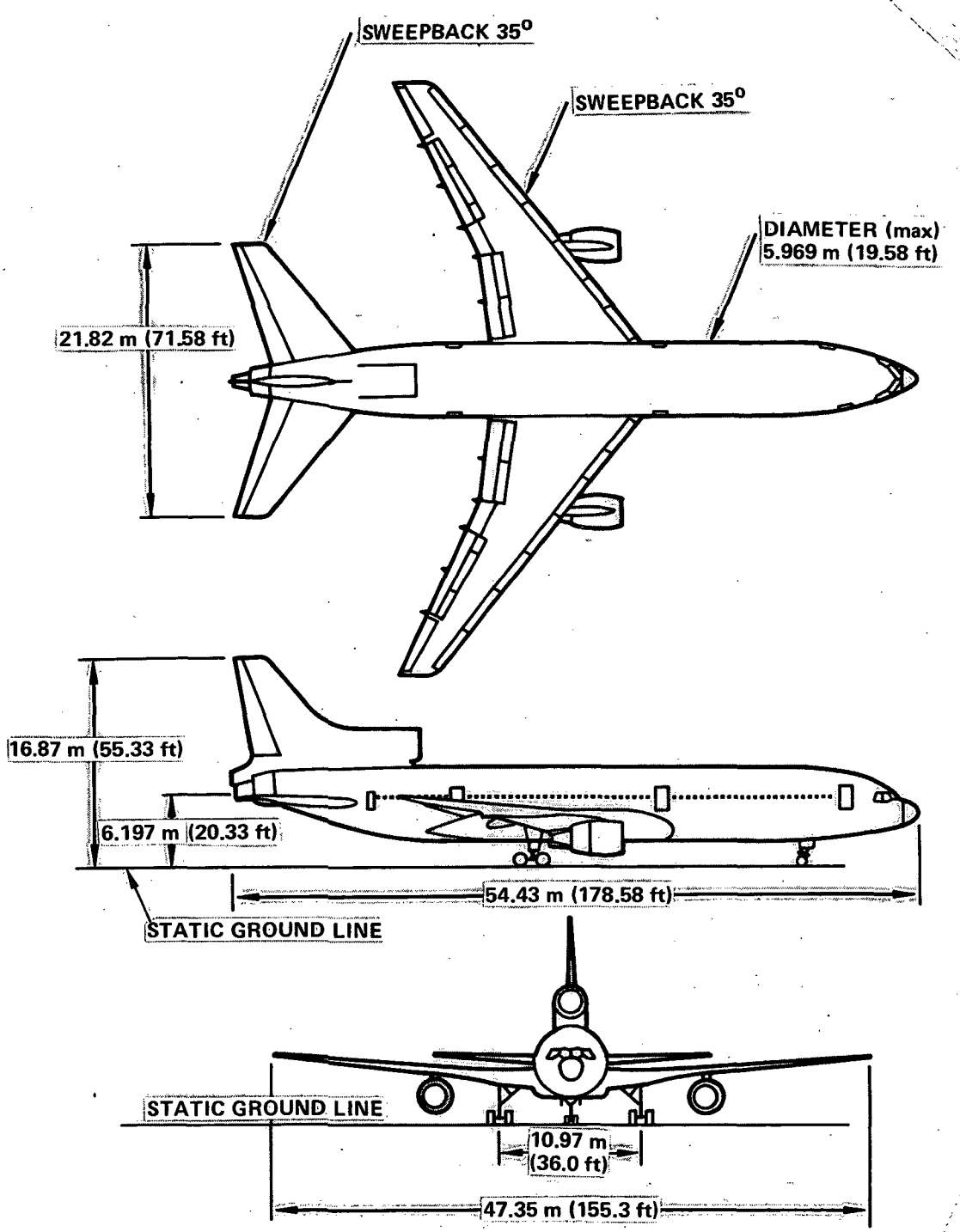

Figure 1. - Three-view drawing of L-1011-1-385

TABLE 1. - AIRCRAFT GEOMETRY

Wing	321.1 m^2 (3456 ft^2) reference, 352.8 m^2 (3797 ft^2) total
Wing Span	47.35 m (155.3 ft)
Flap Angles	4, 10, 18, 22, 27, 33, or 42 d
Number of Trailing Edge Flap Segments	2
Trailing Edge Flap Area	26.9 m^2 (290 ft^2) inboard and 22.9 m^2 (246 ft^2) outboard
Trailing Edge Flap Chord	1.98 m (6.5 ft) inboard (constant) and 30% wing chord outboard
Horizontal Tail Area	119.1 m^2 (1282 ft^2)
Horizontal Tail Span	21.8 m (71.6 ft)
Vertical Tail Area	51.1 m^2 (550 ft^2)
Vertical Tail Span	9.04 m (29.7 ft)
Number of MLG Wheels	8
Diameter of MLG Wheels	1.27 m (4.17 ft) tire O.D.; 0.526 m (1.73 ft) rolling radius
MLG Strut Length	3.63 m (11.9 ft) full extension; 3.54 m (11.6 ft) static at TOGW = 1.913×10^6 N (430 000 lb)
Number of NLG Wheels	2
Diameter of NLG Wheels	0.914 m (3.0 ft) tire, outside diameter; 0.386 m (1.27 ft) rolling radius
NLG Strut Length	2.57 m (8.48 ft) full extension; 2.49 m (8.17 ft) static at TOGW = 1.93×10^6 N (430 000 lb)

turbine plane. The fan duct is fitted with a thrust reverser which is deployed by translating a portion of the fan cowl rearward, exposing the reverser cascades. During the translation of the fan cowl, the fan duct is blocked off, forcing the fan air to be turned and exhausted through the exposed cascades. There is no core thrust spoiler or reverser.

Geometric and performance characteristics of the LP system are presented in table 3.

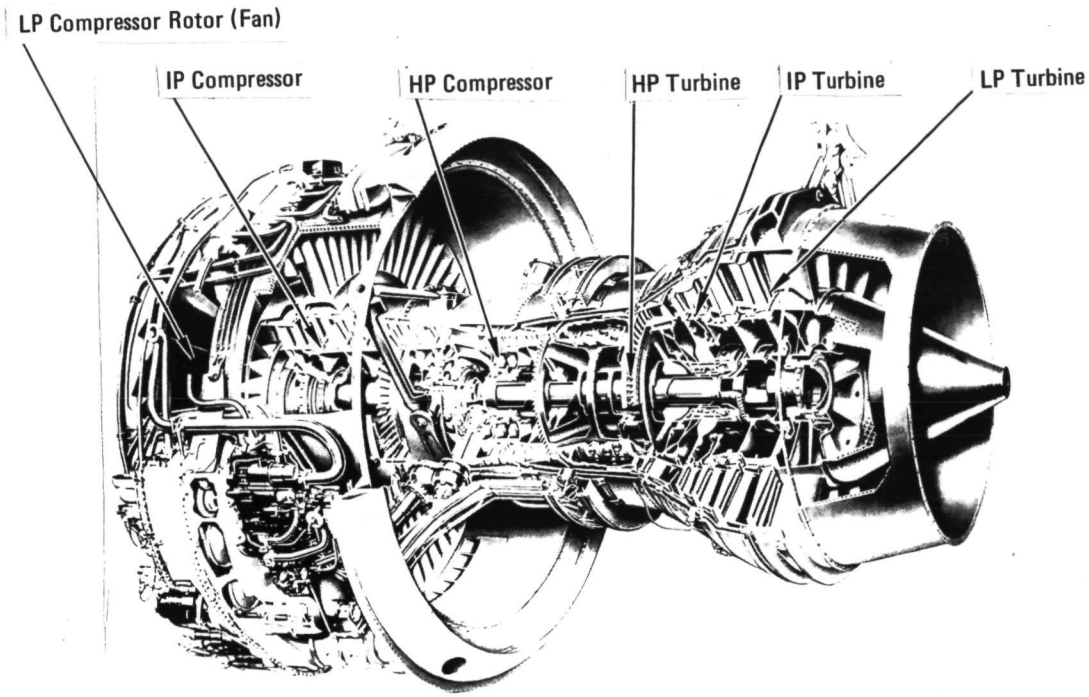

Figure 2. - RB.211 cutaway

In the engine core the IP and HP compressors together provide approximately 19:1 design pressure ratio and when supercharged by the fan root develops an overall pressure ratio of 28:1. The engine has a conventional annular combustor which provides approximately a 1547 degree K (2784 degree R) burner outlet temperature for design takeoff rating. The first and second stage turbine nozzle guide vanes are both cooled. Details of the core engine design are shown in table 4.

TABLE 2. - AIR INDUCTION SYSTEM

Parameter	
Highlight Diameter	2.25 m (7.37 ft)
Throat Diameter	1.99 m (6.52 ft)
Contraction Ratio	1.28

TABLE 3. - LP SYSTEM

Fan			
Pressure ratio (SLS)	1.64		
Airflow (SLS)	657.6 kg/s (1450 lb/sec)		
Diameter	2.18 m (7.17 ft)		
Hub/tip	0.34		
Blades	33		
OGV's	70		
Rotor/OGV spacing	2 Fan Blade Chord Lengths		
Design tip speed	457 m/s (1500 ft/sec)		
LP Turbine			
Number of stages	3		
Cooled	No		
Stage number	1	2	3
Number of blades	124	76	72
Number of vanes	102	93	111
Diameter	1.16 m (3.80 ft)	1.26 m (4.13 ft)	1.27 m (4.17 ft)

TABLE 4. - CORE ENGINE DESIGN

IP Compressor	
Stages	7
Pressure ratio	4.4:1
HP Compressor	
Stages	6
Pressure ratio	4.3:1
HP Nozzle Guide Vanes	
Cooled	Yes
Number of vanes	36
HP Turbine	
Stages	1
Cooled	Yes
Number of blades	102
Diameter	0.937 m (3.08 ft)
IP Nozzle Guide Vanes	
Cooled	Yes
Number of vanes	26
IP Turbine	
Stages	1
Cooled	No
Number of Blades	148
Diameter	1.11 m (3.65 ft)

1.1.3 Acoustic liner. - The RB.211-524B installed on the L-1011, SN 1001, has acoustic liners designed into the

- fan inlet duct
- fan discharge duct
- primary nozzle areas

This acoustic treatment consists of perforated face sheets bonded to a honeycomb core. Specification of the liner location and dimensions are made in table 5. Engine noise source components attenuated by these treatments are:

- fan inlet
- fan discharge
- buzz-saw
- turbine
- core

Rolls-Royce has characterized the source attenuation and directivities from extensive static ground tests of the RB.211-524B engine (reference 2). Results of these tests provide insertion loss as a function of frequency and noise source component. These data are shown in tables 6 and 7. Note that attentuations for buzz-saw noise are a function of normalized frequency, F/BPF (frequency/blade passage frequency). This is the only component insertion loss that has any significant dependence on power setting. Liner attenuation spectra are further modified by directivity exponents that are functions of noise source component and inlet radiation angle, θ. These exponents are shown in table 8.

To obtain the third-octave band sound pressure level attenuation, the insertion loss for a particular frequency is multiplied by the directivity exponent at a specified radiation angle, θ.

Therefore, the change in sound pressure level is

$$\Delta SPL = -\Delta PWL\ (f)\ X\ DE\ (\theta)$$

where $\Delta PWL(f)$ is from table 6 or 7 and DE (θ) is found in table 8.

TABLE 5. - ACOUSTIC LINER DESCRIPTION

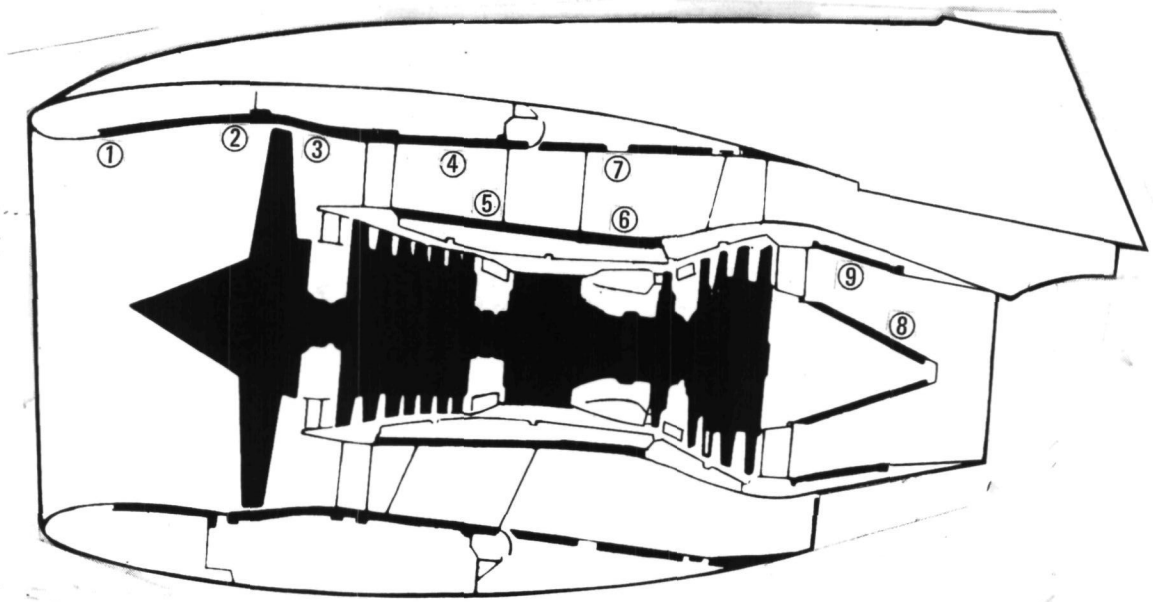

Location	Inlet		Fan Case		Fan Discharge			Tailpipe	
Design Parameter	①	②	③	④	⑤	⑥	⑦	⑧	⑨
Length -m (ft)	0.483 (1.58)	0.152 (.500)	0.137 (.450)	0.582 (1.91)	1.07 (3.5)	0.457 (1.50)	1.52 (5.00)	0.531 (1.74)	0.406 (1.33)
Area -m^2 (ft^2)	2.57 (27.7)	0.706 (7.6)	0.836 (9.0)	3.00 (32.3)	3.07 (33.0)	0.836 (9.0)	5.95 (64.0)	0.650 (7.0)	1.30 (14.0)
Duct Height -m (ft)	2.08 (6.83)	2.08 (6.83)	0.406 (1.33)	0.406 (1.33)	-	-	0.457 (1.50)	-	0.300 (0.983)
Perforate -% Open Area	9.0 **	23.0 *	6.0 *	6.0 *	7.0 *	7.0 **	6.5 *	9.0 **	9.0 **
Core Face Width -m (ft)	0.019 (0.063)	0.019 (0.063)	0.019 (0.063)	0.019 (0.063)	0.019 (0.063)	0.016 (0.053)	0.016 (0.052)	0.013 (0.042)	0.013 (0.042)
Core Depth -m (ft)	0.019 (0.053)	0.076 (0.250)	0.025 (0.083)	0.025 (0.083)	0.019 (0.063)	0.033 (0.11)	0.032 (0.104)	0.013 (0.042)	0.013 (0.042)

*Hex Cell **Rectangular Cell

TABLE 6. - RB.211-524B ACOUSTIC LINER INSERTION LOSS FOR BROADBAND NOISE Δ dB

Frequency Hz	Turbine and Core	Inlet	Discharge
200	0.	0.2	0.
250	0.	0.4	0.2
315	0.	0.7	0.6
400	0.	1.0	1.2
500	0.	2.1	2.0
630	0.	2.3	3.5
800	0.	3.1	5.3
1000	0.2	3.6	7.4
1250	0.6	3.9	9.2
1600	0.9	3.9	10.1
2000	1.3	3.7	10.1
2500	1.8	3.4	9.7
3150	2.6	3.1	9.1
4000	3.7	2.8	8.8
5000	5.1	2.5	8.5
6300	5.2	2.3	8.2
8000	4.0	2.1	7.6
10000	2.6	1.9	7.2

TABLE 7. - RB.211-524B ACOUSTIC LINER, BUZZ INSERTION LOSS FOR BUZZ SAW NOISE AND TONES Δ dB

F/BPF	0.125	0.167	0.208	0.250	0.292	0.458	0.500
ΔPWL	0.3	2.0	3.8	5.5	6.4	6.7	6.0
F/BPF	0.667	0.833	1.000	1.333	1.667	2.000	2.333
ΔPWL	5.3	4.5	3.7	2.8	1.8	0.7	0.

TABLE 8. - RB.211-524B ACOUSTIC LINER ATTENUATION DIRECTIVITY EXPONENT

Theta Deg.	Turbine and Core	Fan Inlet	Fan Discharge	Buzz Saw And Tones
10	1.00	0.70	1.00	0.40
20	1.00	0.70	1.00	0.51
30	1.00	0.76	1.00	0.62
40	1.00	1.00	1.00	0.73
50	1.00	1.13	1.00	0.85
60	1.00	1.18	1.00	0.96
70	1.00	1.20	1.00	1.00
80	1.00	1.20	1.00	0.87
90	1.00	1.20	1.00	0.70
100	1.00	1.20	1.00	0.50
110	1.00	1.20	1.00	0.30
120	1.00	1.20	0.94	0.10
130	0.94	1.20	0.85	0.
140	0.77	1.20	0.74	0.
150	0.56	1.20	0.60	0.
160	0.32	1.20	0.46	0.
170	0.10	1.20	0.30	0.

2.2 Test

The six flight conditions shown in Table 9 have been chosen for the measured noise data base. The corrected fan speed ($N_1/\sqrt{\theta}$) provides an indication of the engine power setting.

2.2.1 Ambient conditions. - The noise tests were conducted at Air Force Plant 42 (Palmdale, California). The test site is a flat desert region free of obstructions. The terrain is sandy soil with sparse vegetation. Ground flow resistance for the surrounding area is assumed to be 2.50×10^5 N-s/m^4 (4.85.1 lb-sec/ft^4). Airport reference altitude is 762 m (2500 ft).

Weather conditions during the period of noise measurements were within the requirements of FAR 36. These conditions were:

TABLE 9. - FLIGHT CONDITIONS FOR TEST DATA BASE

Nominal Corrected Fan Speed (% $N_1/\sqrt{\theta}$)	Flight Mode	Flap Setting (Degrees)	Landing Gear Position	Altitude m (ft)	True Air Speed m/sec (knots)
100	Takeoff	10	Up	304 (1000)	99.3 (193)
90	Level	33	Down	366 (1200)	94.1 (183)
80	Level	33	Up	335 (1100)	95.7 (186)
70	Level	27	Up	91.4 (300)	83.3 (162)
66	Approach	42	Down	91.4 (300)	74.6 (145)
60	Level	4	Up	91.4 (300)	84.9 (165)

- no rain or other precipitation
- relative humidity between 30 and 90 percent
- ambient temperature range from 5 deg C (41 deg F) to 30 deg C (86 deg F)
- wind not above 5.14 m/s (10 knots) and crosswind component not above 2.57 m/s (5 knots) at 10 meters (32.8 ft) above the ground
- no temperature inversion or anomalous wind conditions that would affect noise data acquisition

Temperature, pressure, relative humidity, and wind velocity measurements were made at a 10 m (32.8 ft) tower located directly under the flight path approximately 2408 m (7900 ft) east of the runway threshold. Also, temperature, pressure, and relative humidity measurements were made with onboard aircraft equipment. All onboard meteorological measurements were made as a function of altitude. When level flyover noise measurements were being made, a climbout of the aircraft was performed approximately every 30 minutes to measure ambient conditions as a function of altitude.

A summary of the average weather measurements made during the six test flights at Palmdale is shown in table 10.

2.2.2 Flight trajectory. - Takeoff was from west to east while approach and level flyover flights were made from east to west. All aircraft flyovers were tracked with a Lockheed developed system, space tracking airborne recording system (STARS). It consists of an aircraft mounted camera that photographs precisely surveyed ground targets. Tracking data, aircraft performance data, and noise were synchronized using IRIG B format time code. This is the same method used during L-1011 FAA certification tests.

TABLE 10. - WEATHER CONDITIONS

% $N_1/\sqrt{\theta}$	Altitude - m (ft)	Temperature -deg K (deg R)	Relative Humidity %	Wind Speed m/s (ft/sec)
60	10. (32.8) 91.4 (300.)	288.5 (519.3) 286.4 (515.5)	66.0 69.8	2.5 (8.1) 0. 0.
66	10. (32.8) 91.4 (300.)	287.8 (518.1) 286.6 (515.8)	55.0 55.4	4.0 (13.2) 0. 0.
70	10. (32.8) 91.4 (300.)	287.7 (517.8) 285.6 (514.1)	64.8 65.6	0. 0. 0. 0.
80	10. (32.8) 335. (1100.)	287.3 (517.2) 283.1 (509.5)	55.3 71.6	2.8 (9.3) 0. 0.
90	10. (32.8) 366. (1200.)	286.8 (516.2) 282.6 (508.6)	61.9 73.1	2.3 (7.4) 0. 0.
100	10. (32.8) 304. (1000.)	282.7 (508.8) 281.1 (506.0)	87.0 81.3	0. 0. 0. 0.

Time history plots of aircraft position in x, y, z coordinates correlated to IRIG are presented in Figures 3 through 8. Basic airplane data (BAD) produced from onboard performance measurements provide aircraft velocity and lift coefficients for each test condition as a function of time. This is shown in figures 9 through 14.

Angle of attack versus lift coefficient for test condition flap angles is given in figure 15.

Engine axis orientation with respect to the ground plane can be computed from

$$ROT = \epsilon + \alpha + \gamma ,$$

where

ϵ is the angle between engine and fuselage reference plane,

α is the angle between fuselage reference plane and aircraft motion vector, and

γ is the angle between aircraft motion vector and ground plane.

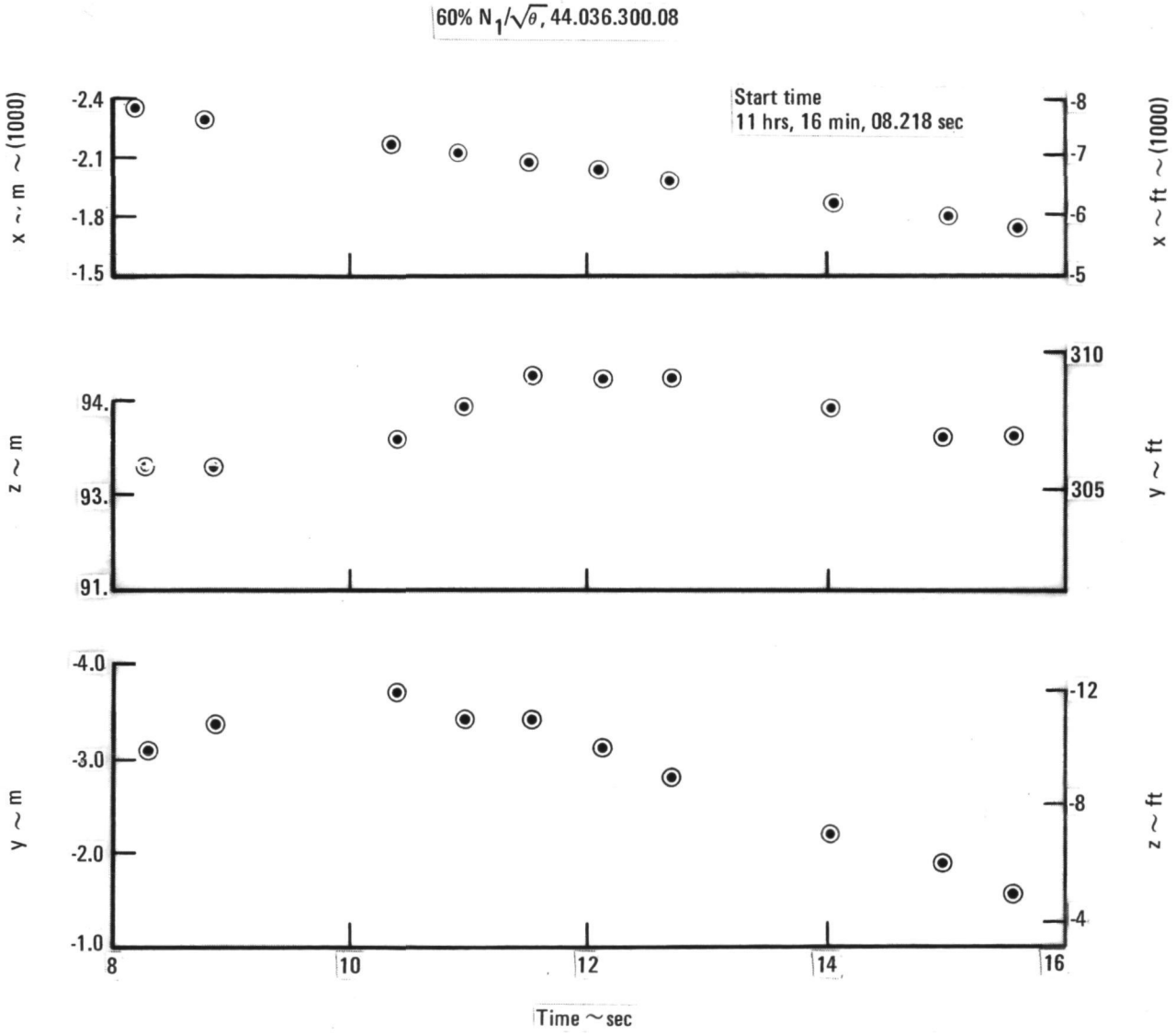

Figure 3. - Aircraft position time history plots, condition no. 44.036.300.08.

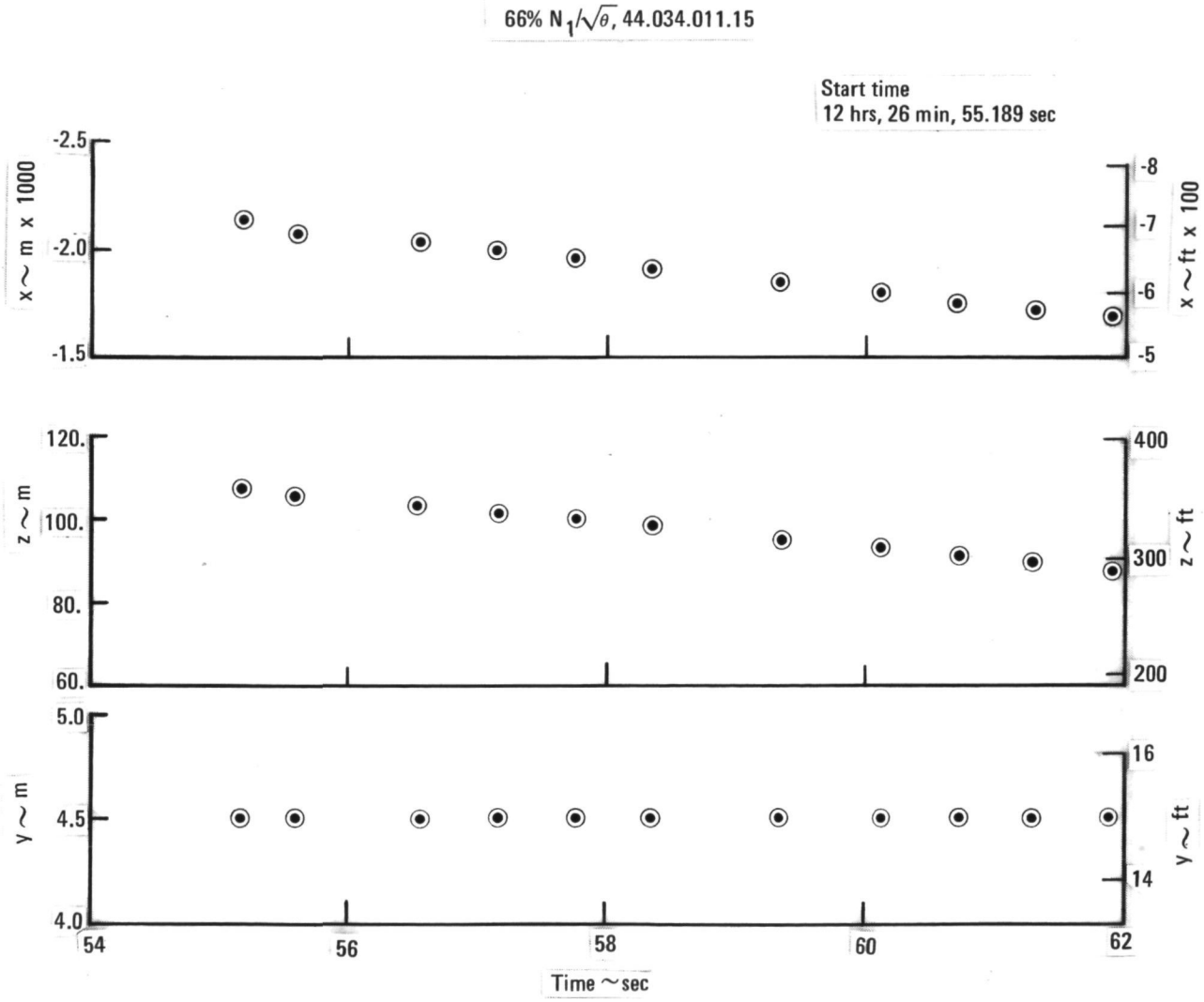

Figure 4. - Aircraft position time history plots, condition no. 44.034.011.15.

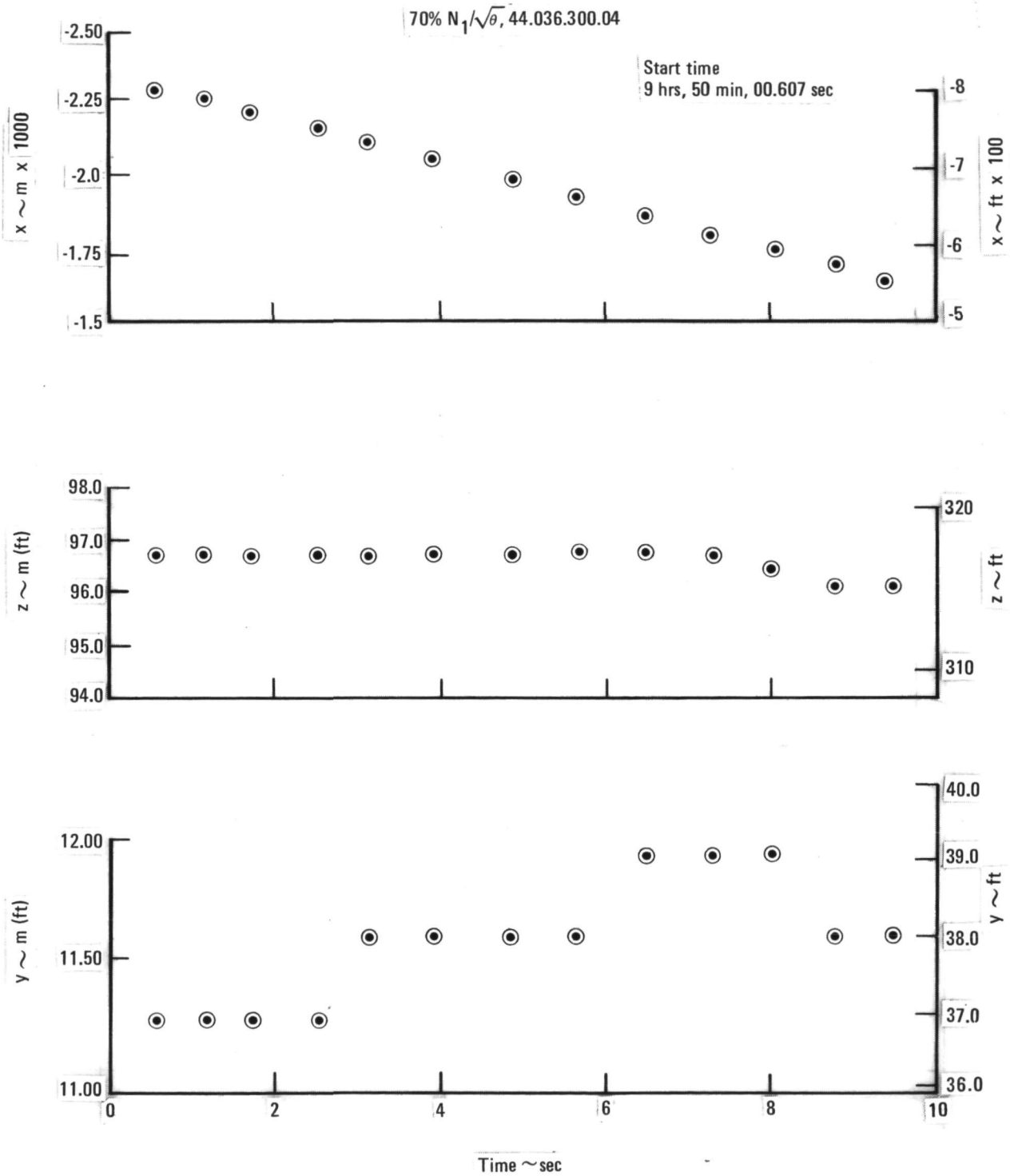

Figure 5. - Aircraft position time history plots, condition no. 44.036.300.04.

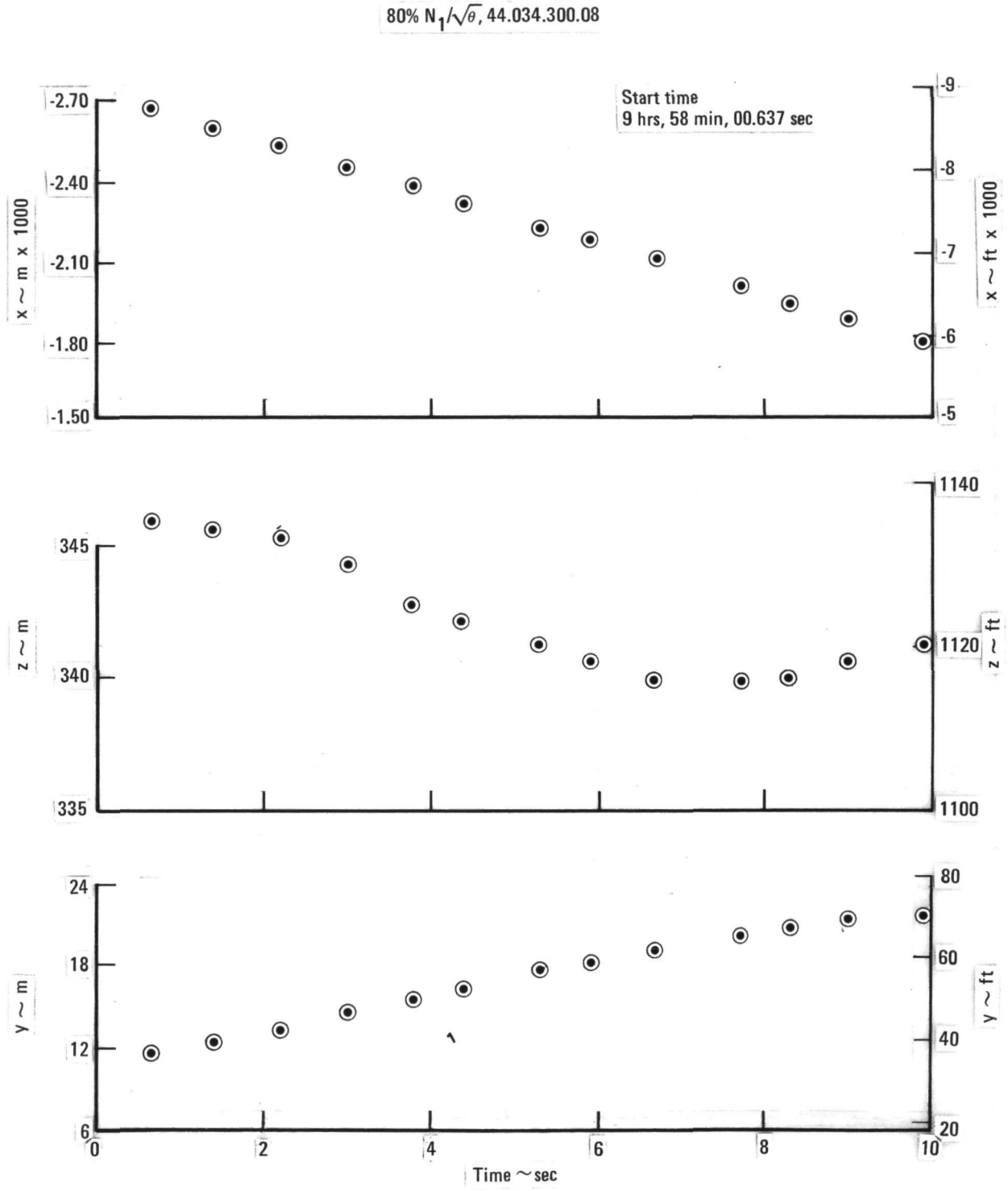

Figure 6. - Aircraft position time history plots, condition no. 44.034.300.08.

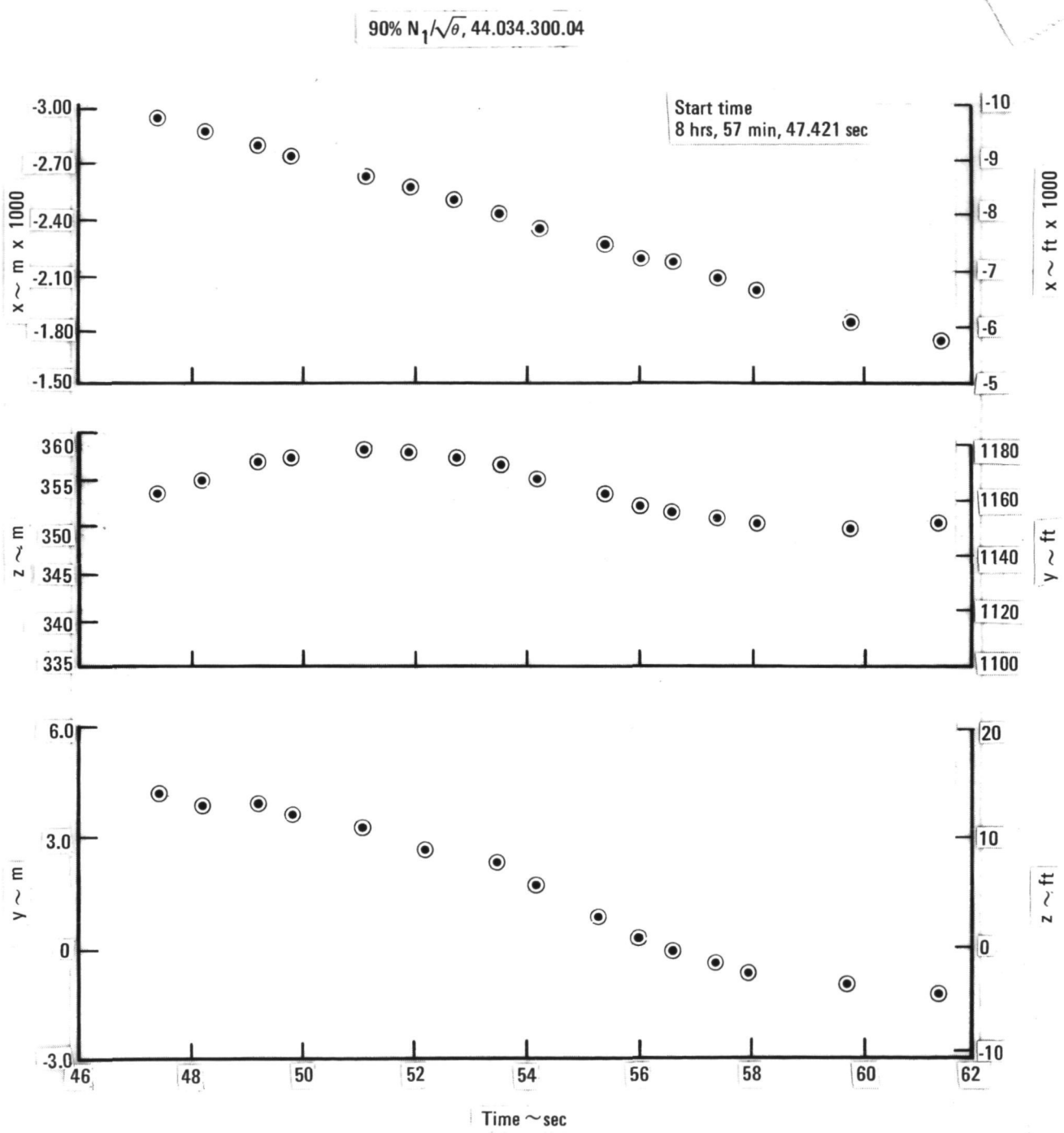

Figure 7. - Aircraft position time history plots, condition no. 44.034.300.04.

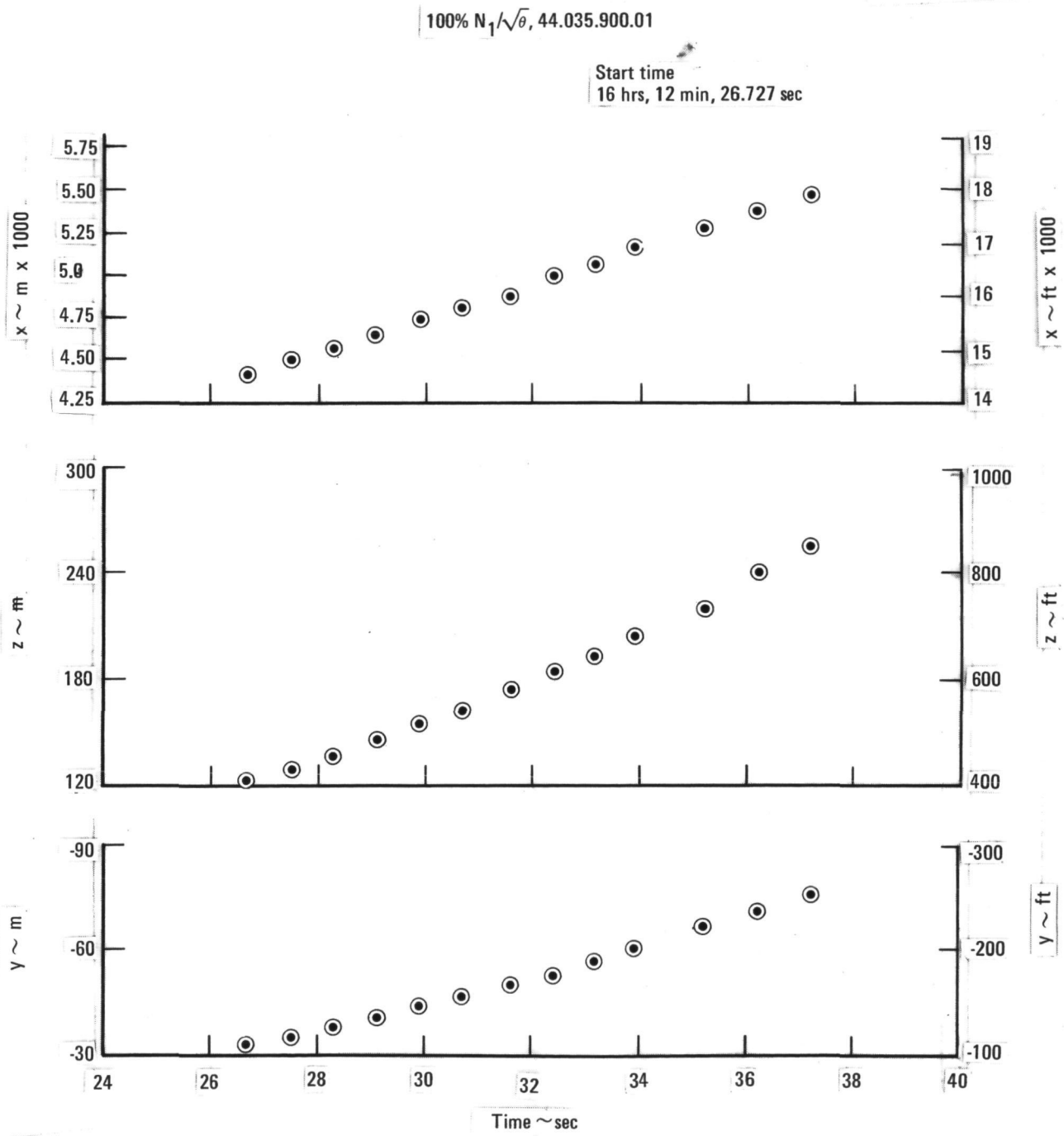

Figure 8. - Aircraft position time history plots, condition no. 44.035.900.01.

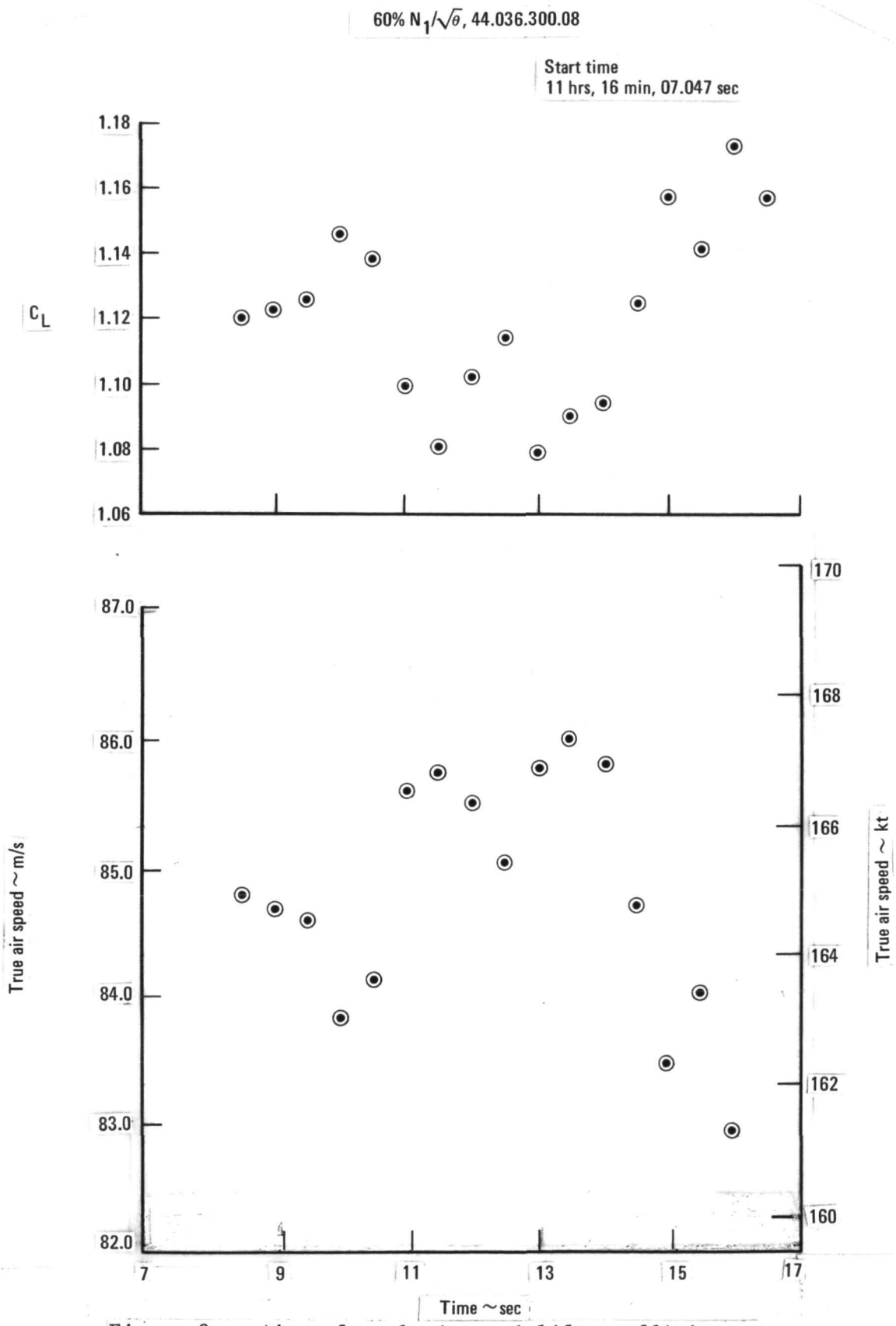

Figure 9. - Aircraft velocity and lift coefficients, condition no. 44.036.300.08

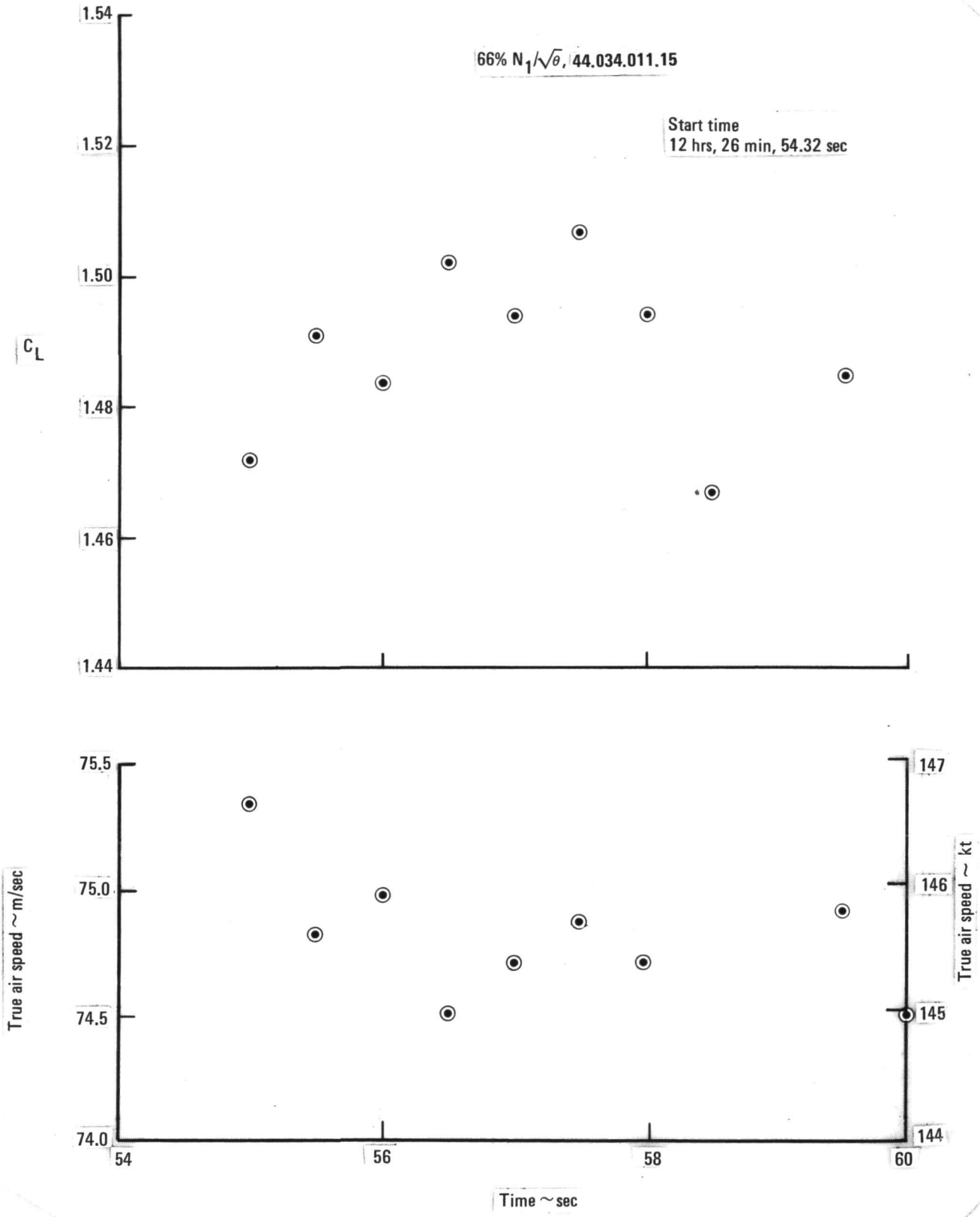

Figure 10. - Aircraft velocity and lift coefficients, condition no. 44.034.011.15.

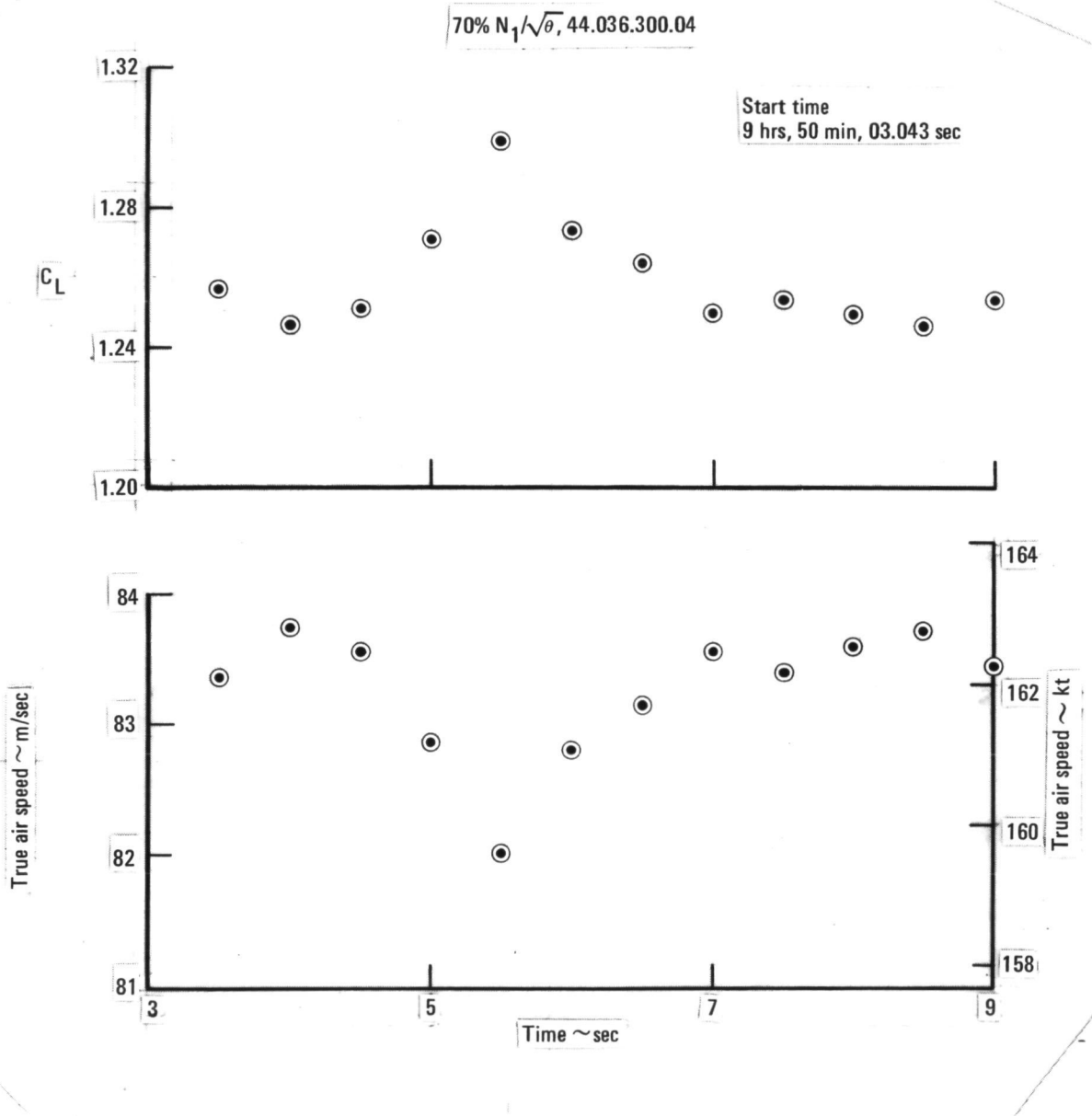

Figure 11. - Aircraft velocity and lift coefficients, condition no. 44.036.300.04.

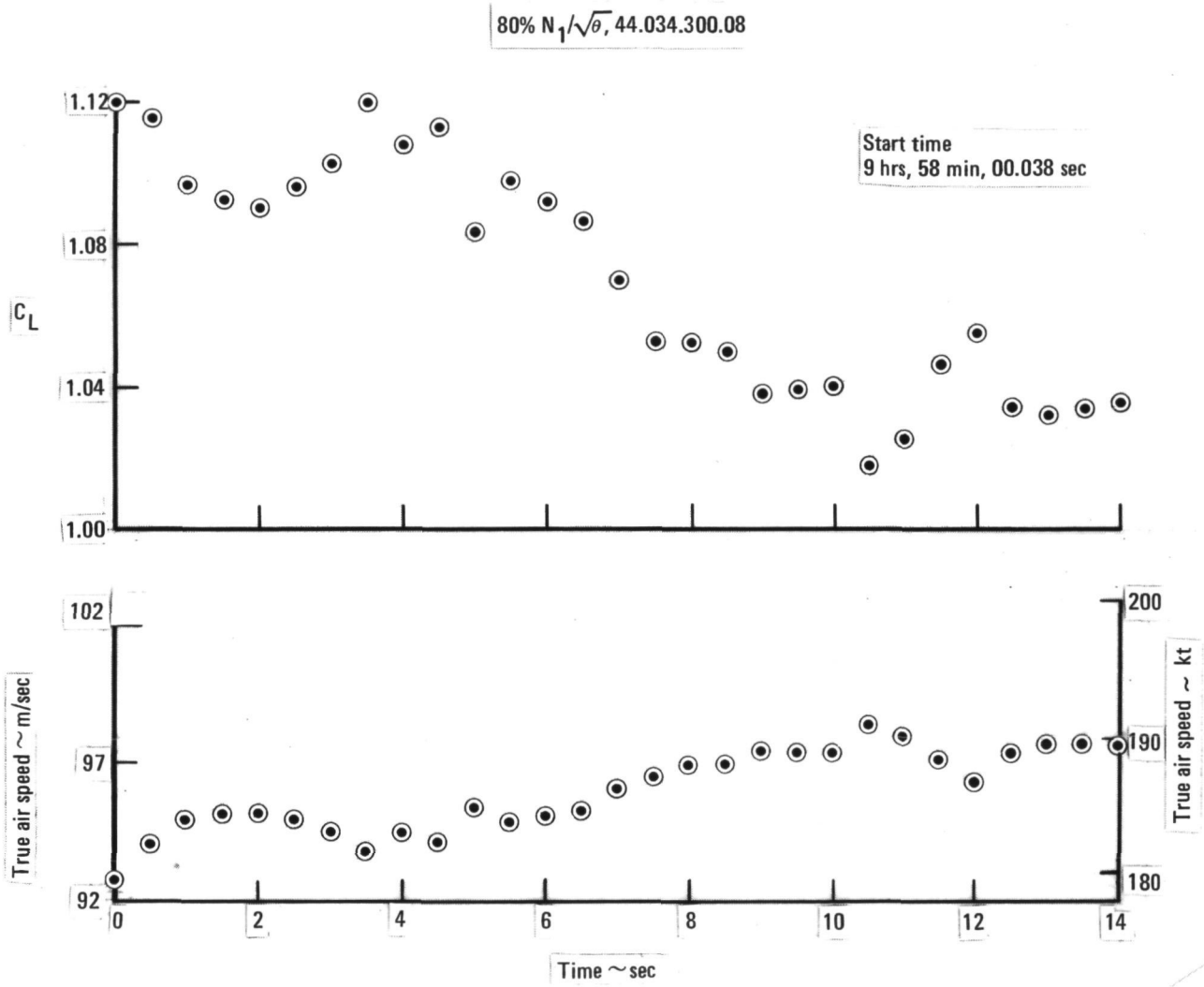

Figure 12. - Aircraft velocity and lift coefficients, condition no. 44.034.300.08.

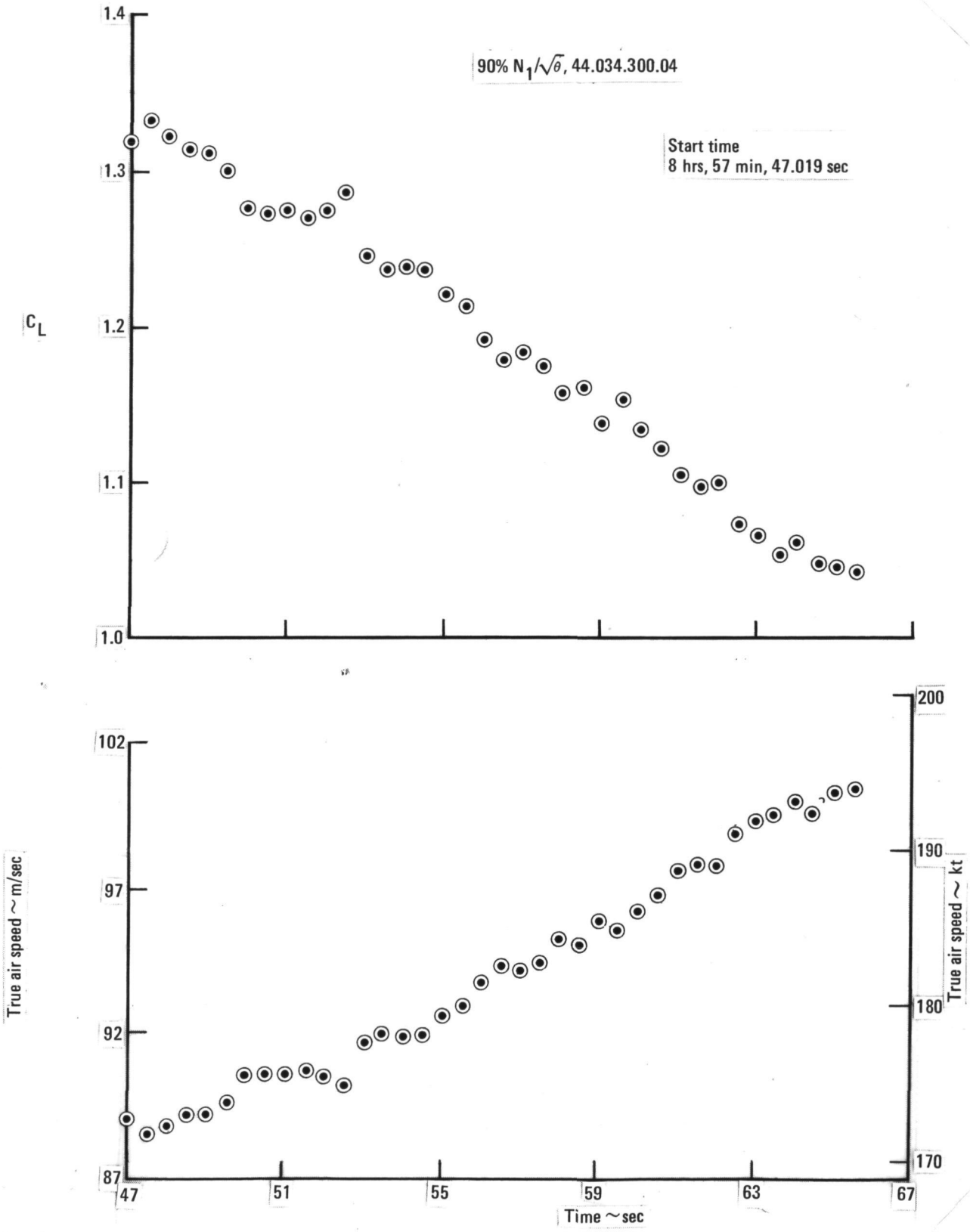

Figure 13. - Aircraft velocity and lift coefficients, condition no. 44.034.300.04.

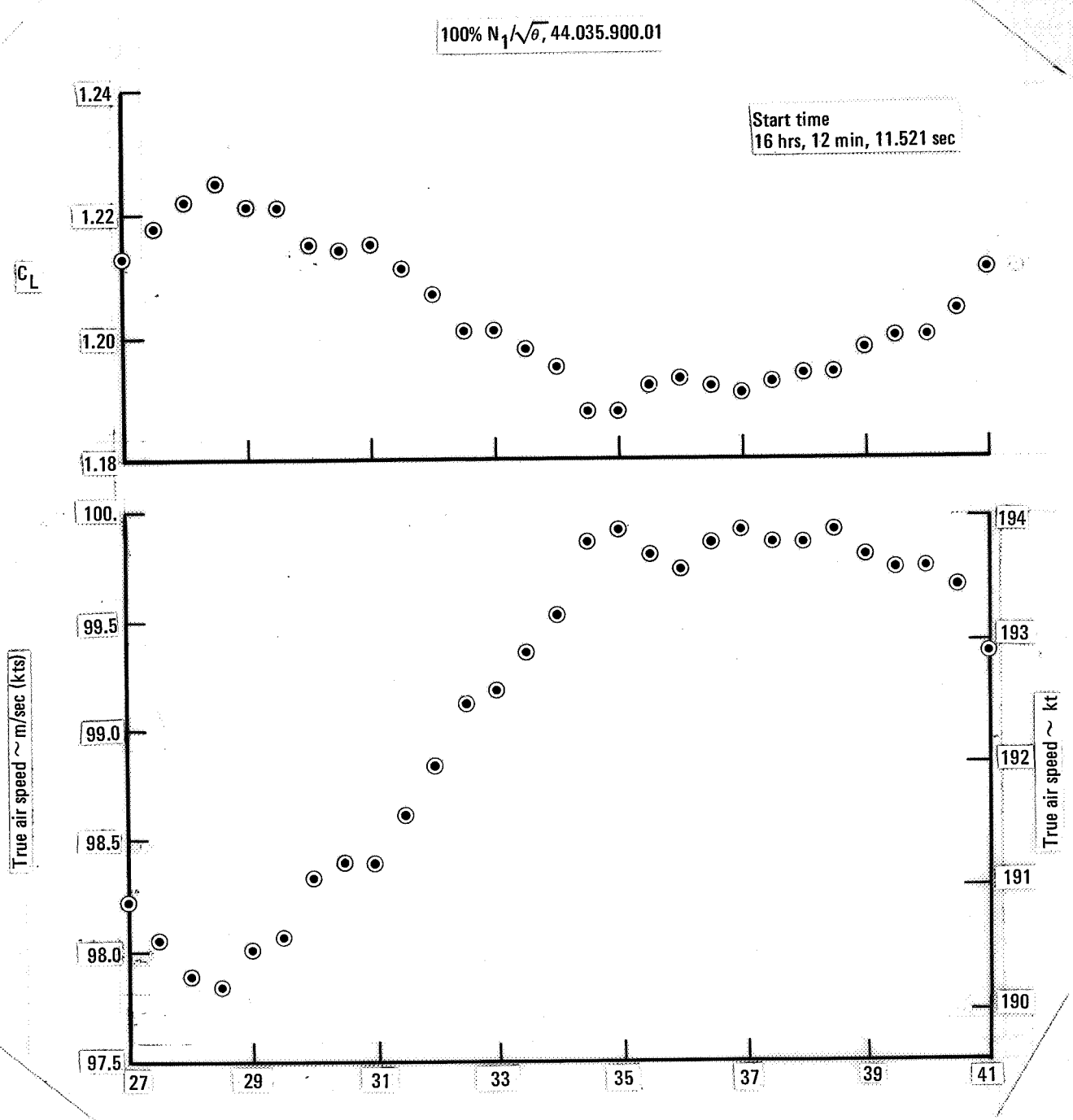

Figure 14. - Aircraft velocity and lift coefficients, condition no. 44.035.900.01.

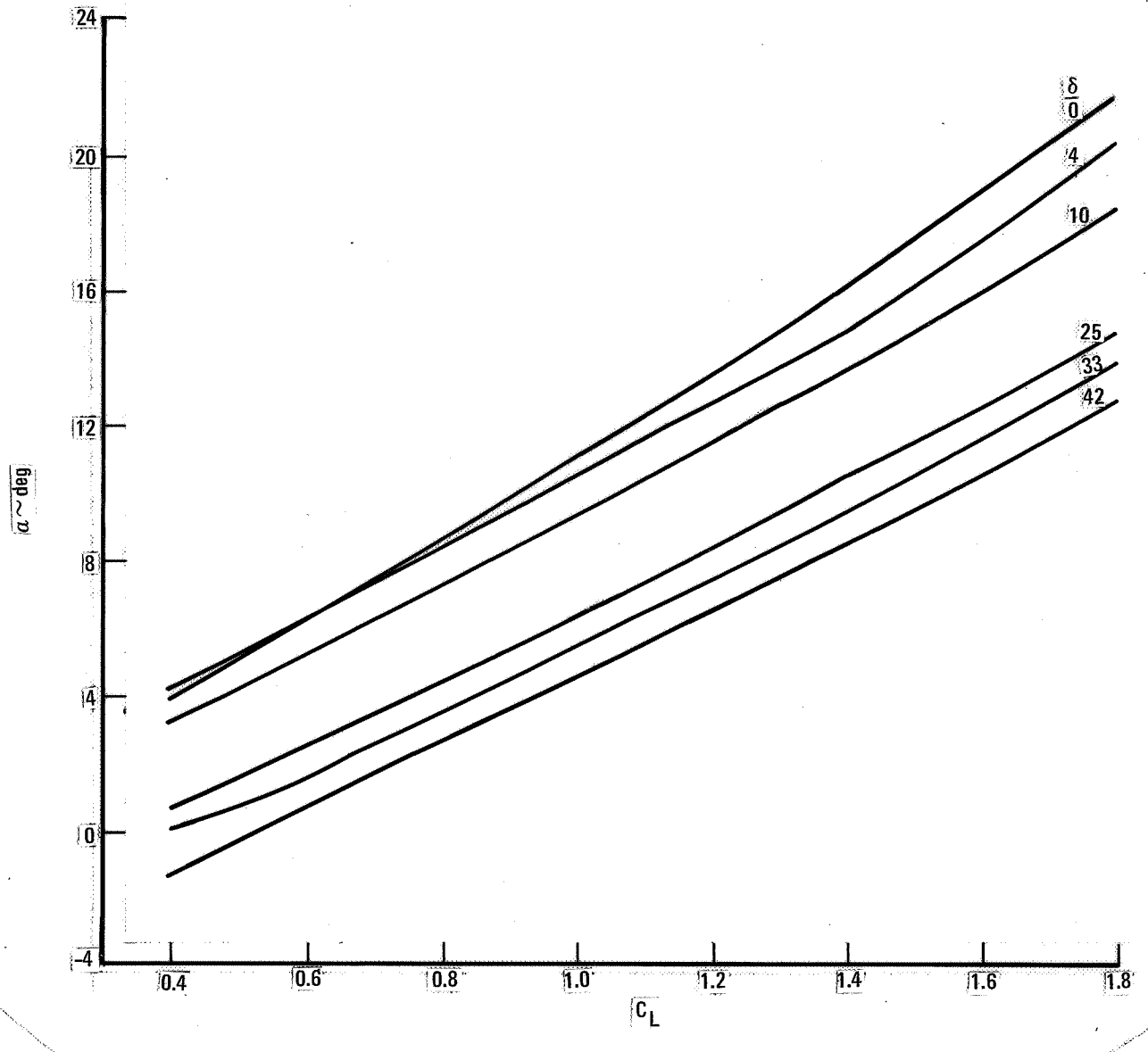

Figure 15. - Angle of attack vs lift coefficient

Average values of ROT were used in this study because it varied insignificantly during each test. ROT angles for each flight condition are given in table 11.

2.2.3 Engine operating Conditions. - Speed of the three engine rotors (N_1, N_2, and N_3), IEPR (core + bypass nozzle pressure/inlet pressure), turbine gas temperature, fan face temperature were measured throughout each test. The engines were operated in a steady state condition and engine data were averaged for each flight. Input data for the RB.211-524B engine simulation program are shown in table 12.

Results of this engine simulation showed insignificant variation in operating parameters for different engines during the same test. Therefore, the three sets of engine data were averaged to provide flow parameters for each test condition. A summary of the engine information is given in table 13.

2.2.4 Noise Measurements. - The noise data used in this study are those recorded by a microphone located as shown in figure 16 and Table 14. This microphone is on the runway extended centerline 1853 m (6080 ft) from the runway threshold. It was mounted 1.2 m (4 ft) above the ground surface

The noise measurement equipment required for data acquisition includes:

- microphone system with remote signal conditioning
- central signal conditioning, monitoring, and recording equipment
- calibration sources for frequency and amplitude.

A schematic of the system is shown in figure 17.

A 141B portable microphone system was used. This equipment conforms with applicable IEC 179 acoustical and electrical specifications for precision sound level meters when used at 90° (grazing) incidence with a one-half inch microphone. The system includes windscreen, pre-emphasis filter (per FAR Part 36, A36.2), cable-loss compensation, and support tripod. The system is connected to a central acoustics van via 200-ohm balanced, twisted, and shielded line.

The central recording system includes a 14-channel FM tape recorder with low-level, differential inputs, oscilloscope monitoring, and Lockheed attenuators. The lines are terminated in the van and the signals are attenuated as required for the low-level tape recorder inputs. Data signals are monitored at the record input and playback output for waveform. Acoustical monitoring is done on simultaneous playback with an amplifier/speaker unit. One-third octave spectrum monitoring is accomplished with a 3347 Real-Time Analyzer. Synchronizer IRIG B time code is recorded on a direct mode channel of the tape recorder.

TABLE 11. - ENGINE AXIS ORIENTATION

Condition No.	δ deg	C_L	α deg	γ deg	ROT* deg
44.036.300.08	4	1.113	11.6	0.	14.6
44.034.011.15	42	1.492	9.4	-3.0	9.4
44.036.300.04	27	1.261	8.6	0.	11.6
44.034.300.08	33	1.103	6.4	0.	9.4
44.034.300.04	33	1.131	6.7	0.	9.7
44.035.900.01	10	1.200	11.5	8.2	22.7

*ϵ = 3 deg

During noise measurements the microphone was set to measure grazing incidence noise. It was calibrated before and after each test. The noise data were recorded on magnetic tape at 30 ips in a wideband FM mode. Ambient noise measurements were made immediately preceeding each flight.

The calibration equipment consists of a pistonphone and microphone calibration apparatus. The pistonphone establishes the amplitude sensitivity of the system at a single frequence (250 Hz) in the field before and after each test series. The calibration apparatus uses an electrostatic actuator to determine system frequency response.

The system electrical response is determined by a pink noise insert voltage calibration in the field. An 8057A precision noise generator is used in conjunction with an 15124A insert voltage adaptor prior to and after recording the aircraft flyover noise.

The dynamic range of the system is optimized by:

- vernier setting of remote preamplifier gain
- use of the pre-emphasis filter on recording (with de-emphasis on playback or analysis).

The system one-third octave band signal-to-noise ratios vary from 60 to 70 dB (with reference to the sine clipping level) plus that achieved with the use of pre-emphasis.

TABLE 12. - L-1011-524 FLYOVER ENGINE DATA

Condition Number	Nominal $N_1/\sqrt{\theta}$ (%)	Tower		Aircraft		Total Air Temp.	Mach #	Engine Pressure Ratio		
		T_s C^o (F^o)	PN/m2 (lb/ft^2)	T_s C^o (F^o)	PN/m^2 (lb/ft^2)	T_s C^o (F^o)		Engine # 1	Engine # 2	Engine # 3
44.036.300.08	60	15.3 (59.6)	9.346×10^4 (1938.5)	13.2 (55.8)	9.213×10^4 (1910.8)	16.8 (62.2)	.250	1.135	1.131	1.133
44.034.011.15	66	14.7 (58.4)	9.346×10^4 (1937.1)	13.4 (56.1)	9.203×10^4 (1908.8)	16.2 (61.2)	.220	1.173	1.187	1.194
44.036.300.04	70	14.5 (58.1)	9.346×10^4 (1938.5)	12.4 (54.4)	9.211×10^4 (1910.6)	15.9 (60.6)	.246	1.216	1.214	1.216
44.034.300.08	80	14.2 (57.5)	9.339×10^4 (1937.1)	9.9 (49.8)	8.931×10^4 (1852.4)	14.6 (58.3)	.287	1.321	1.310	1.318
44.034.300.04	90	13.6 (56.5)	9.339×10^4 (1937.1)	9.4 (48.9)	8.923×10^4 (1850.7)	14.6 (57.2)	.285	1.472	1.458	1.463
44.035.900.01	100	9.5 (49.1)	9.288×10^4 (1926.5)	7.9 (46.3)	8.959×10^4 (1858.2)	12.9 (55.2)	.297	1.663	1.645	1.673

TABLE 13. - RB.211-524B - AVERAGE ENGINE OPERATING PARAMETERS

Condition Number	44.036. 300.08.	44.034. 011.05	44.036. 300.04
$N_1/\sqrt{\theta}$ $N_2/\sqrt{\theta}$ $N_3/\sqrt{\theta}$	60 83 77	66 87 80	70 86 81
Primary Jet			
Area m^2 (ft^2)	0.587 (6.32)	0.591 (6.36)	0.592 (6.37)
Density kg/m3 (lb/ft^3) x 10^{-4}	157.0 (9.804)	154.2 (9.629)	150.0 (9.366)
Temperature ^oK (^oR)	646.1 (1162.9)	661.9 (1191.4)	670.5 (1206.9)
Velocity m/s (ft/sec)	183.2 (601.0)	211.6 (694.3)	231.5 (759.5)
Secondary Jet			
Area m^2 (ft^2)	1.571 (16.91)	1.573 (16.93)	1.571 (16.91)
Density kg/m^3 (lb/ft^3) x 10^{-3}	34.07 (2.127)	33.93 (2.118)	34.01 (2.123)
Temperature ^oK (^oR)	306.6 (551.8)	310.6 (559.0)	313.1 (563.5)
Velocity m/s (ft/sec)	176.6 (579.4)	192.9 (632.7)	207.7 (681.4)
Fan			
Temperature rise ^oK (^oR)	15.80 (28.44)	20.36 (36.64)	23.13 (41.63)
Mass flow kg/s (lb/sec)	11.252 (24.807)	12.363 (27.256)	13.370 (29.475)
Angular speed rev/sec	37.27	41.49	44.06
Combustor			
Mass flow kg/s (lb/sec)	1.369 (3.018)	1.564 (3.449)	1.708 (3.766)
Inlet pressure n/m^2 (lb/ft) x 10^4	104.8 (2.188)	127.9 (2.567)	136.2 (2.844)
Inlet temperature ^oK (^oR)	644.8 (1160.6)	670.1 (1206.2)	684.4 (1232.0)
Exit temperature ^oK (^oR)	1134.8 (2042.6)	1194.7 (2150.4)	1229.8 (2213.7)
Low Speed Turbine			
Local speed of sound m/s (ft/sec)	504.1 (1654.)	510.2 (1674.)	513.6 (1685.)
Mass flow kg/s (lb/sec)	1.690 (3.725)	1.929 (4.252)	2.055 (4.531)
Relative tip speed m/s (ft/sec)	235.9 (774)	255.1 (837)	283.8 (931)

TABLE 13. - Concluded.

Condition Number	44.036. 300.08.	44.034. 011.05	44.036. 300.04
$N_1/\sqrt{\theta}$ $N_2/\sqrt{\theta}$ $N_3/\sqrt{\theta}$	80 89 83	90 94 87	100 98 90
Primary Jet			
Area m^2 (ft^2)	0.598 (6.44)	0.610 (6.57)	0.628 (6.76)
Density kg/m3 (lb/ft^3) x 10^{-4}	145.2 (9.066)	139.5 (8.710)	137.5 (8.269)
Temperature ^oK (^oR)	698.9 (1258.1)	745.2 (1341.4)	705.4 (1469.7)
Velocity m/s (ft/sec)	290.8 (953.9)	360.8 (1183.6)	450.3 (1477.4)
Secondary Jet			
Area m^2 (ft^2)	1.568 (16.88)	1.566 (16.86)	1.566 (16.86)
Density kg/m3 (lb/ft^3) x 10^{-3}	33.09 (2.066)	33.0 (2.060)	33.09 (2.066)
Temperature ^oK (^oR)	320.3 (576.5)	329.8 (593.6)	341.7 (615.1)
Velocity m/s (ft/sec)	244.2 (801.3)	278.8 (914.7)	317.5 (1041.5)
Fan			
Temperature rise ^oK (^oR)	31.62 (56.91)	42.41 (75.98)	55.3 (99.54)
Mass flow kg/sec (lb/sec)	15.363 (33.870)	17.734 (39.097)	20.470 (45.130)
Angular speed rev/sec	51.19	58.17	65.12
Combustor			
Mass flow kg/sec (lb/sec)	2.048 (4.514)	2.487 (5.482)	3.025 (6.668)
Inlet pressure N/m^2 (lb/ft^2) x 10^4	169.7 (3.544)	215.6 (4.504)	275.7 (5.758)
Inlet temperature ^oK (^oR)	723.3 (1301.9)	768.3 (1384.7)	823.6 (1482.4)
Exit temperature ^oK (^oR)	716.5 (1289.7)	1450.8 (2611.5)	1612.6 (2902.7)
Low Speed Turbine			
Local speed of sound m/s (ft/sec)	524.3 (1720.)	541.3 (1776.)	565.8 (1859.)
Mass flow kg/s (lb/sec)	2.526 (5.569)	3.072 (6.773)	3.746 (8.258)
Relative tip speed m/s (ft/sec)	382.8 (1256)	428.9 (1407)	520.3 (1707)

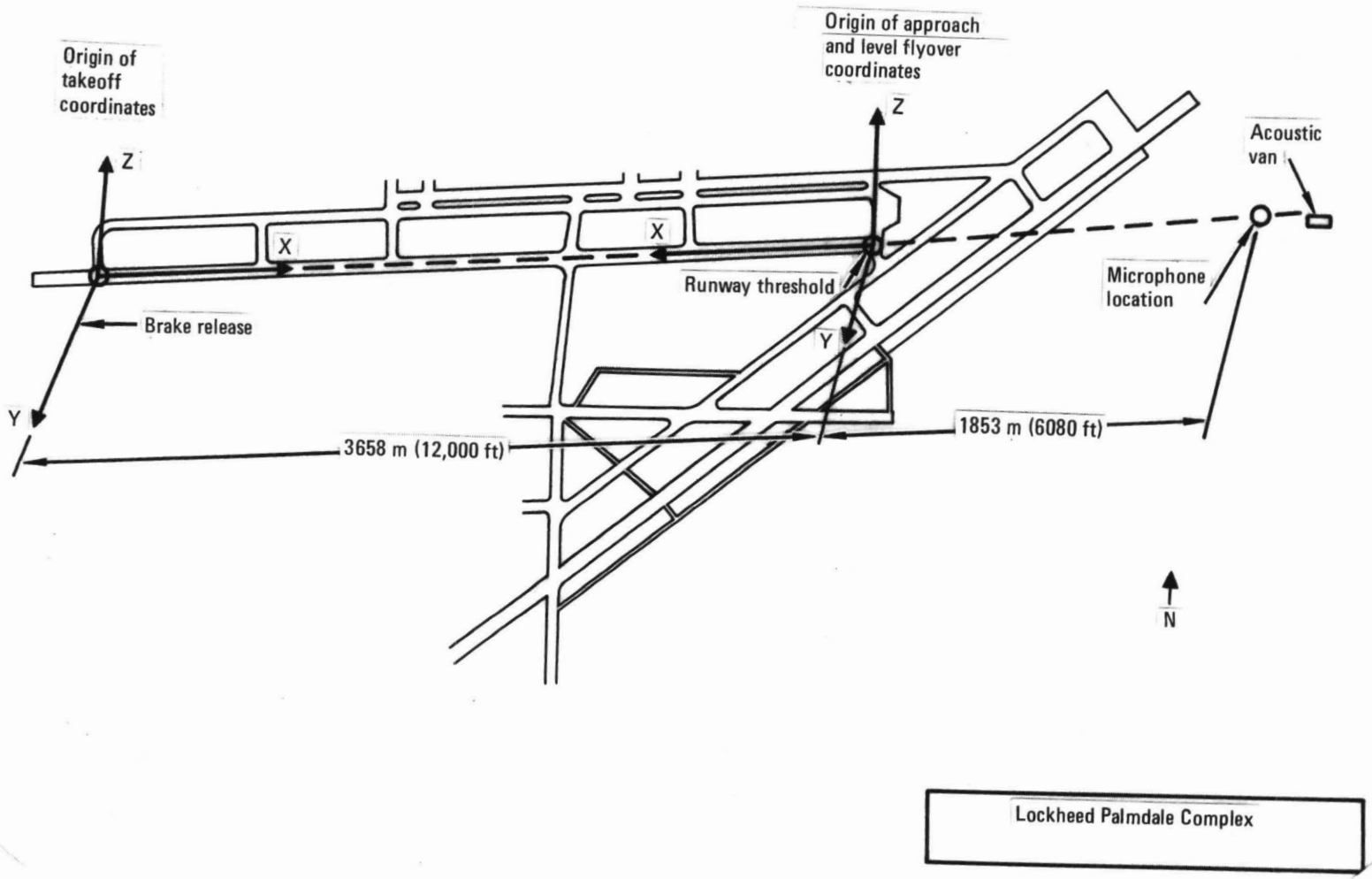

Figure 16. - Microphone location.

TABLE 14. - OBSERVER LOCATIONS

Condition No.	X m (ft)	Z m (ft)	Y m (ft)
44.036.300.08	-1853.(-6080.)	-13.4 (-44.)	0.
44.034.011.15	-1853.(-6080.)	- .61(- 2.)	0.
44.036.300.04	-1853.(-6080.)	-13.4 (-44.)	0.
44.034.300.08	-1853.(-6080.)	-13.4 (-44.)	0.
44.034.300.04	-1853.(-6080.)	-13.4 (-44.)	0.
44.035.900.01	5486.(18000.)	-13.4 (-44.)	0.

Spectral data are obtained by data reduction of the analog flight tape at a 0.1 second sampling rate and a 0.5 second averaging interval. Considering the change of θ with respect to time during the flyover and the smoothness of the third-octave sound pressure levels, it is felt that this fast sampling rate and averaging time provide a better quality noise data base.

3. ANOPP VALIDATION

Procedures used for making ANOPP predictions, establishing the noise data base, and comparing predicted levels with test data are discussed here.

3.1 Program Requirements

3.1.1 Computer Facility. - The noise predictions are made by accessing the ANOPP computer program that is stored on a NASA CYBER 175 computer located at Langley Research Center in Hampton, Virginia. Lockheed access to the ANOPP program is through a special account provided by NASA. Input/output with the NASA CYBER is via a phone line from Burbank, California to Hampton. Transmission is at 4800 baud through a 208B modem. Computer facilities located at Lockheed include a 200 UT terminal station with card reader, 300-lines-per-minute printer, and a tape unit.

3.1.2 Functional Modules. - ANOPP functional modules and component noise source or source propagation procedures used in this validation effort are shown in table 15. These procedures are described in reference 3.

A special note is made concerning liner attenuation of the RB.211-524B in ANOPP applications. Since the noise reduction from absorptive lining is a function of radiation angle and frequency, it is necessary to alter the input table to SUP1. This table is normally a function of Strouhal number and radiation angle. Strouhal number ($f \cdot D/V$) dependence is changed to frequency dependence by setting $D = 1$ and $V = 1$.

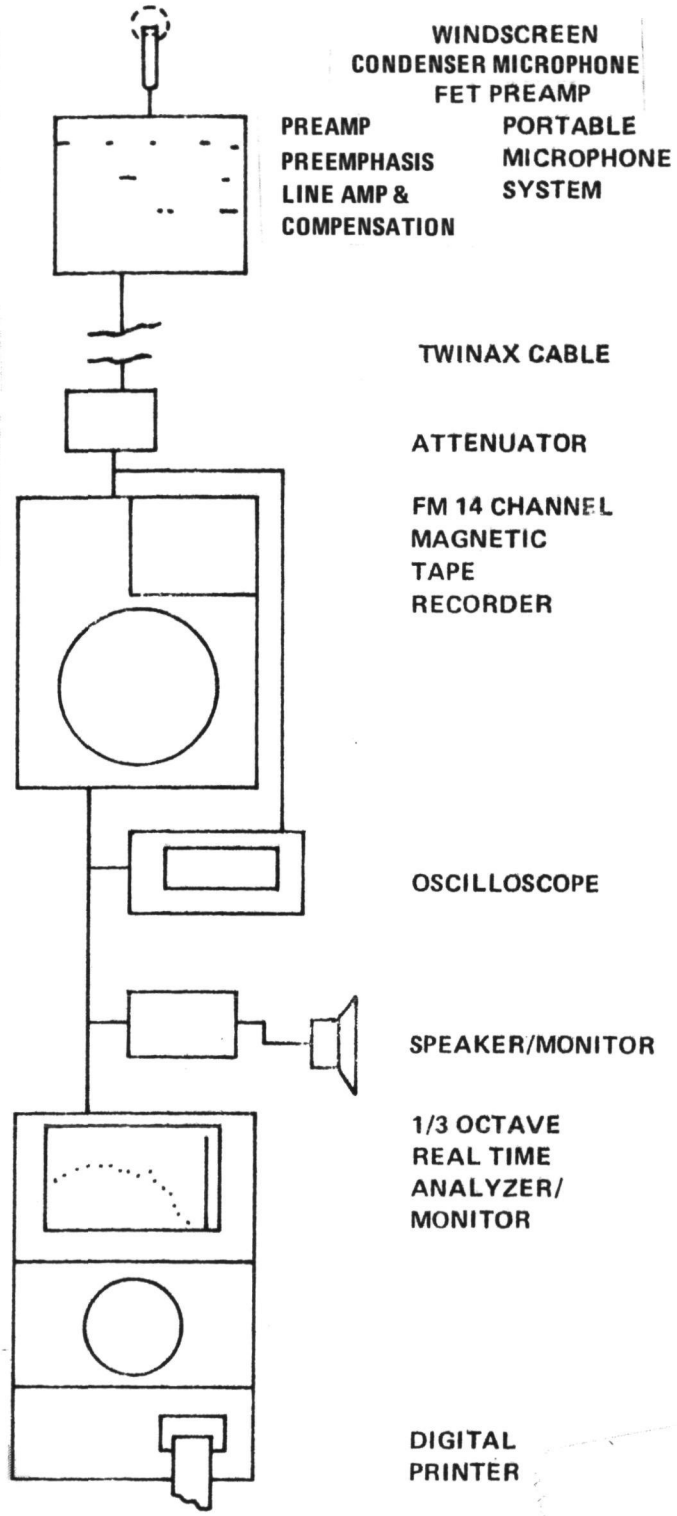

Figure 17. - Noise data acquisition equipment.

TABLE 15. - ANOPP MODULES EXECUTED

Module	Function
AFM	Airframe noise
ASP	Sound pressure level at observer
ATMD	Atmospheric model data
ATT	Propagation effects
COR	Core noise
FAN	Fan noise
JRSJET	Jet mixing noise
SRI	Tone perceived noise level time history
SUM	Sum noise sources
SUP1	Suppress source noise
TDG	Observer to aircraft coordinate transform
TDV	Time dependent aircraft parameter input
TUR	Turbine noise

3.1.3 Run deck description. - Organization of the typical ANOPP run deck is shown in figure 18. Input data were formulated from aircraft parameters and test results shown earlier. When aircraft parameters varied slightly with time, average values were computed over the duration of the test. If a parameter varied significantly with time, then it was input as a time-dependent variable. Table 16 represents the input data used to simulate the six test conditions with ANOPP.

Noise predictions were made from θ equals 30 to 150 degrees in 10 degree increments to minimize the number of jobs run. Results presented in this study include PNLT versus θ from 30 to 150 degrees and SPL third-octave band spectra at θ equals 30, 60, 90, 120, and 150 degrees.

3.2 Aircraft Noise Predictions and Measured Data

To compare aircraft noise, predicted versus measured, ANOPP was executed first for the required radiation angles. Then, based on the retarded times output at the microphone location, a list of time correlated to θ can be made for each test. With these time data, measured noise values are extracted from the reduced flight data at the same IRIG B time.

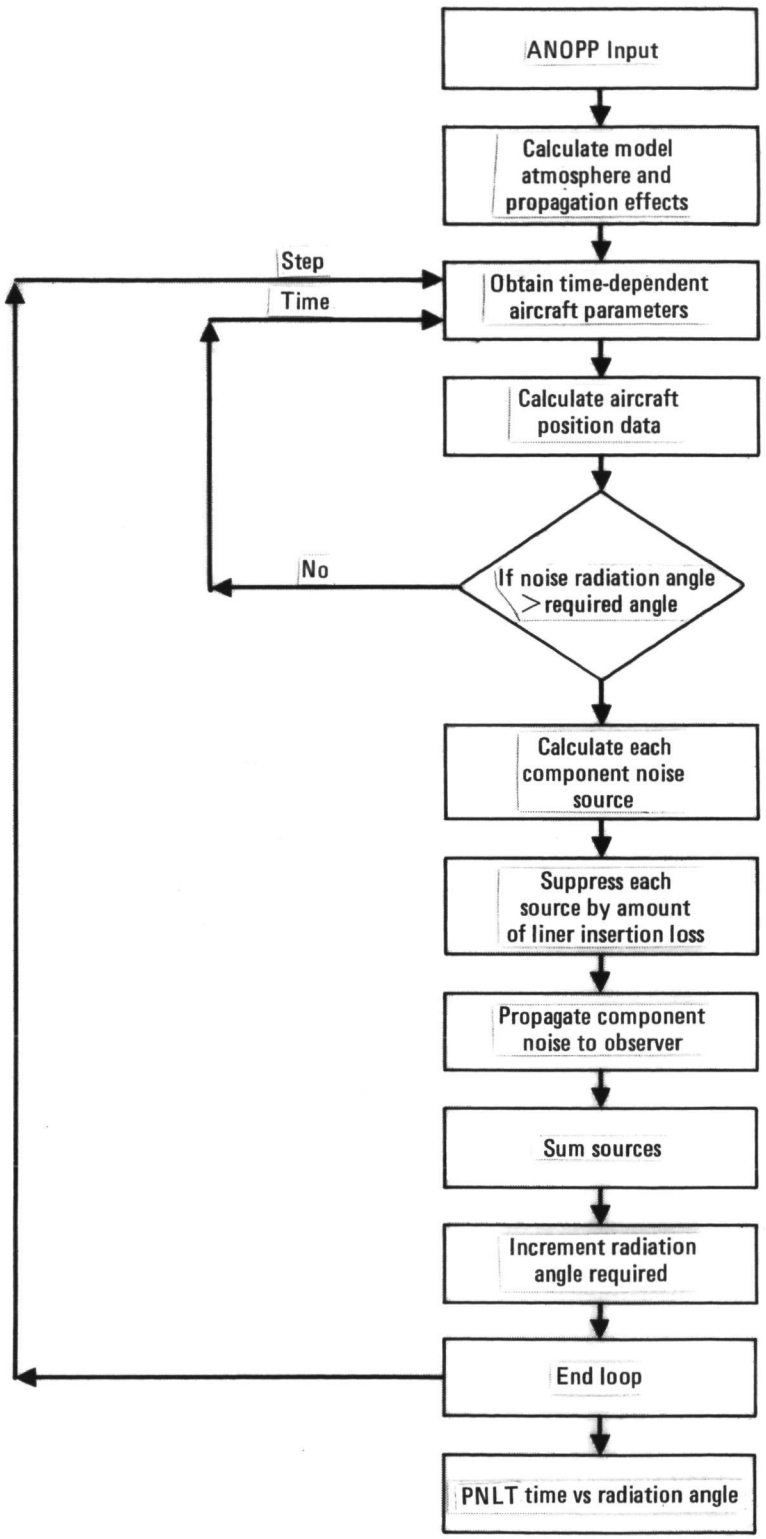

Figure 18. - ANOPP run deck schematic.

TABLE 16. - L-1011 DATA INPUT FOR ANOPP*

Airframe Noise Constants for AFM

AW	= 3456.0	AF	= 536.0	TDNG	= 3.0
BW	= 155.33	CF	= 6.5	CNG	= 2.828
AH	= 1282.0	NF	= 2.0	NNG	= 2.0
BH	= 71.58	TDMG	= 4.167	ITEFN	= 1.0
AV	= 550.0	CMG	= 2.860	ITYPW	= 1.0
BV	= 29.67	NMG	= 4.0		

Fan Noise Constants for Fan

AREA	= 29.5	IGV	= 0	RSS	= 206.0
DIAM	= 7.17	NB	= 33.0		
DM	= 1.52	NV	= 70.0		

Core Noise Constant for COR

TDDELT = 425.0

Turbine Noise Constants

NB	= 72.0	SRS	= 0.86

Observer Coordinates for OBSERV

X	Y	Z	
-6080.0	-44.0	0.0	
-6080.0	-2.0	0.0	Condition Number 44.034.011.15 Only
18000.0	-44.0	0.0	Condition Number 44.035.900.01 Only

Aircraft Performance Data for TDV and TDG

Condition Number 44.036.300.08, Start Time: 11:16:08:218 (Approach)

TA	XA	YA	ZA	VA
9.84	- 7405.0	- 9.0	308.0	278.0
16.27	- 5210.0	- 9.0	308.0	278.0

Delta = 14.6 ROT = 14.6

Condition Number 44.034.011.15 Start Time: 12:26:55.189

TA	XA	YA	ZA	VA
55.51	- 6990.0	15.0	350.0	245.0
57.16	- 6990.0	↓	336.0	↓
58.07	- 6450.0		326.0	
58.57	- 6320.0		322.0	
58.94	- 6220.0		320.0	
59.31	- 6150.0		315.0	
59.58	- 6100.0		312.0	
59.83	- 6080.0		310.0	
60.09	- 6010.0		308.0	
60.39	- 5920.0		305.0	
60.63	- 5870.0		302.0	
60.94	- 5800.0		300.0	
61.41	- 5700.0		295.0	
63.24	- 5300.0	15.0	278.0	245.0

Delta = 12.4 ROT = 9.4

Condition Number 44.036.300.04, Start Time: 9:50:00:607

TA	XA	YA	ZA	VA
3.25	- 7150.0	38.0	274.0	274.0
8.82	- 5650.0	38.0	274.0	274.0

Delta = 11.6 ROT = 11.6

Condition Number 44.034.300.08 Start Time: 9:58.00.637

TA	XA	YA	ZA	VA
0.32	- 8800.0	56.0	1123.0	314.0
18.57	- 3400.0	56.0	1123.0	314.0

Delta = 9.4 ROT = 9.4

TABLE 16. - L-1011 DATA INPUT FOR ANOPP* (Continued)

Condition Number 44.034.300.08 Start Time: 8:57:47.421

TA	XA	YA	ZA	VA
48.62	- 9400.0	5.0	1165.0	292.0
53.44	- 8050.0			300.0
59.99	- 7600.0			302.0
56.68	- 7160.0			308.0
57.95	- 6750.0			311.0
58.75	- 6570.0			312.0
59.51	- 6180.0			312.0
60.25	- 6000.0			315.0
60.97	- 5890.0			318.0
61.70	- 5780.0			319.0
62.51	- 5400.0			320.0
63.52	- 5100.0			326.0
64.88	- 4700.0			326.0
69.51	- 3400.0	5.0	1165.0	337.0

Delta = 9.7 ROT = 9.7

Condition Number 44.035.900.01 Start Time: 16:12:26.727 (Takeoff)

TA	XA	YA	ZA	VA
27.7	14900.0	-122.0	440.0	326.0
31.47	15950.0	-165.0	575.0	
33.21	16650.0	-192.0	650.0	
34.28	17040.0	-208.0	700.0	
35.13	17520.0	-220.0	727.0	
35.68	17450.0	-230.0	770.0	
36.21	17600.0	-238.0	800.0	
36.74	17800.0	-249.0	830.0	
37.31	17990.0	-255.0	860.0	
38.03	18200.0	-265.0	900.0	
38.75	18450.0	-280.0	945.0	
39.47	18700.0	-290.0	975.0	
40.19	18900.0	-300.0	1100.0	
43.56	20000.0	-353.0	1354	326.0

Delta = 14.5 ROT = 22.7

SUP 1 Input - Tables 7, 8 and 9 Section 2.1.3
ATMD 1 Input - Table 11

Run Constants

VJ = 1.0	DJ = 1.0	NENG = 3.0	R = 1.1
REFL = 1.0	PREF = 4.177×10^{-7}	RREF = 1.0	Sigma = 485.1
OH = 4.0	HO = 2500.0	POWREF = 7.3756×10^{-13}	

Condition Number	44.036.300.08	44.034.011.05	44.036.300.04	44.034.300.08	4.034.300.04	44.035.900.01
Functional Module and Variables						
JRSJET						
A1	6.32	6.36	6.37	6.44	6.57	6.76
RH01	9.804E-4	9.629E-4	9.366E-4	9.066E-4	8.710E-4	8.269E-4
T1	1162.9	1191.4	1206.9	1258.1	1341.4	1469.7
V1	601.0	694.3	759.5	953.9	1183.6	1477.4
A2	16.91	16.93	16.91	16.88	16.86	16.86
RH02	2.127E-3	2.118E-3	2.123E-3	2.066E-3	2.060E-3	2.066E-3
T2	551.8	559.0	563.5	576.5	593.6	615.1
V2	579.4	632.7	681.4	801.3	914.7	1041.5
FAN	28.44	36.64	41.63	56.91	75.98	99.54
DOTM	24.807	27.256	29.476	33.870	39.097	45.130
OMEGA	37.27	41.49	44.06	51.19	58.17	65.12
COR						
DOTM	3.018	3.449	3.766	4.514	5.482	6.668
P3	21883.0	25668.0	28441.0	35437.0	45037.0	57584.0
T3	1160.6	1206.2	1232.0	1301.9	1384.7	1482.4
T4	2042.6	2150.5	2213.7	1289.7	2611.5	2902.7
TUR						
CL	1654.0	1674.0	1685.0	1720.0	1776.0	1859.0
MA	0.250	0.220	0.246	0.287	0.286	0.296
DOTM	3.725	4.252	4.531	5.569	6.773	8.258
VTR	774.0	837.0	931.0	1256.0	1407.0	1707.0
AFM						
GAMMA	4.0	42.0	27.0	33.0	33.0	10.0
IMGN	1	0	0	0	1	0
INGN	1	0	0	0	1	0

*English Units Option

3.2.1 Perceived noise level field shapes. - Field shapes were plotted from tone corrected perceived noise levels, predicted and measured. These are shown in Figures 19 through 24 for each flight test condition. For most cases, the predicted PNLT differs from the measured with a much greater significance in the forward quadrant than the aft. In fact, the differences in the forward quadrant increase with corresponding increase in $N_1/\sqrt{\theta}$. The forward and aft quadrant differences are shown vividly in figures 25 and 26.

3.2.2 Third-octave band sound pressure level. - Plots were made from third-octave sound pressure levels, predicted and measured, at frequencies of 50 Hz to 10,000 Hz for radiation angles of approximately 30, 60, 90, 120 and 150 degrees. These comparisons are shown in figures 27 through 56 for each combination of radiation angle and test condition.

The character of the spectral differences between predicted and measured data can be divided into two categories. Under those test conditions that have $N_1/\sqrt{\theta}$ equal to 70% or less spectral differences are greatest at frequencies 100 Hz to 200 Hz, and 1,600 to 10,000 Hz. For the other test conditions, $N_1/\sqrt{\theta}$ greater than 70%, the largest differences occur in the range of frequencies from 500 Hz through 3,150 Hz. In both categories, the predicted spectra are generally higher than measured.

4. COMPONENT ANALYSIS AND VALIDATION

This section deals with the separation of the total flyover noise into source components and subsequent correction of predicted noise levels to measured values.

4.1 Source Separation of Predicted Data

4.1.1 Perceived Noise Levels. - Field shapes were made from tone corrected perceived noise levels output from ANOPP for fan, jet, turbine, core and airframe noise sources for radiation angles from 30 to 150 degrees. These are shown in Figures 57 through 62, It is apparent that the major noise source components are fan and core as shown in table 17.

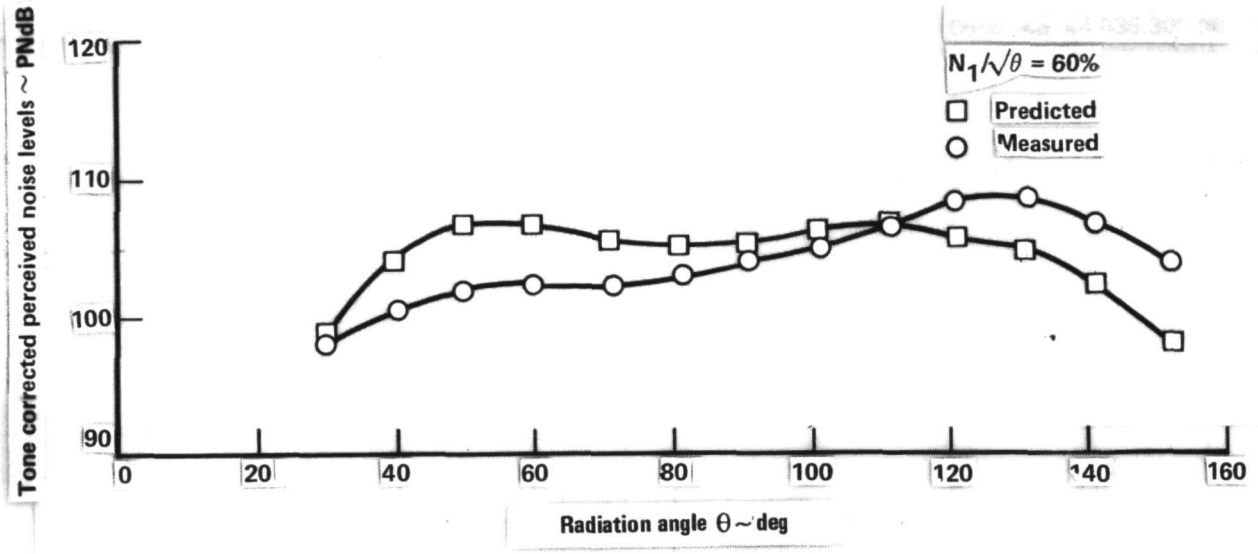

Figure 19. - Field shape comparison, condition no. 44.036.300.08

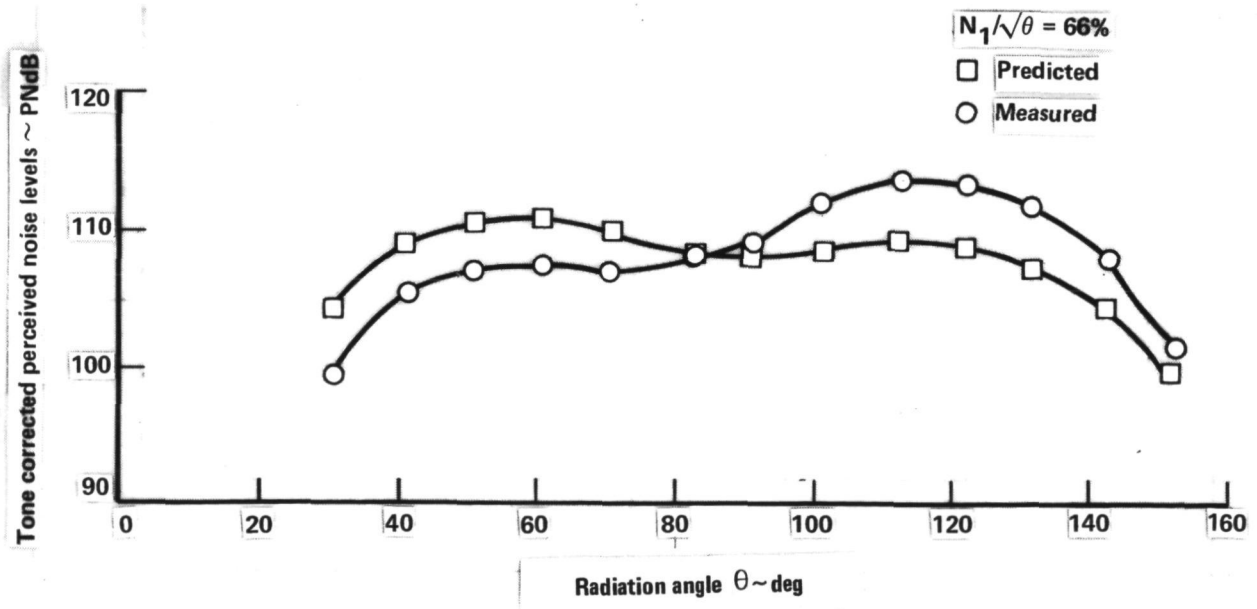

Figure 20. - Field shape comparison, condition no. 44.034.011.15

Preceding Page Blank

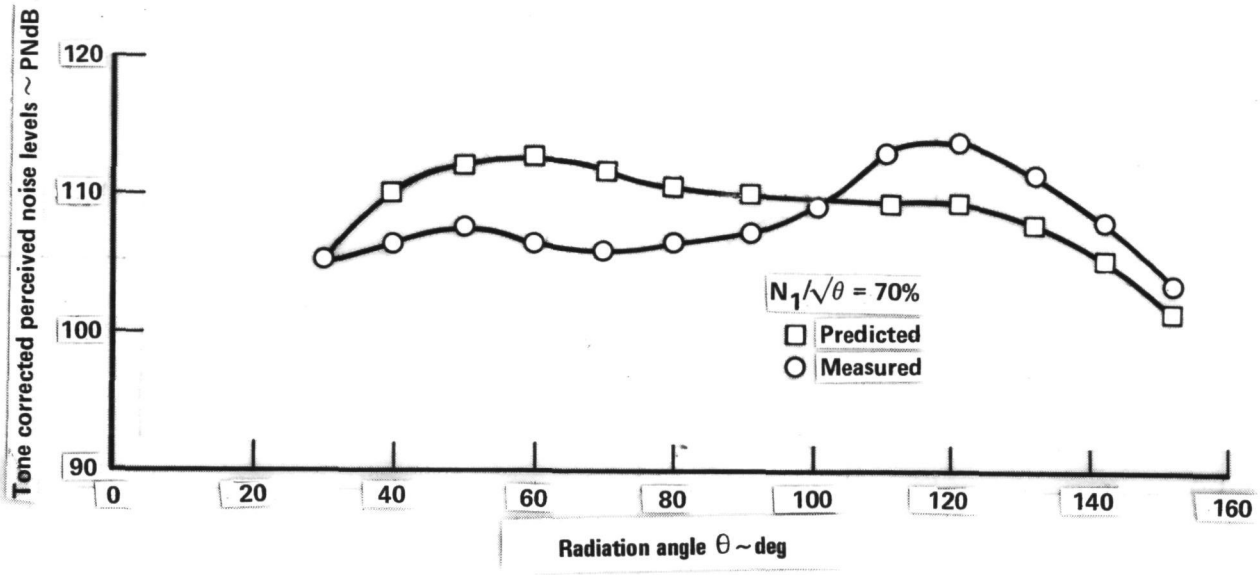

Figure 21. - Field shape comparison, condition no. 44.036.300.04

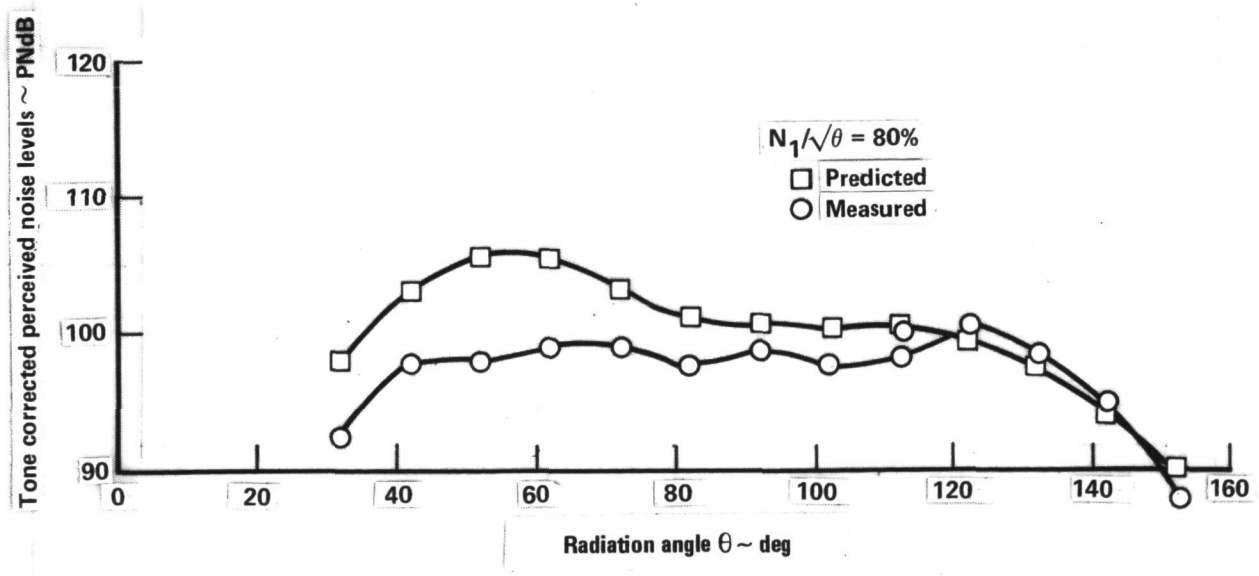

Figure 22. - Field shape comparison, condition no. 44.034.300.08

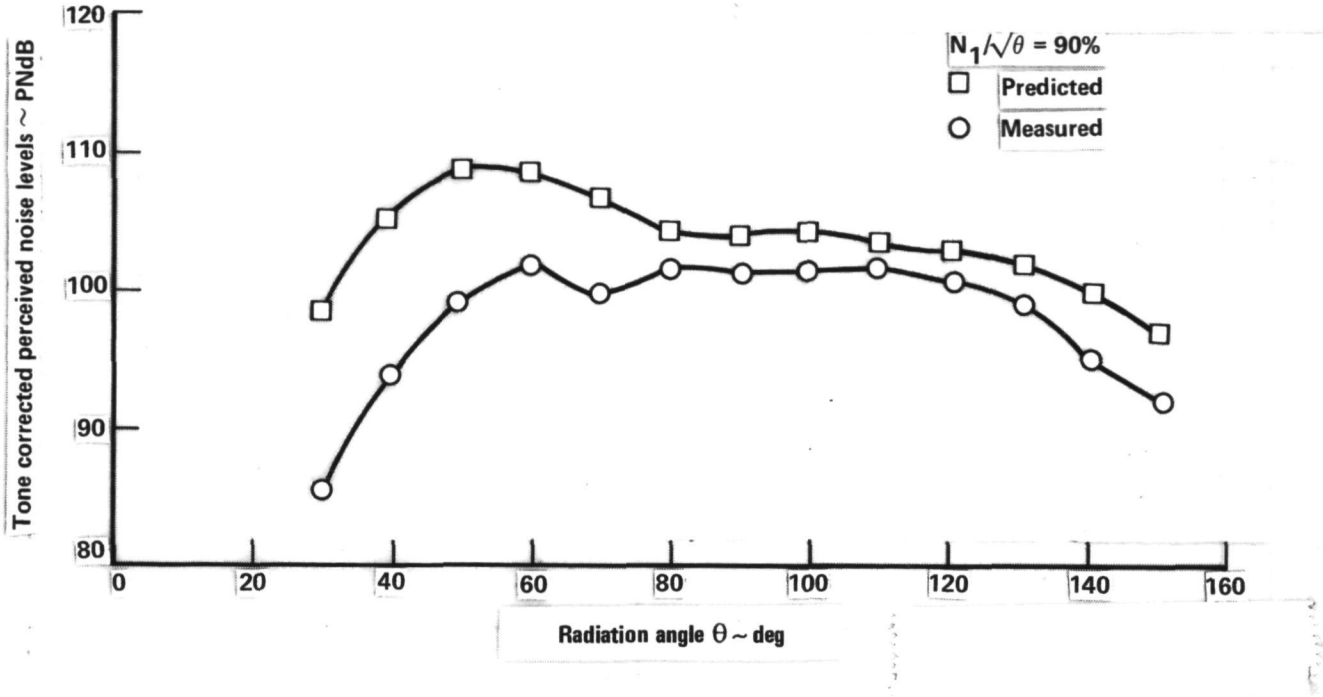

Figure 23. - Field shape comparison, condition no. 44.034.300.04

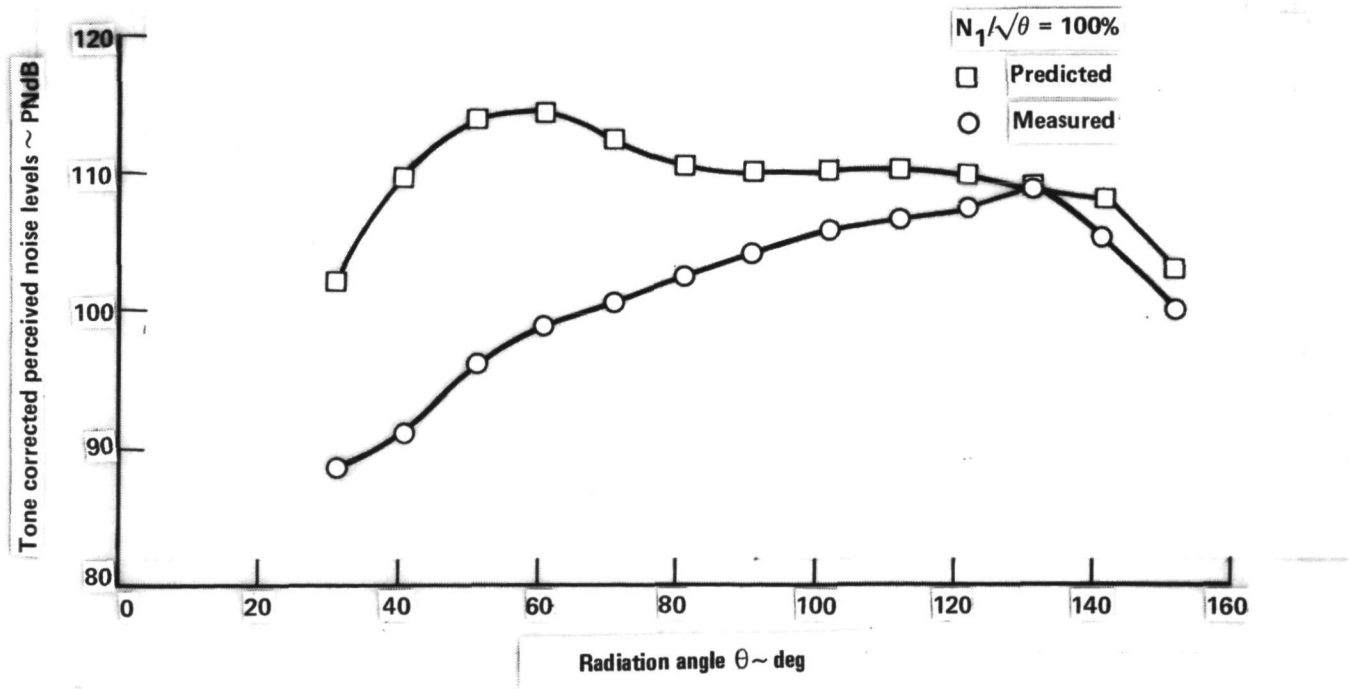

Figure 24. - Field shape comparison, condition no. 44.035.900.01

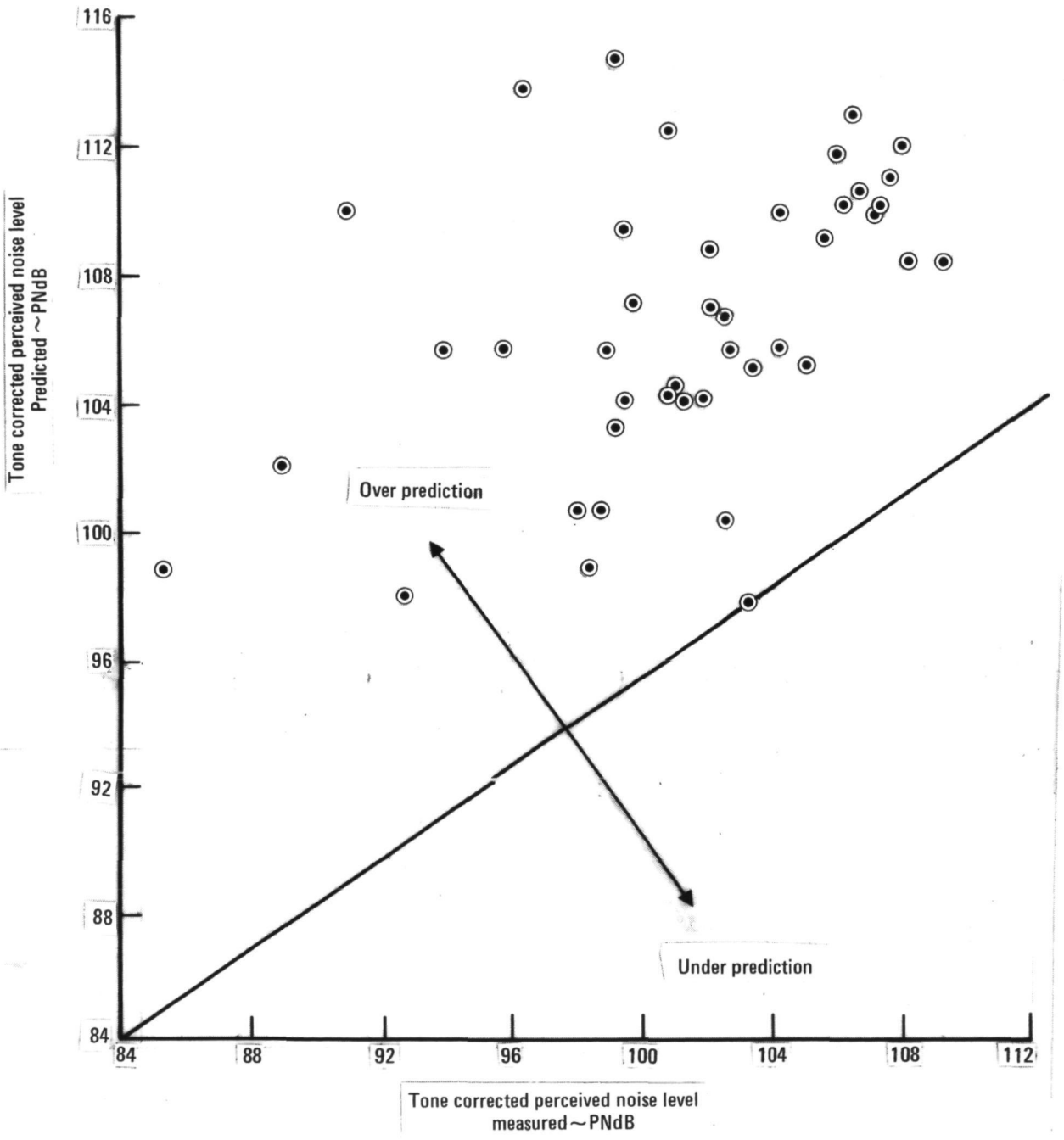

Figure 25. - Noise comparison, forward quadrant ($\theta = 30^{o}$ to 90^{o})

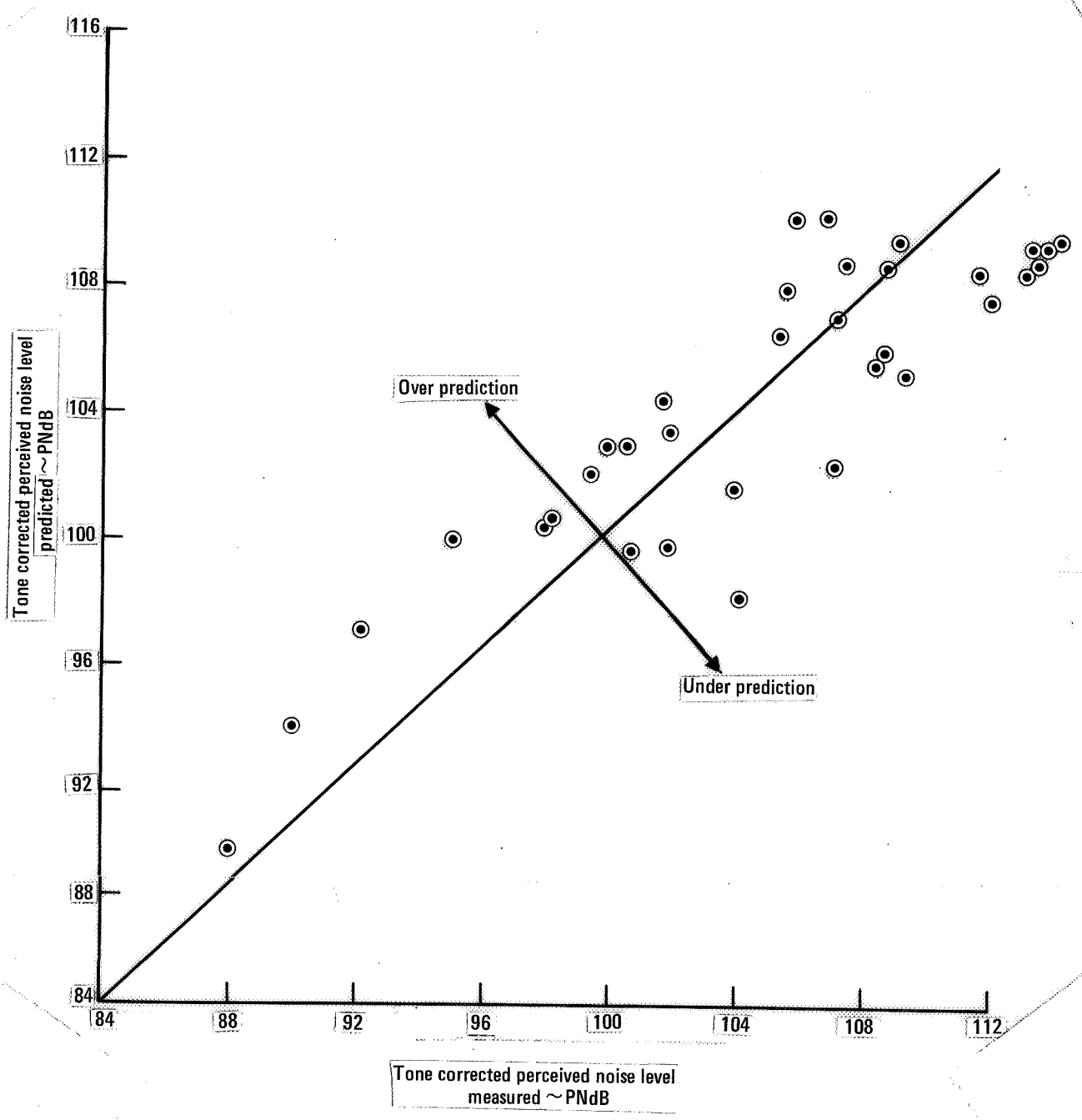

Figure 26. - Noise comparison, aft quadrant (θ = 100 to 150°)

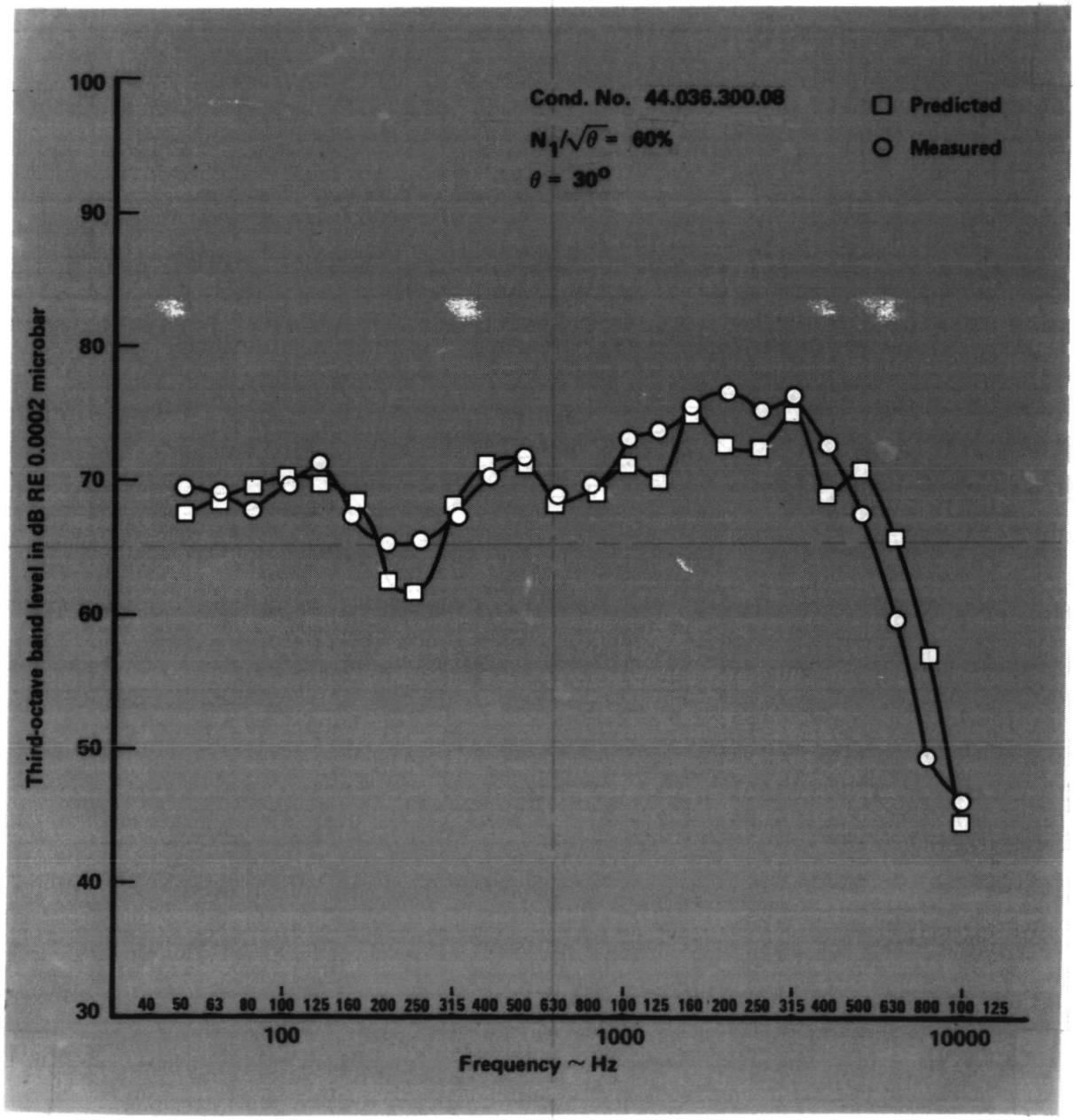

Figure 27. – Comparison of component spectra, condition no. 44.036.300.08, $\theta = 30^{\circ}$.

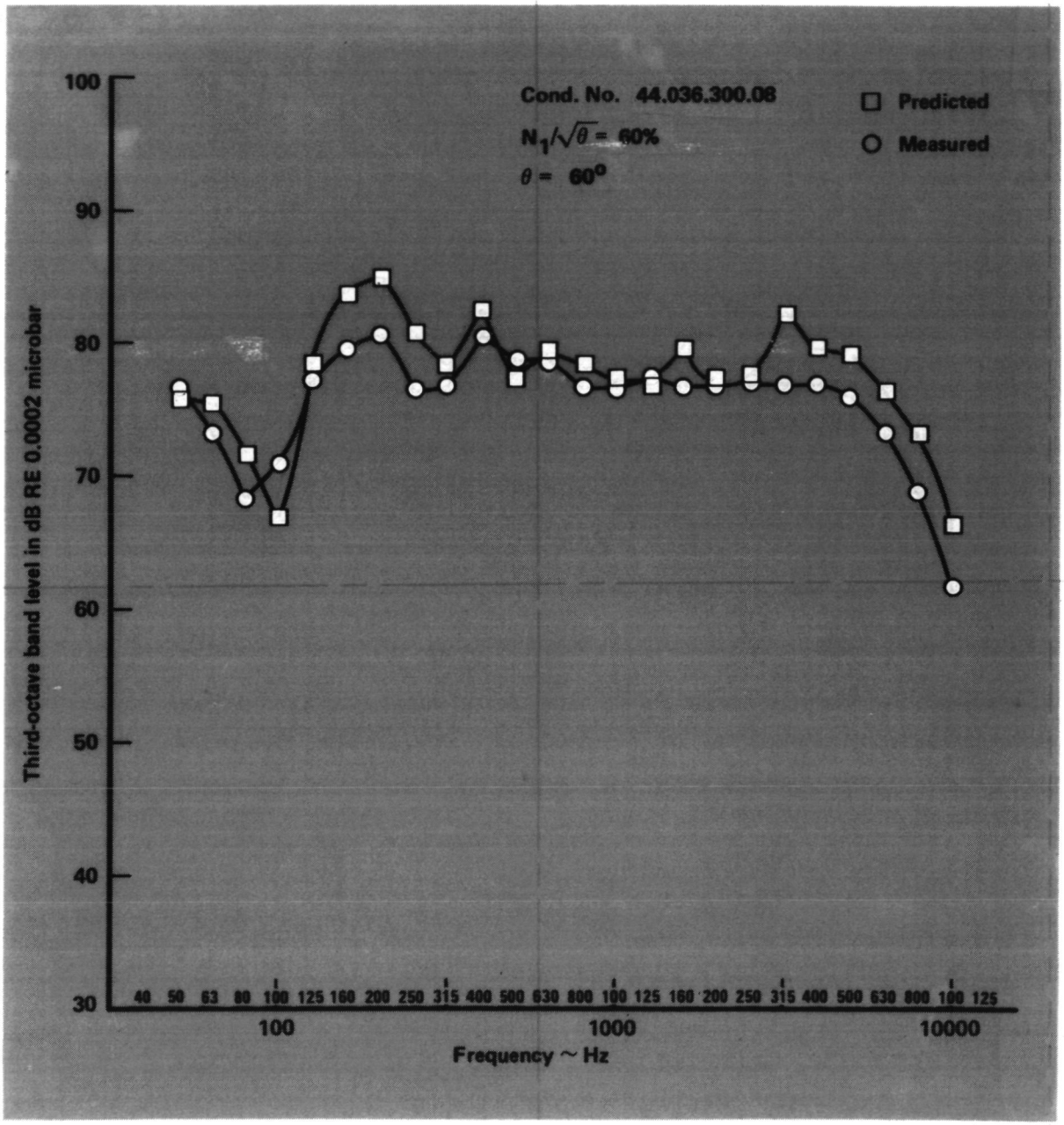

Figure 28. - Comparison of component spectra, condition no. 44.036.300.08, $\theta = 60^{\circ}$.

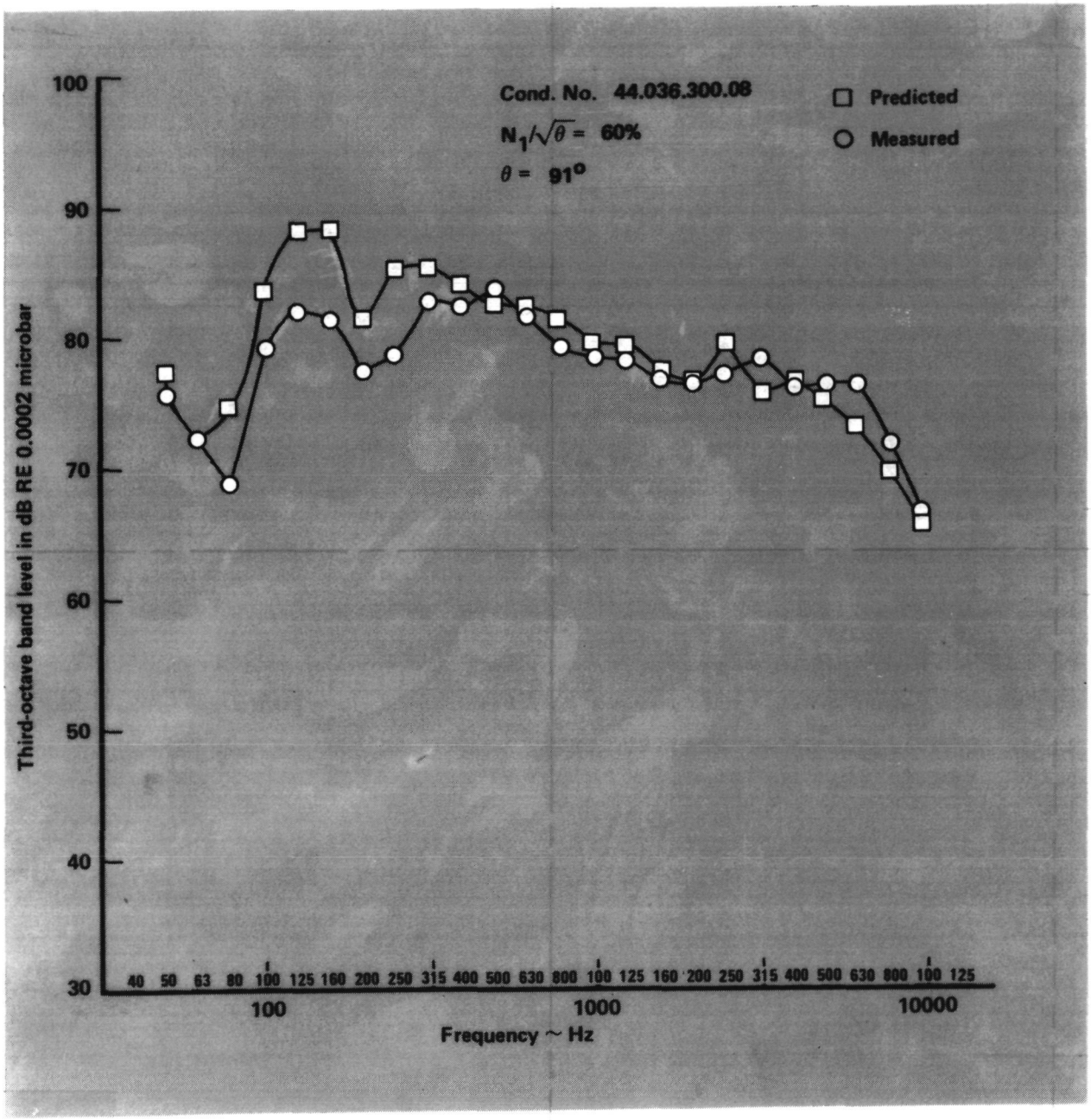

Figure 29. - Comparison of component spectra, condition no. 44.036.300.08, $\theta = 91^{\circ}$.

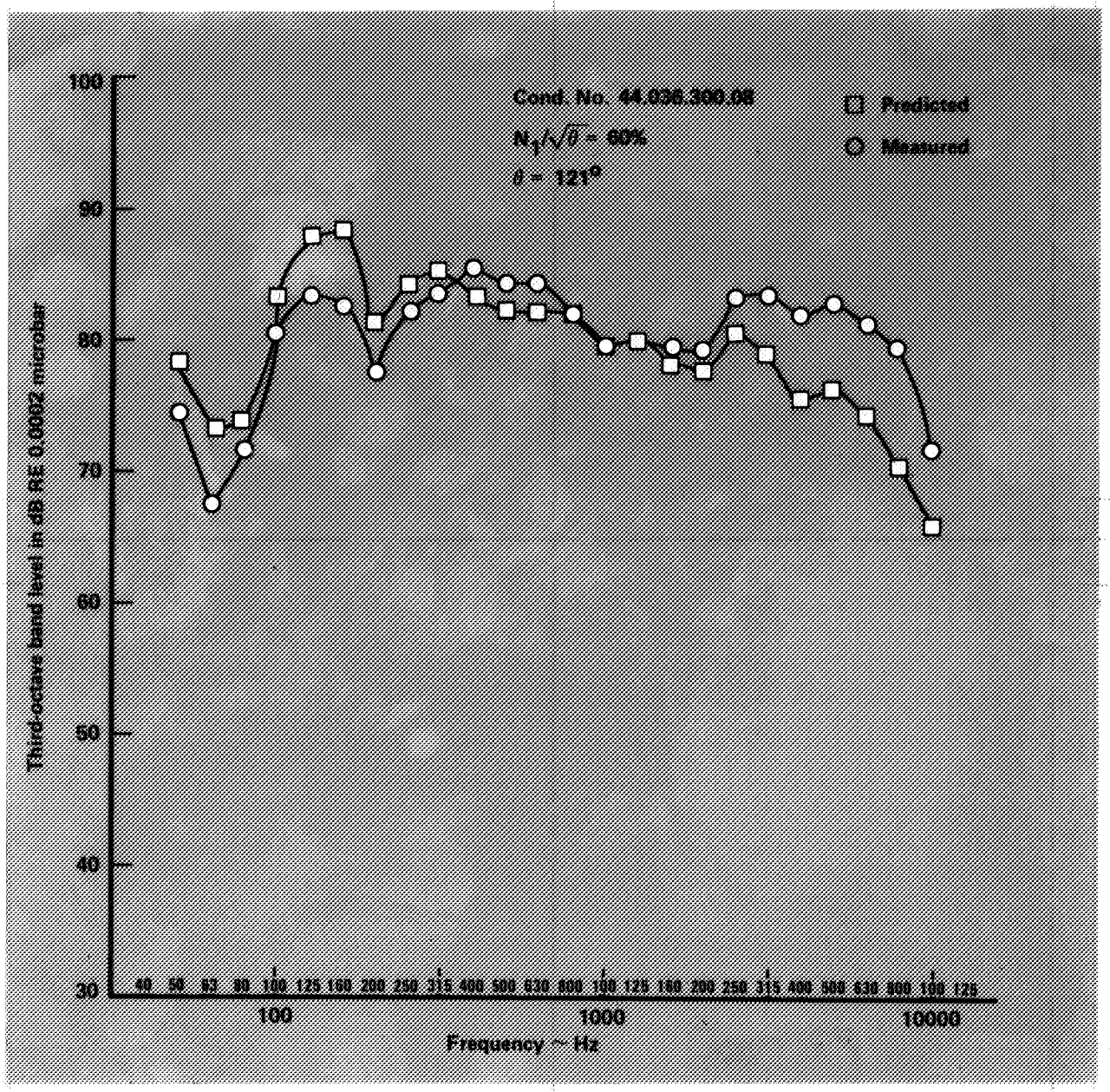

Figure 30. - Comparison of component spectra, condition no. 44.036.300.08, $\theta = 121^{\circ}$.

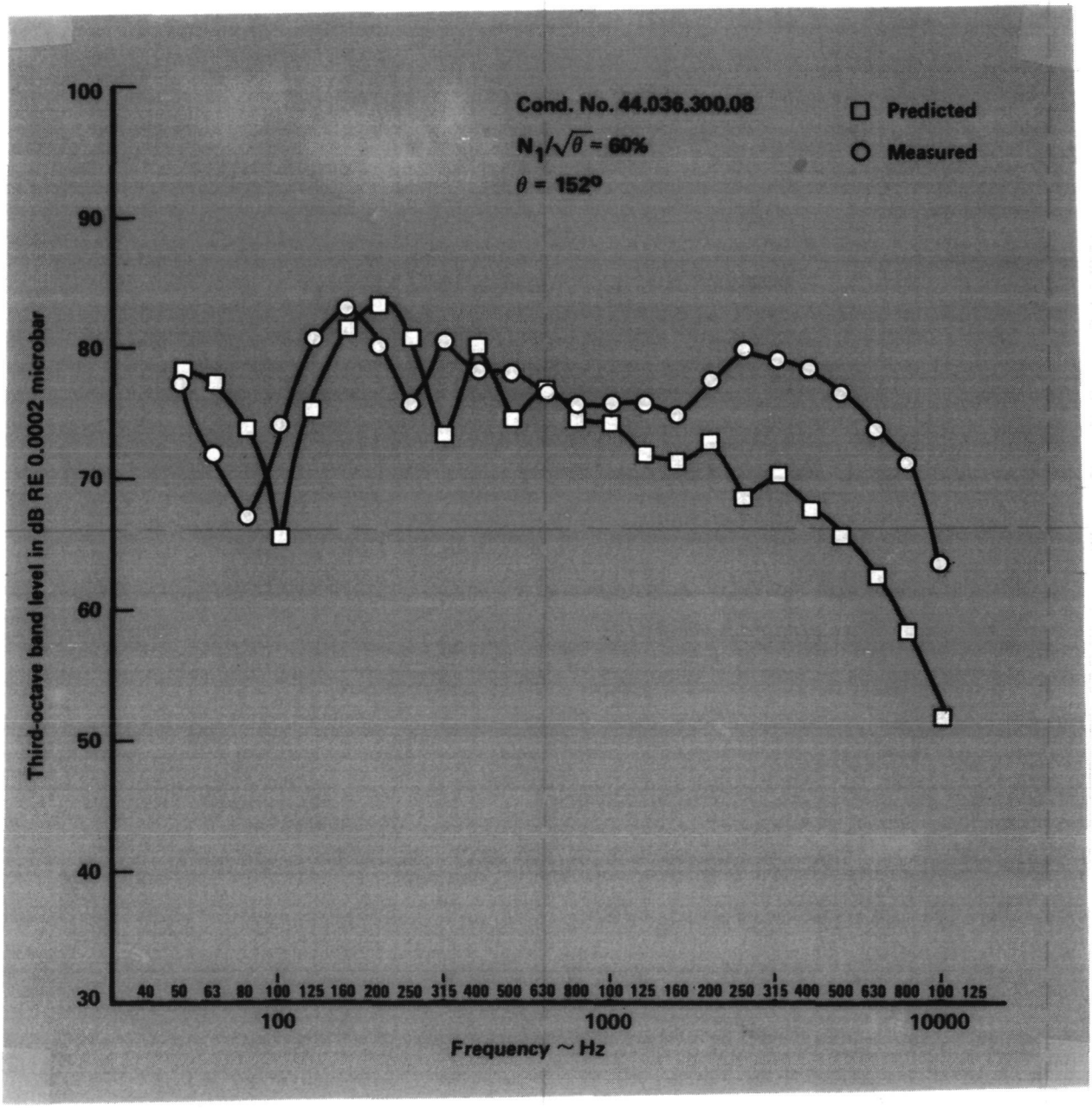

Figure 31. - Comparison of component spectra, condition no. 44.036.300.08, $\theta = 152^{\circ}$.

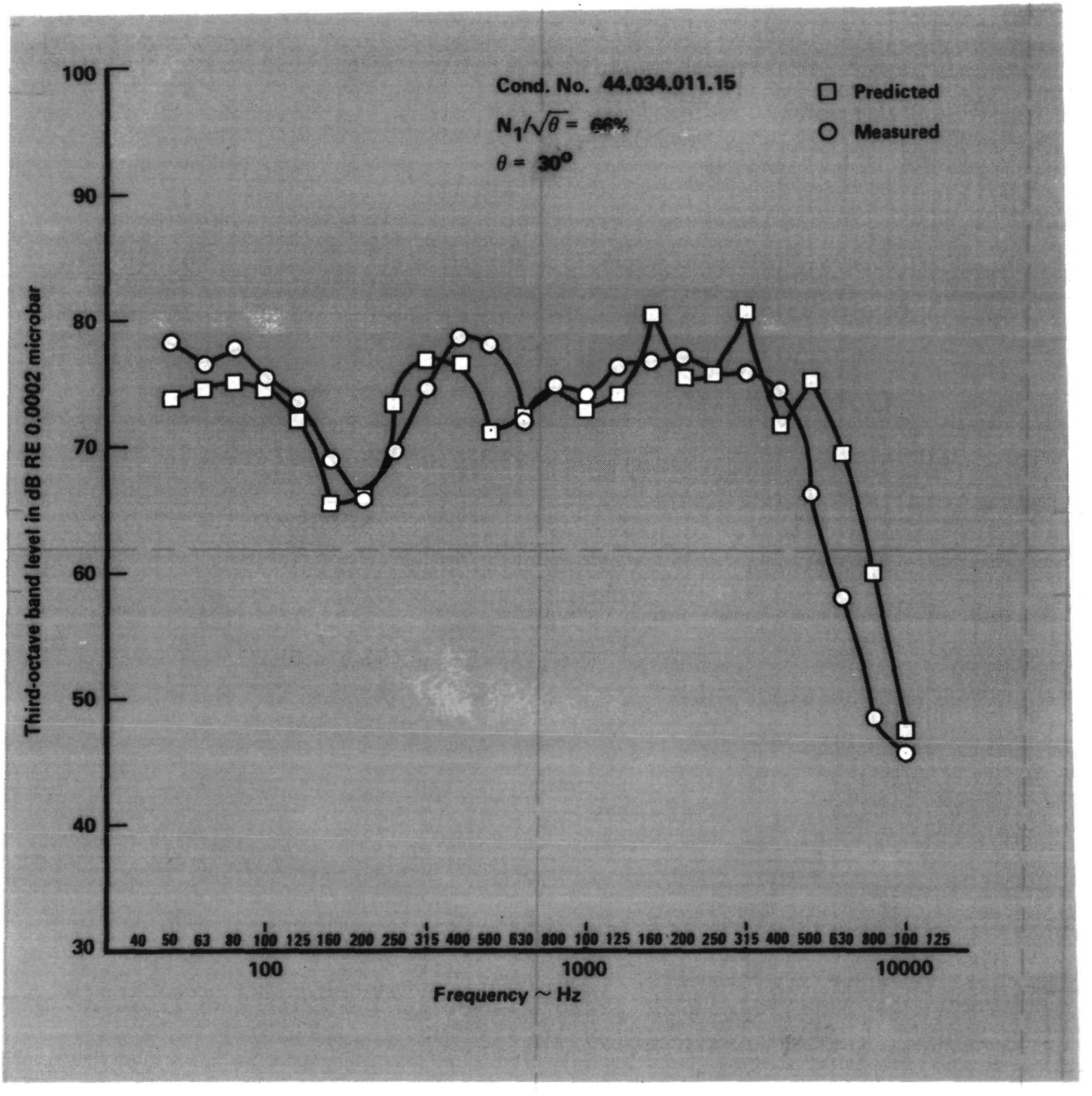

Figure 32. - Comparison of component spectra, condition no. 44.034.011.15, $\theta = 30^{\circ}$.

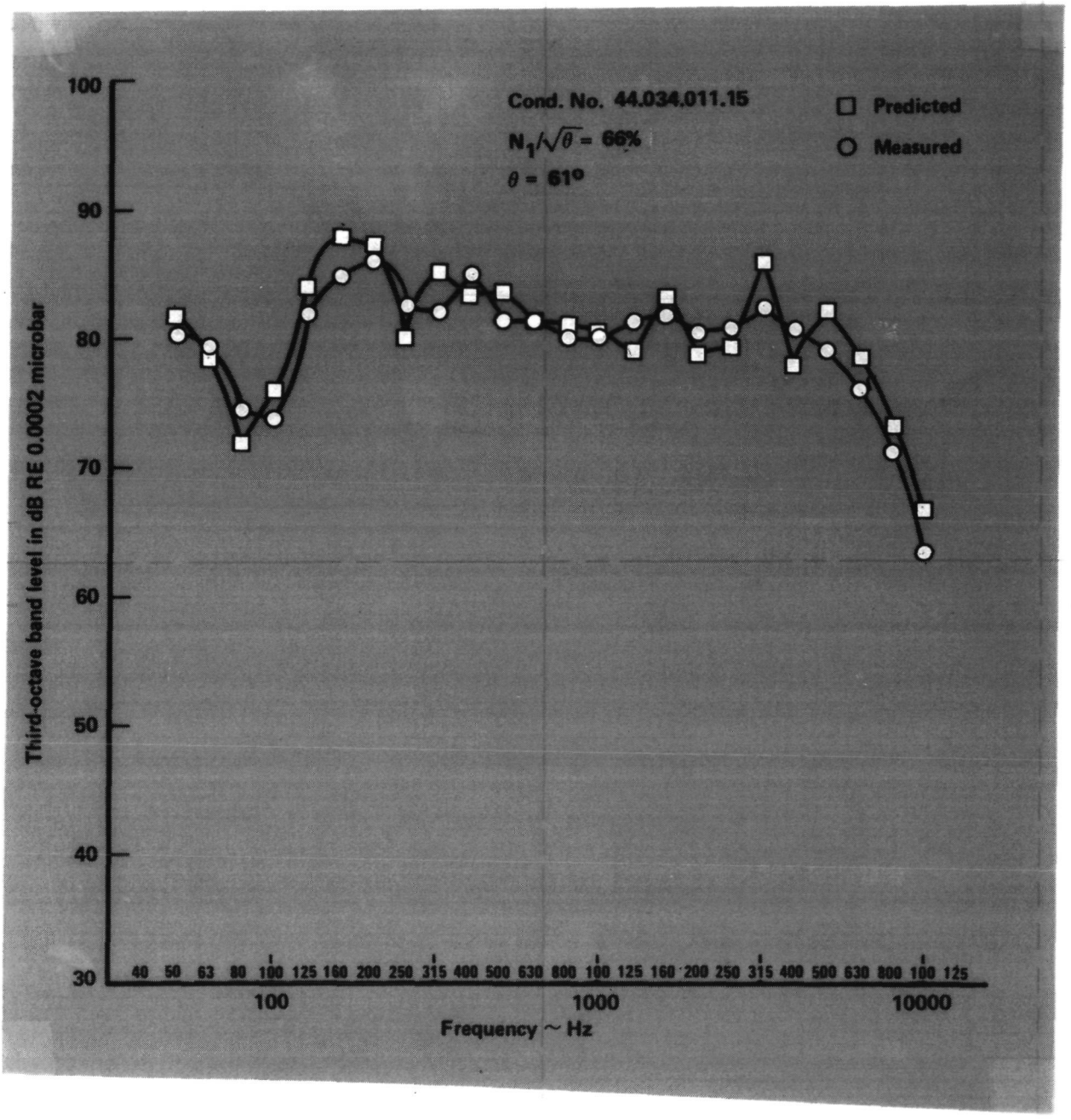

Figure 33. - Comparison of component spectra, condition no. 44.034.011.15, $\theta = 61^{o}$.

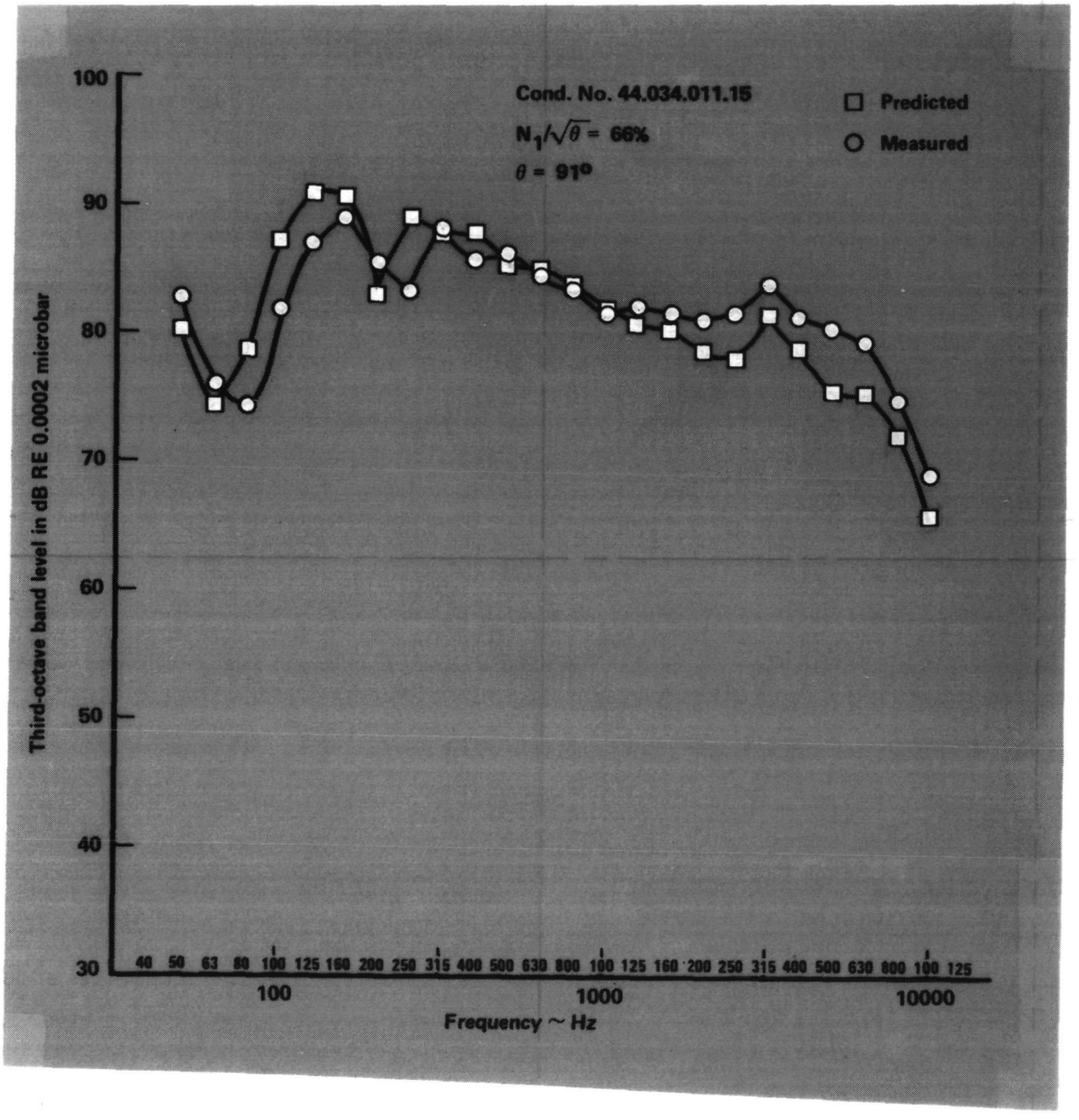

Figure 34. - Comparison of component spectra, condition no. 44.034.011.15, $\theta = 91^{\circ}$.

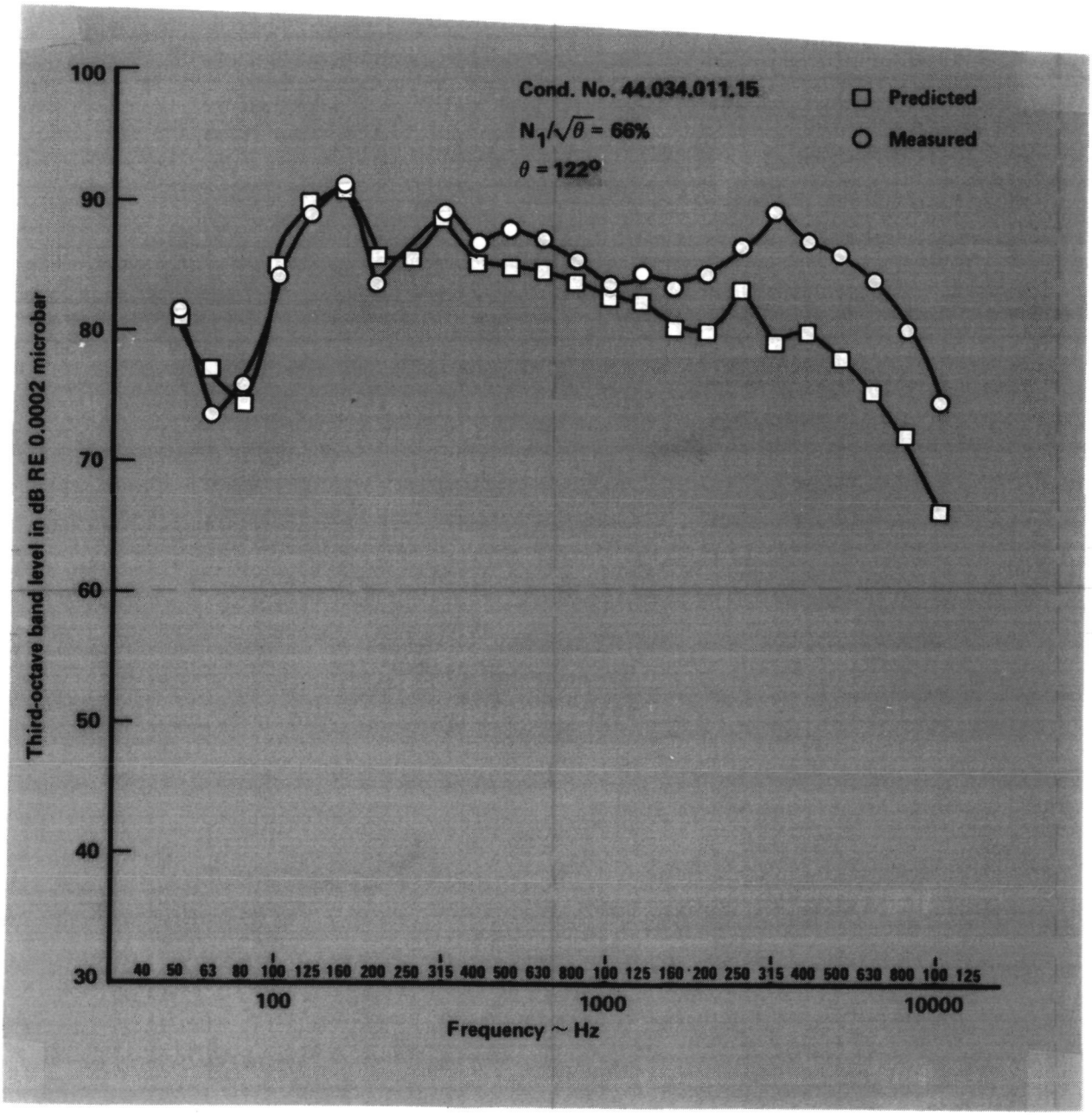

Figure 35. - Comparison of component spectra, condition no. 44.034.011.15, $\theta = 122^{\circ}$.

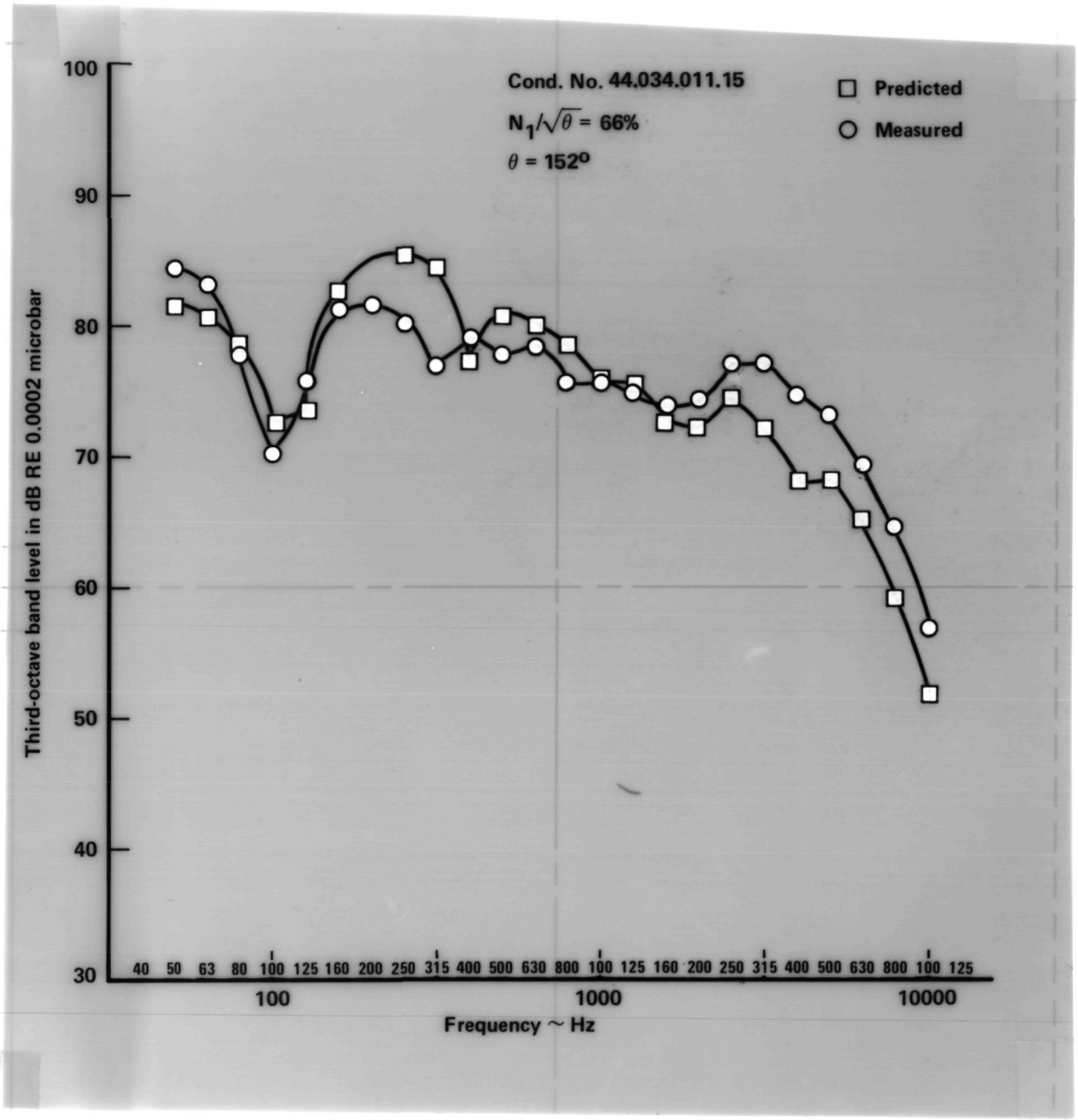

Figure 36. - Comparison of component spectra, condition no. 44.034.011.15, $\theta = 152^{o}$.

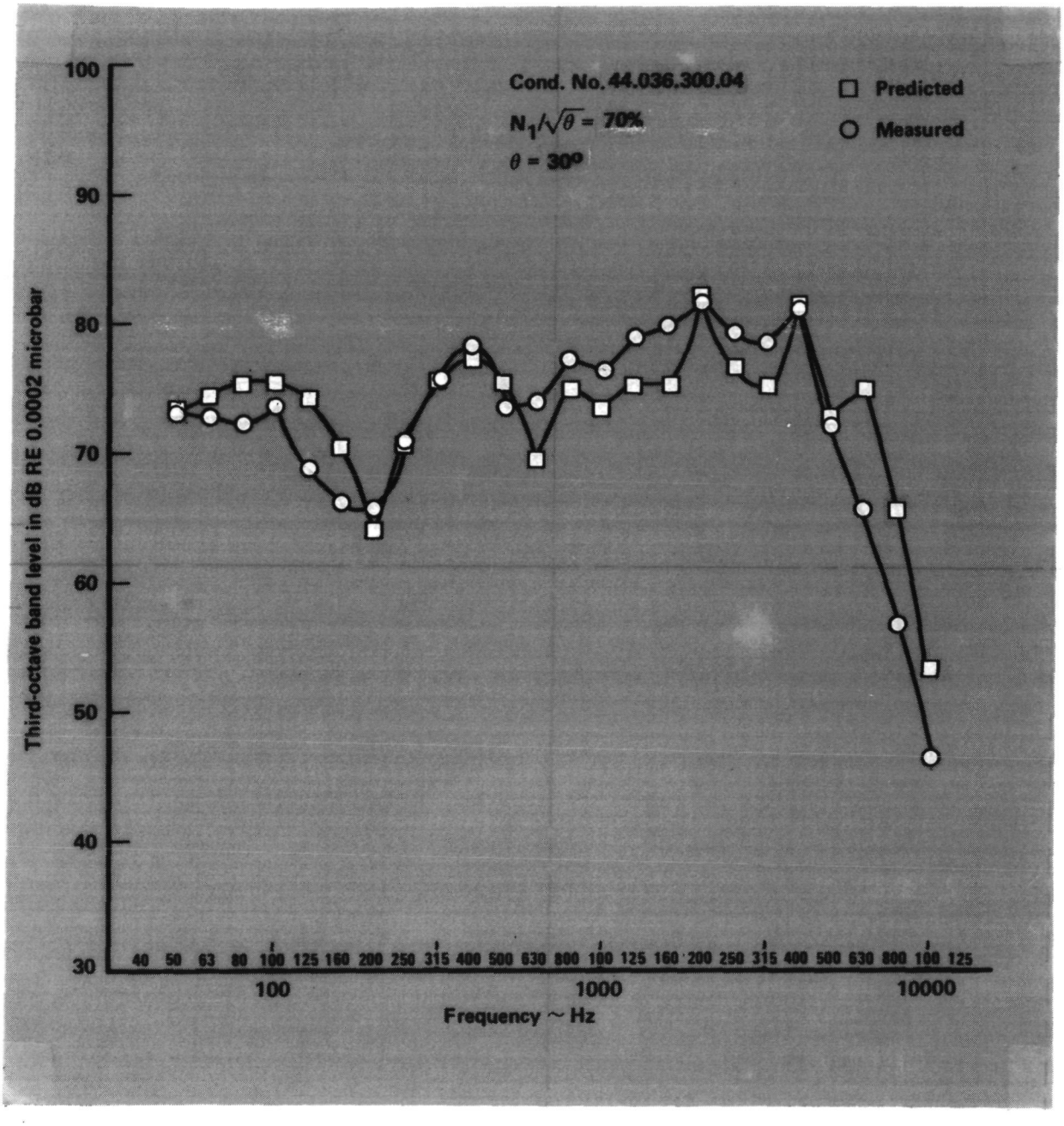

Figure 37. - Comparison of component spectra, condition no. 44.036.300.09, $\theta = 30^{\circ}$.

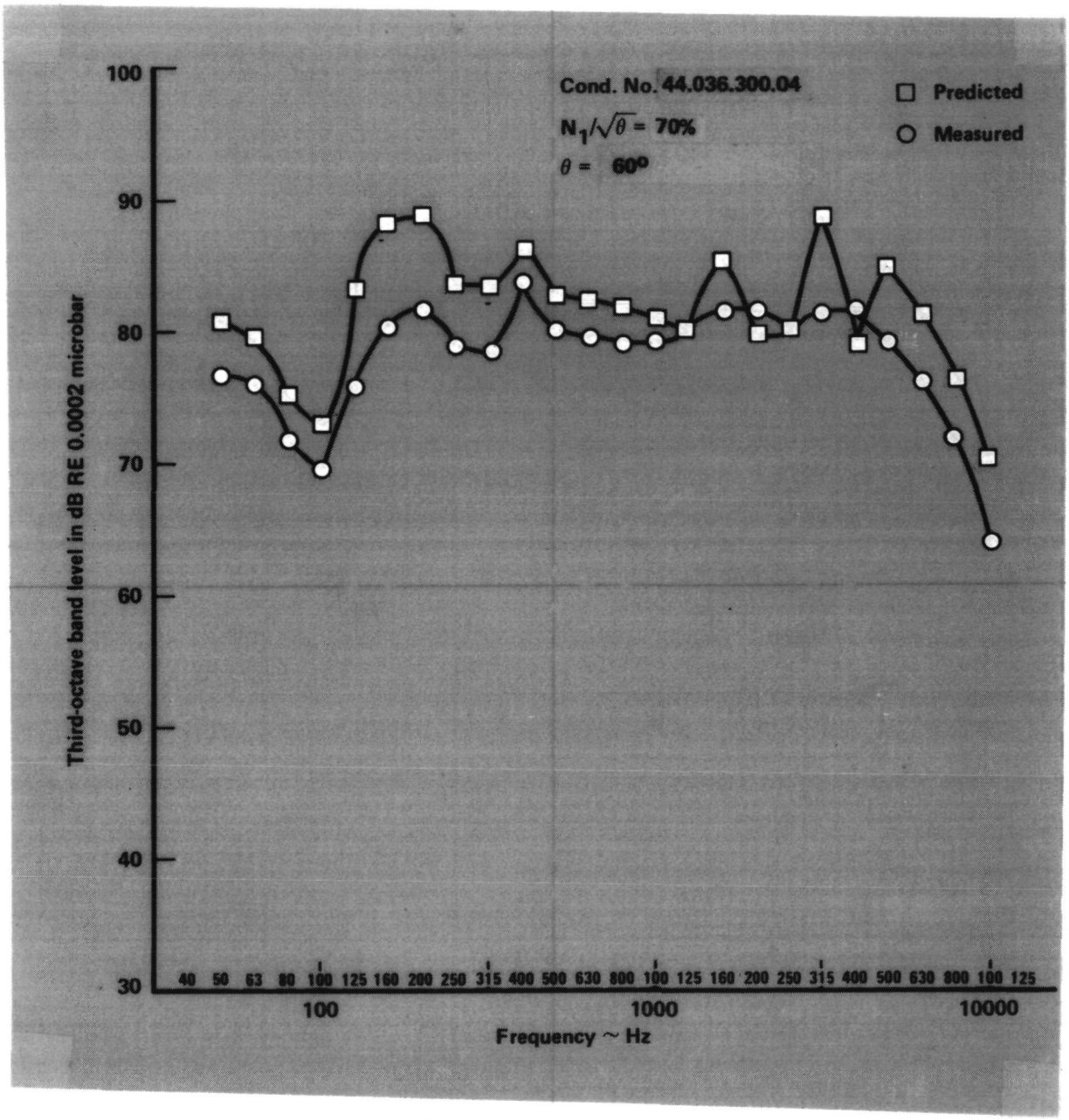

Figure 38. - Comparison of component spectra, condition no. 44.036.300.04, $\theta = 60^{\circ}$.

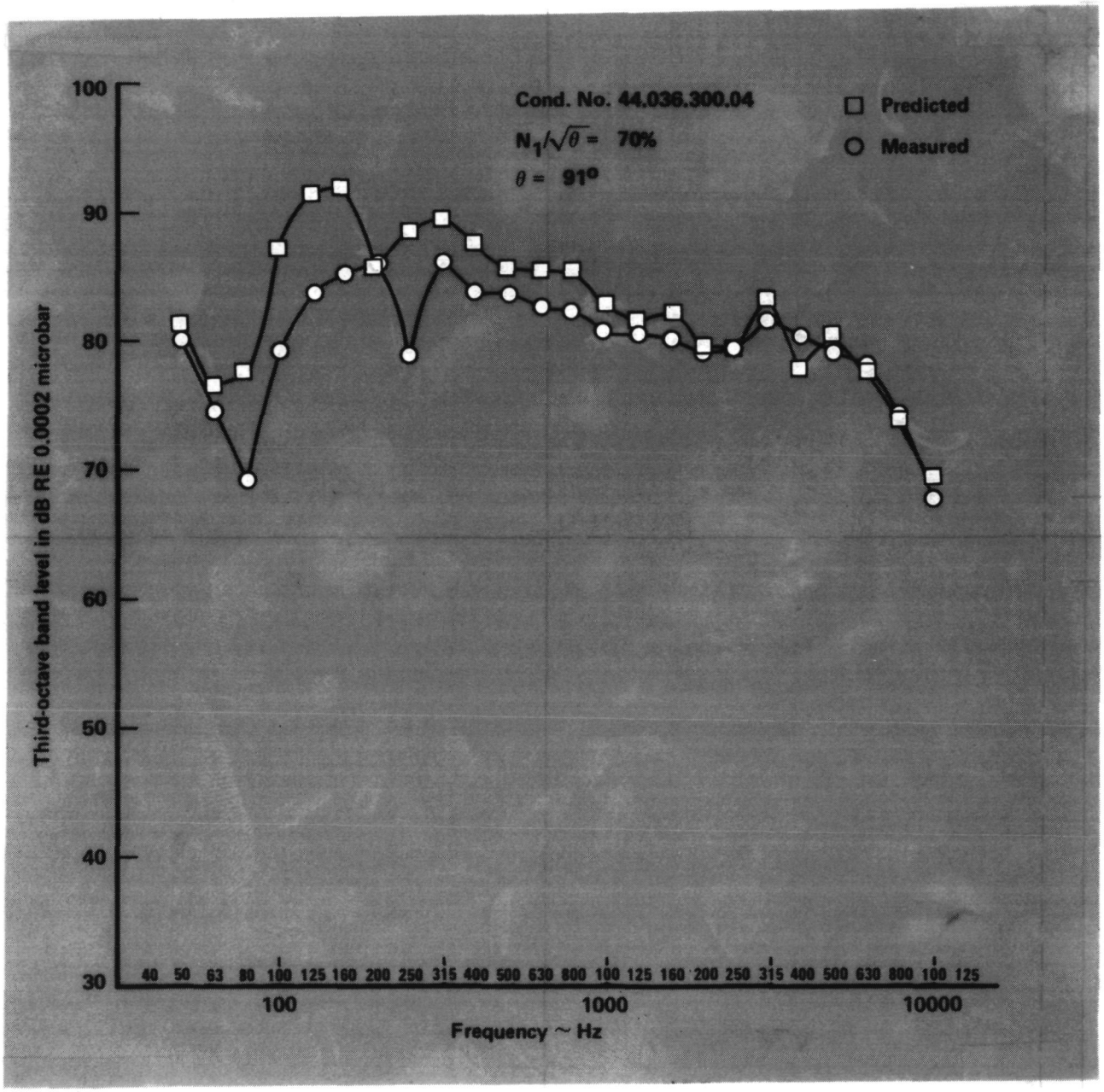

Figure 39. - Comparison of component spectra, condition no. 44.036.300.04, $\theta = 91^{\circ}$.

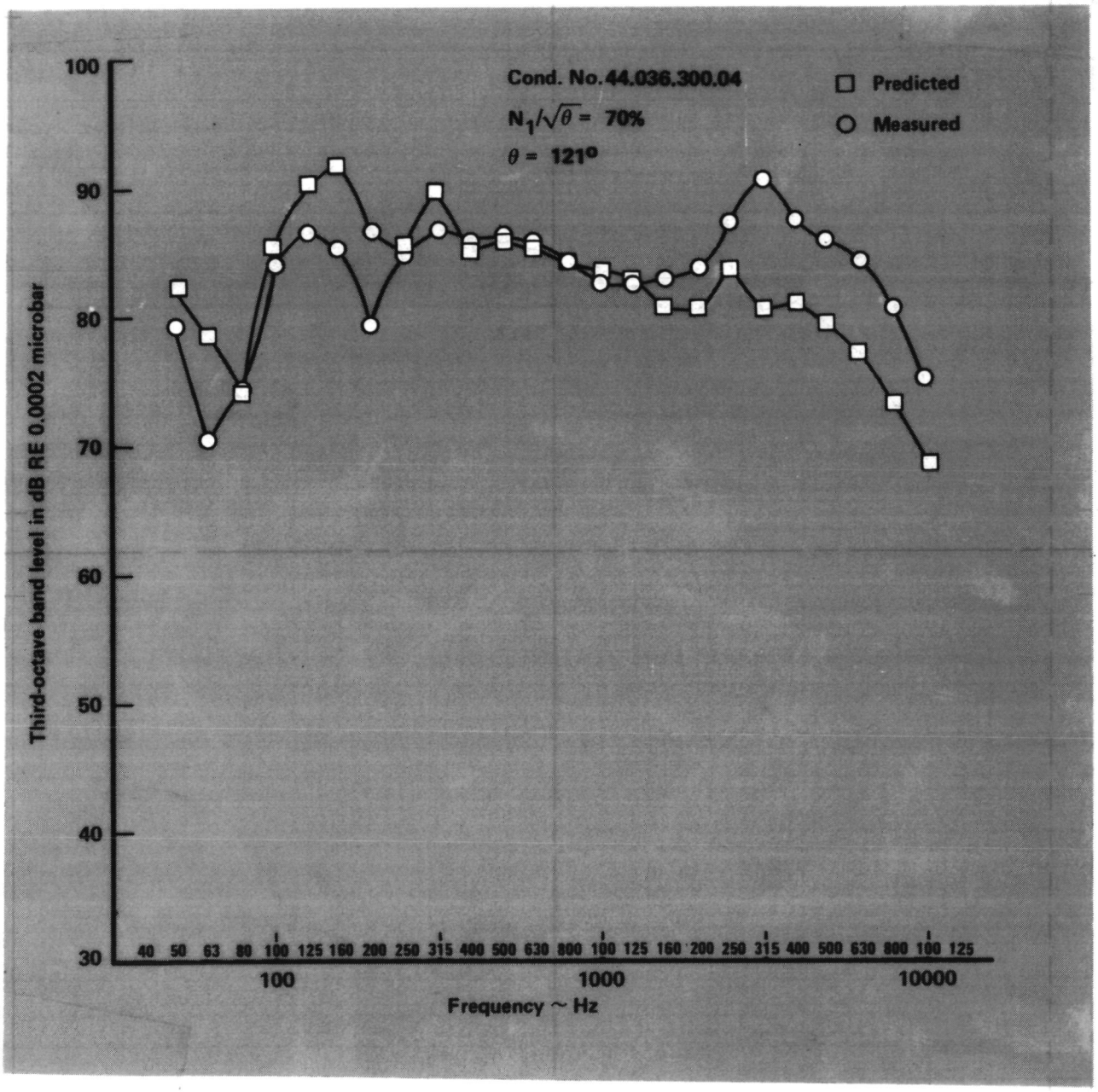

Figure 40. - Comparison of component spectra, condition no. 44.036.300.04, $\theta = 121^{\circ}$.

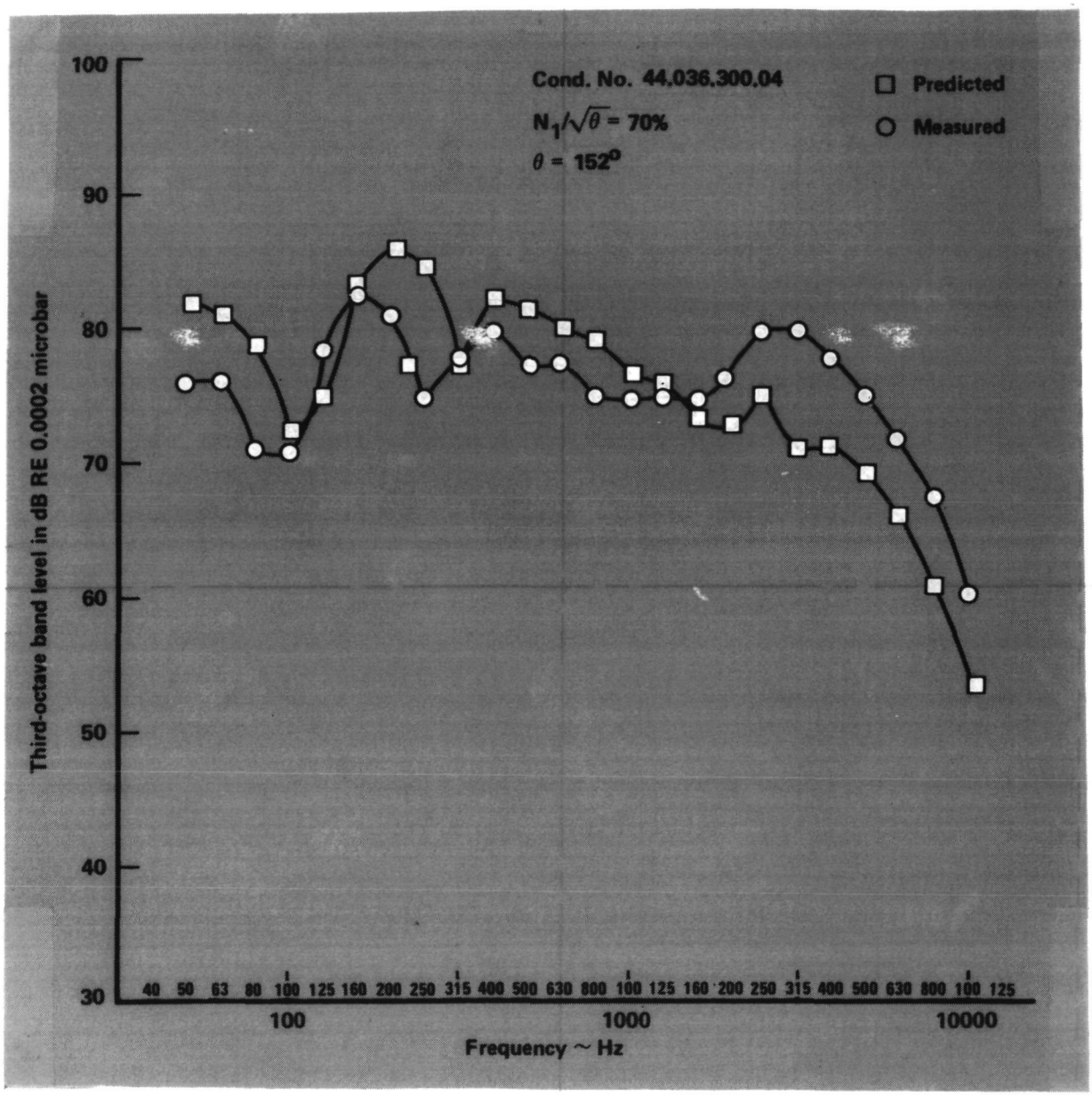

Figure 41. - Comparison of component spectra, condition no. 44.036.300.04, $\theta = 152^{\circ}$.

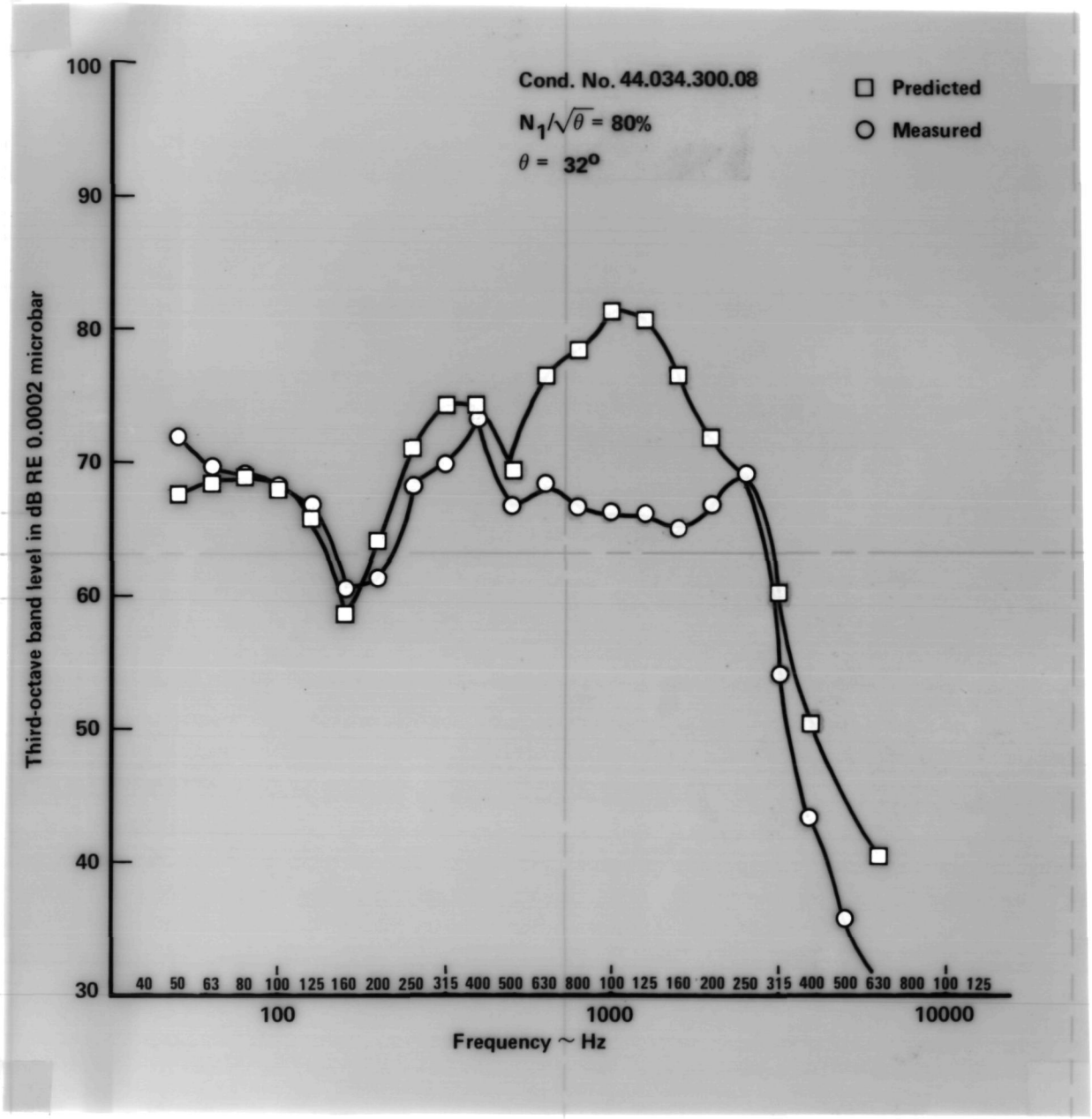

Figure 42. - Comparison of component spectra, condition no. 44.034.300.08, $\theta = 32^{o}$.

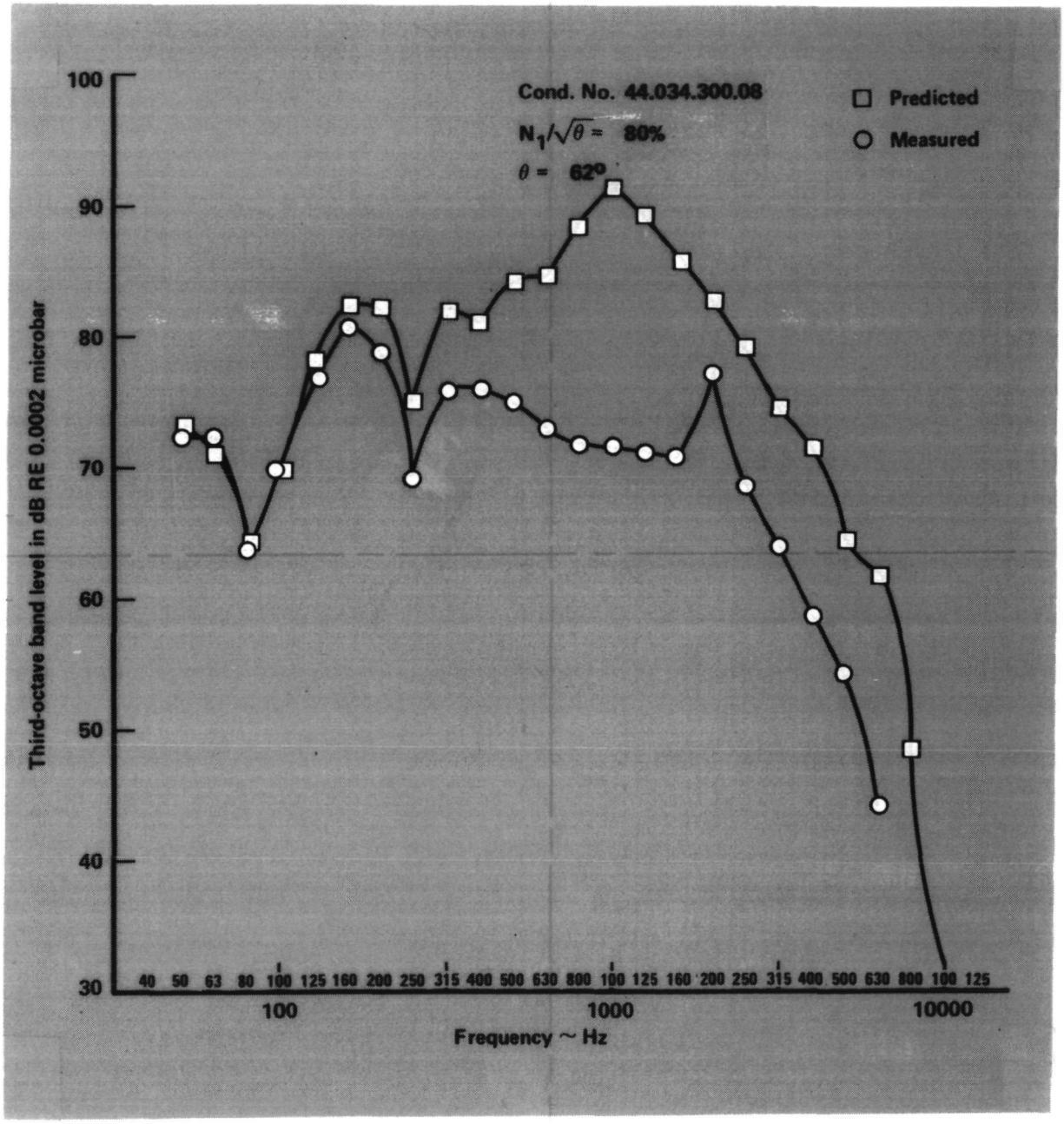

Figure 43. - Comparison of component spectra, condition no. 44.034.300.08, $\theta = 62^{o}$.

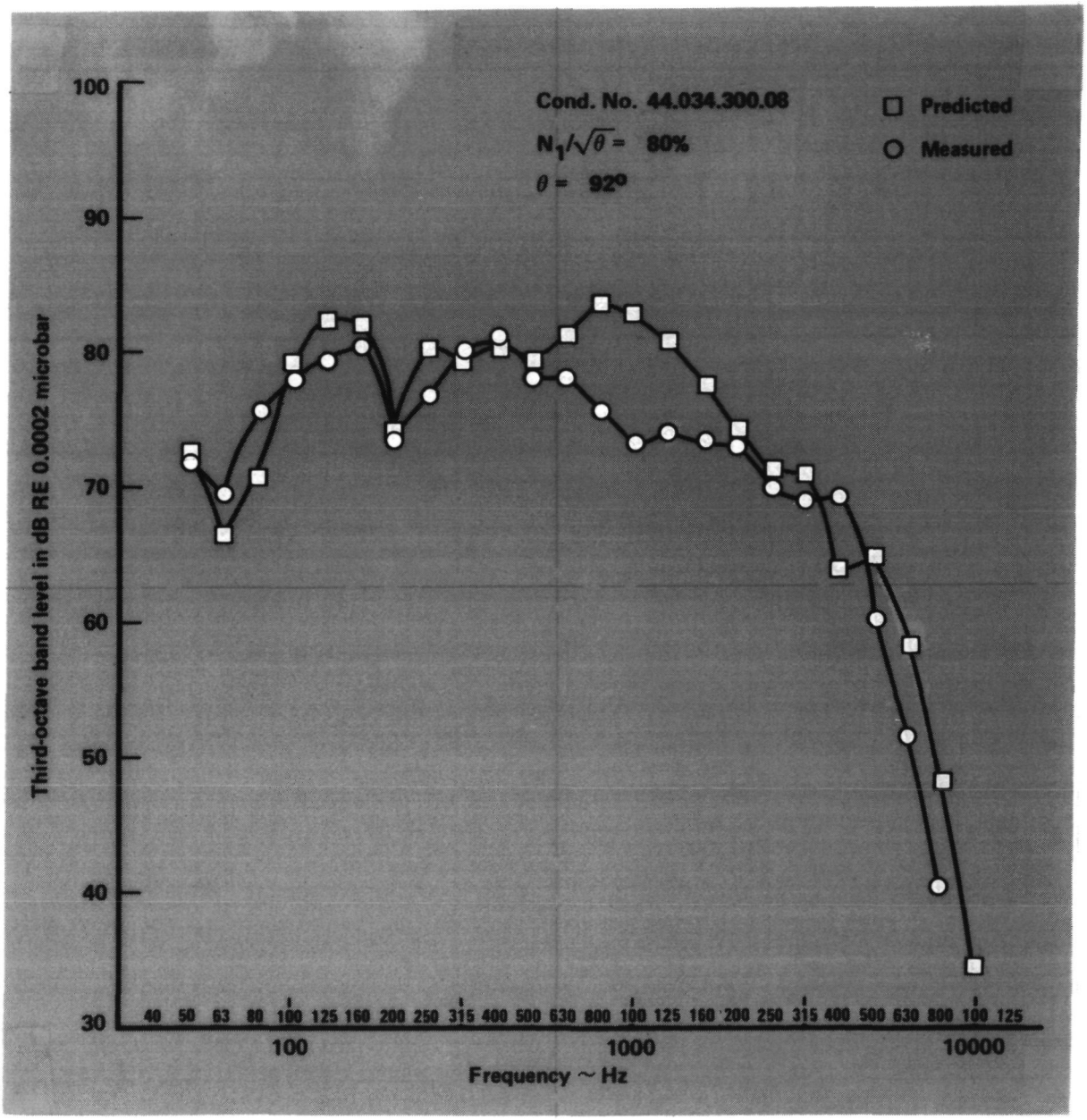

Figure 44. - Comparison of component spectra, condition no. 44.034.300.08, $\theta = 92^{\circ}$.

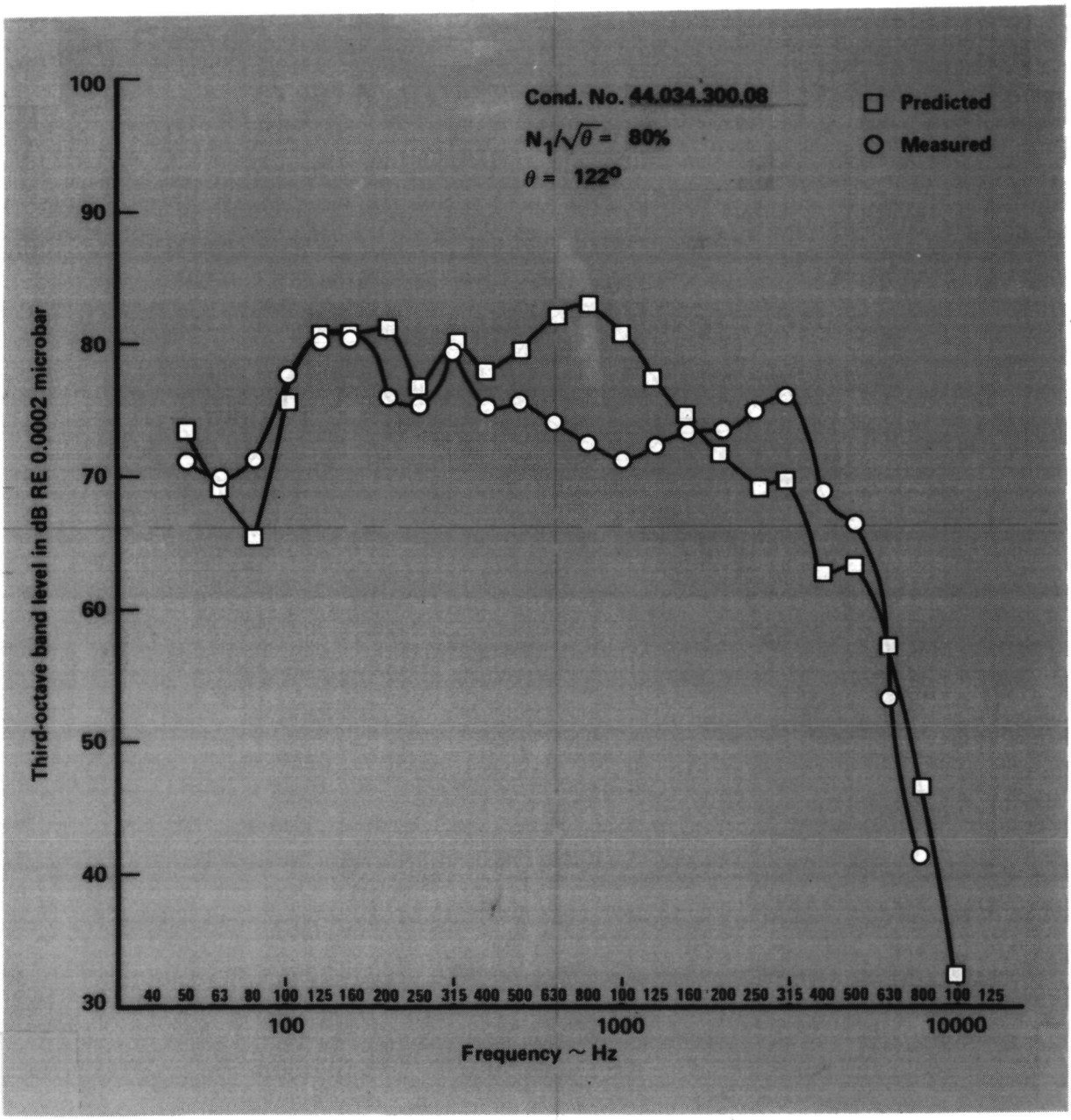

Figure 45. - Comparison of component spectra, condition no. 44.034.300.08, $\theta = 122^{\circ}$.

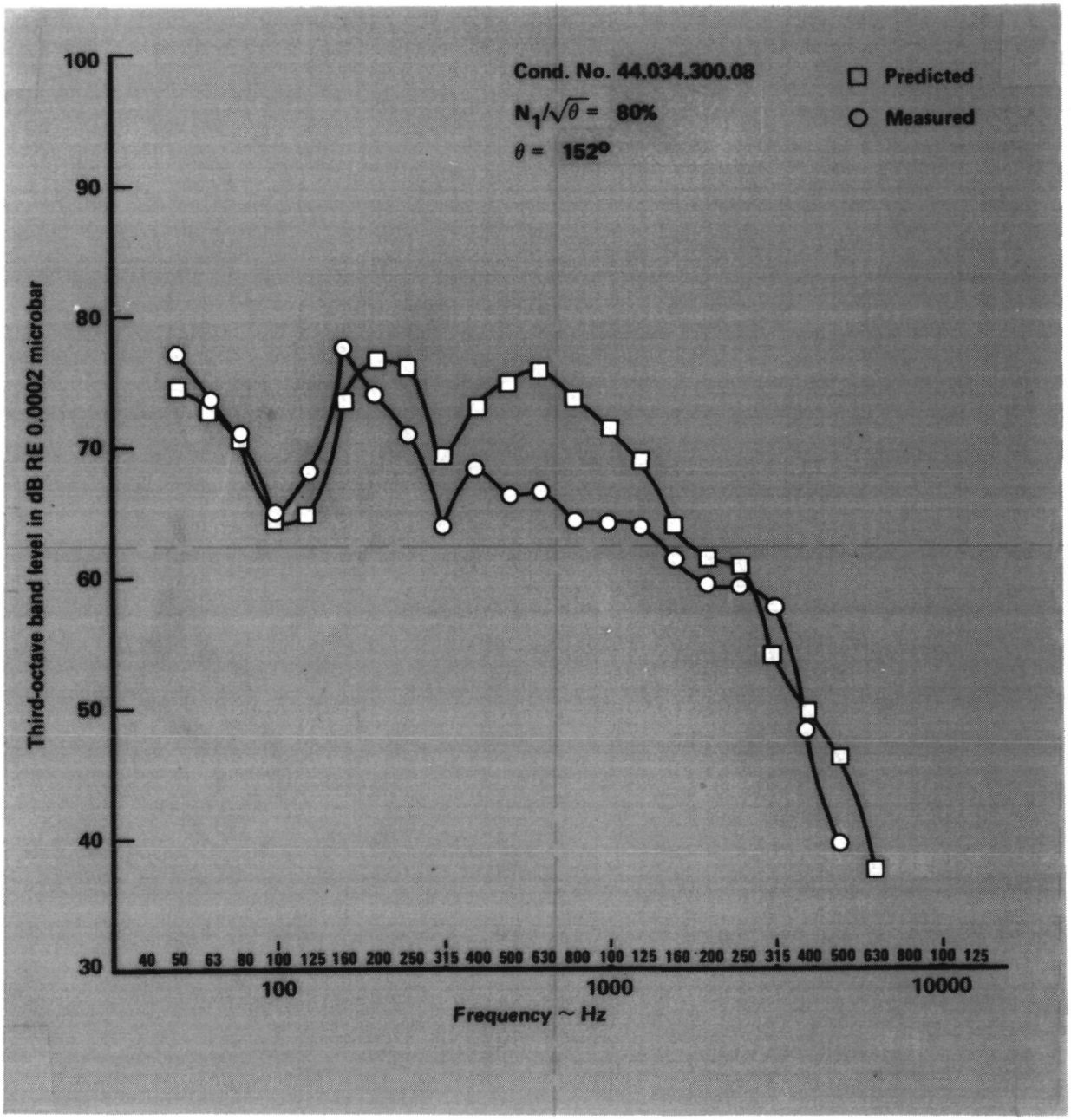

Figure 46. - Comparison of component spectra, condition no. 44.034.300.08, $\theta = 152^{\circ}$.

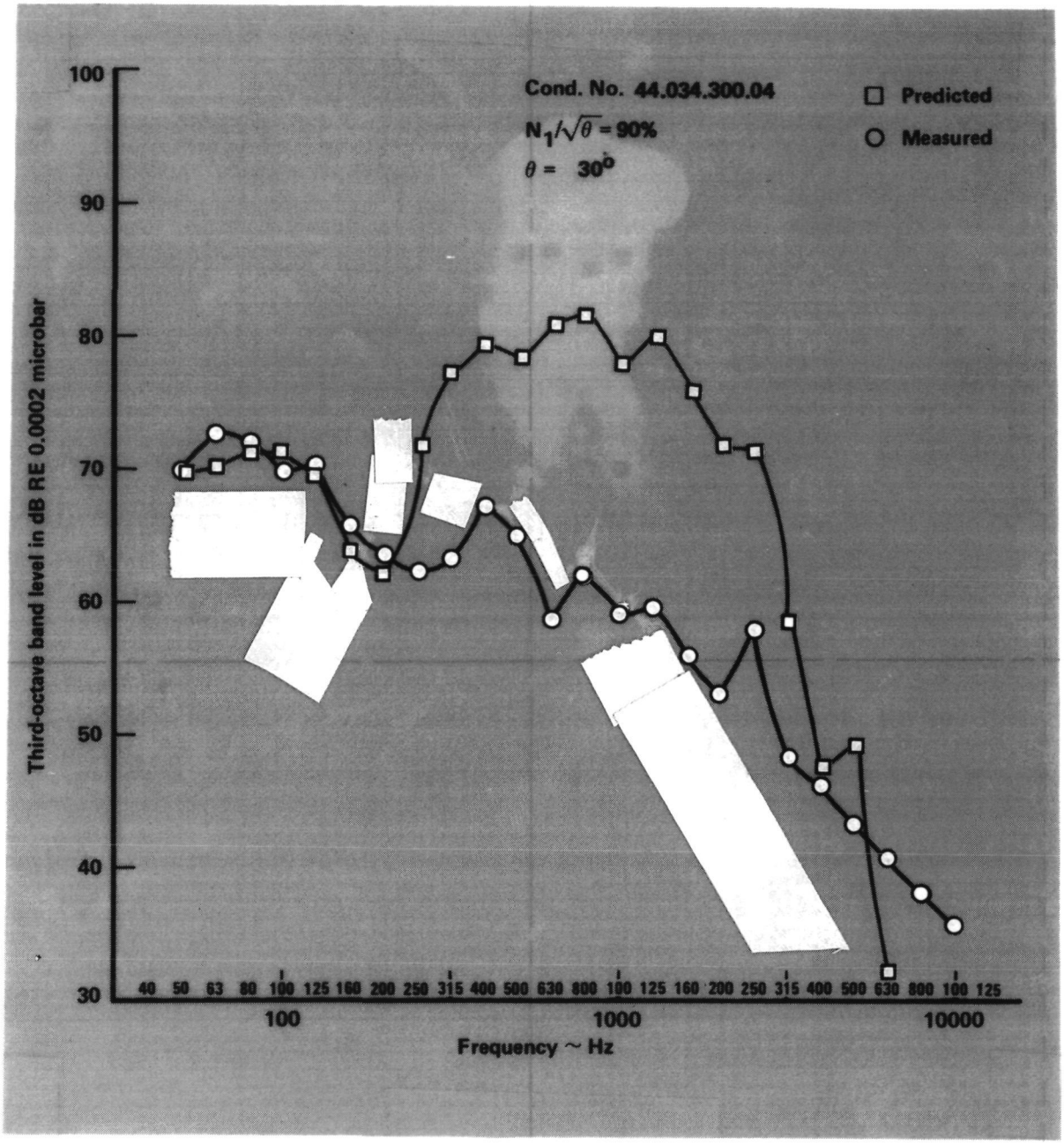

Figure 47. - Comparison of component spectra, condition no. 44.034.300.04, $\theta = 30^{\circ}$

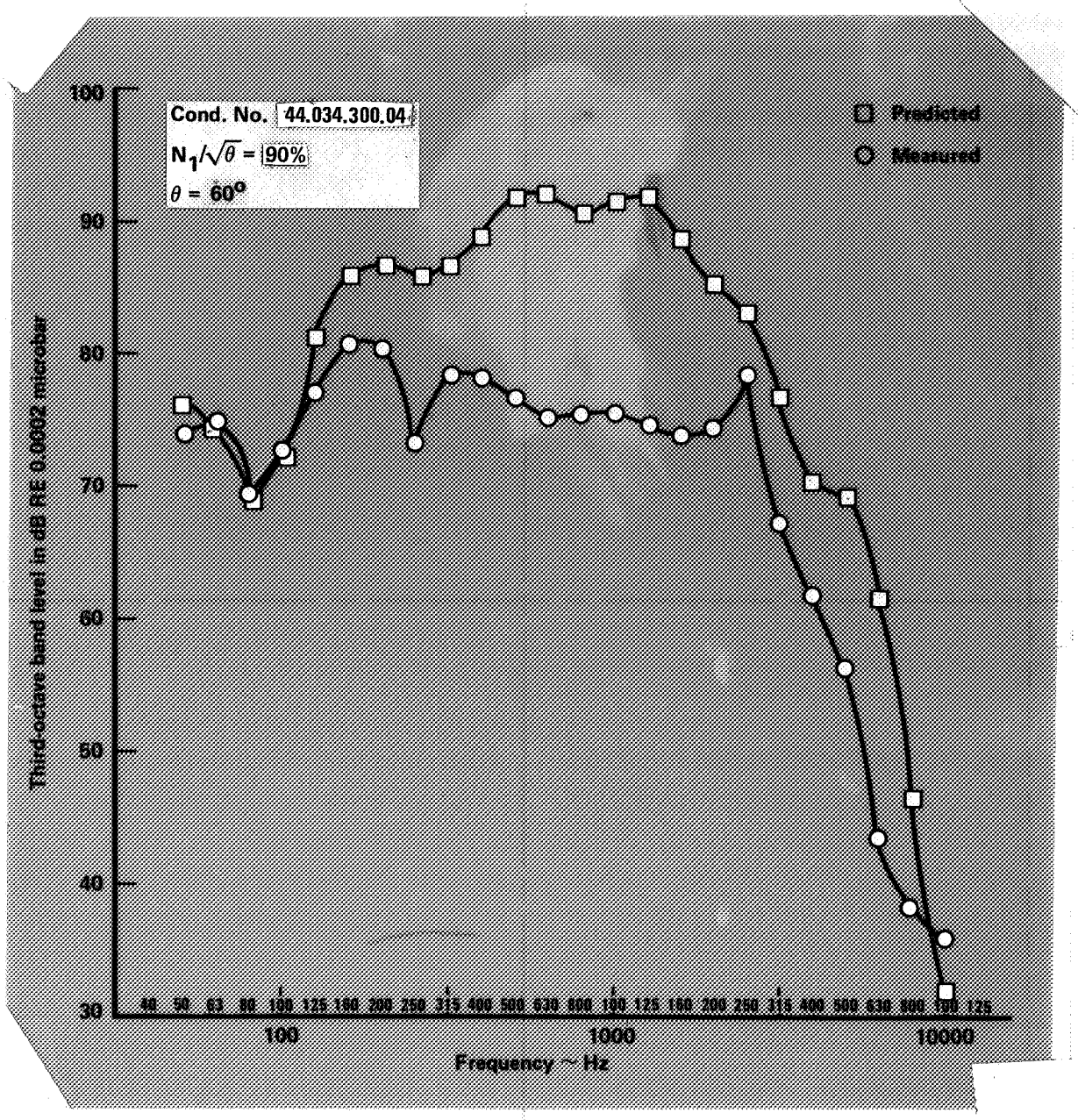

Figure 48. - Comparison of component spectra, condition no. 44.034.300.04, $\theta = 60^{\circ}$.

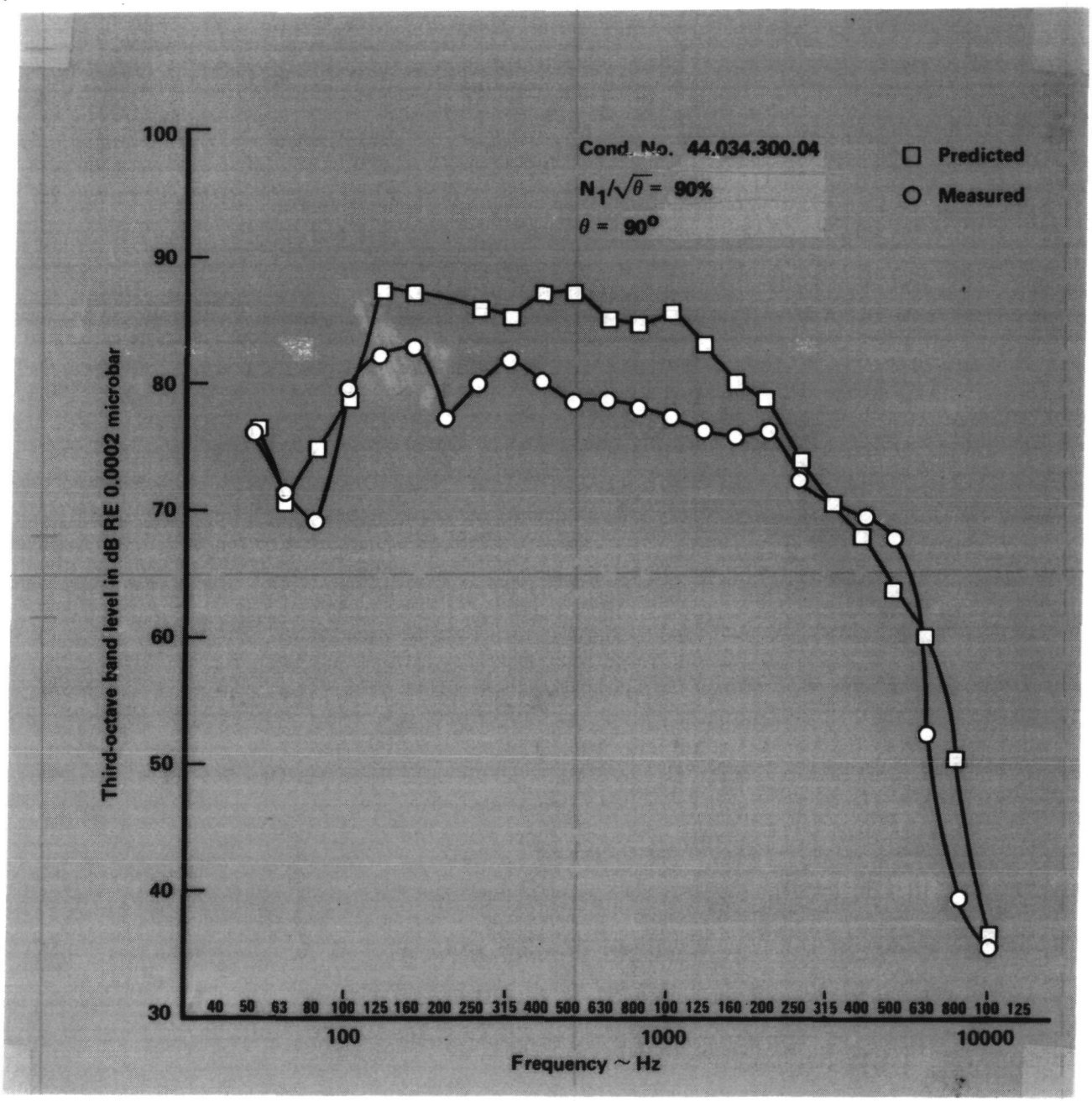

Figure 49. - Comparison of component spectra, condition no. 44.034.300.04, $\theta = 90^{\circ}$.

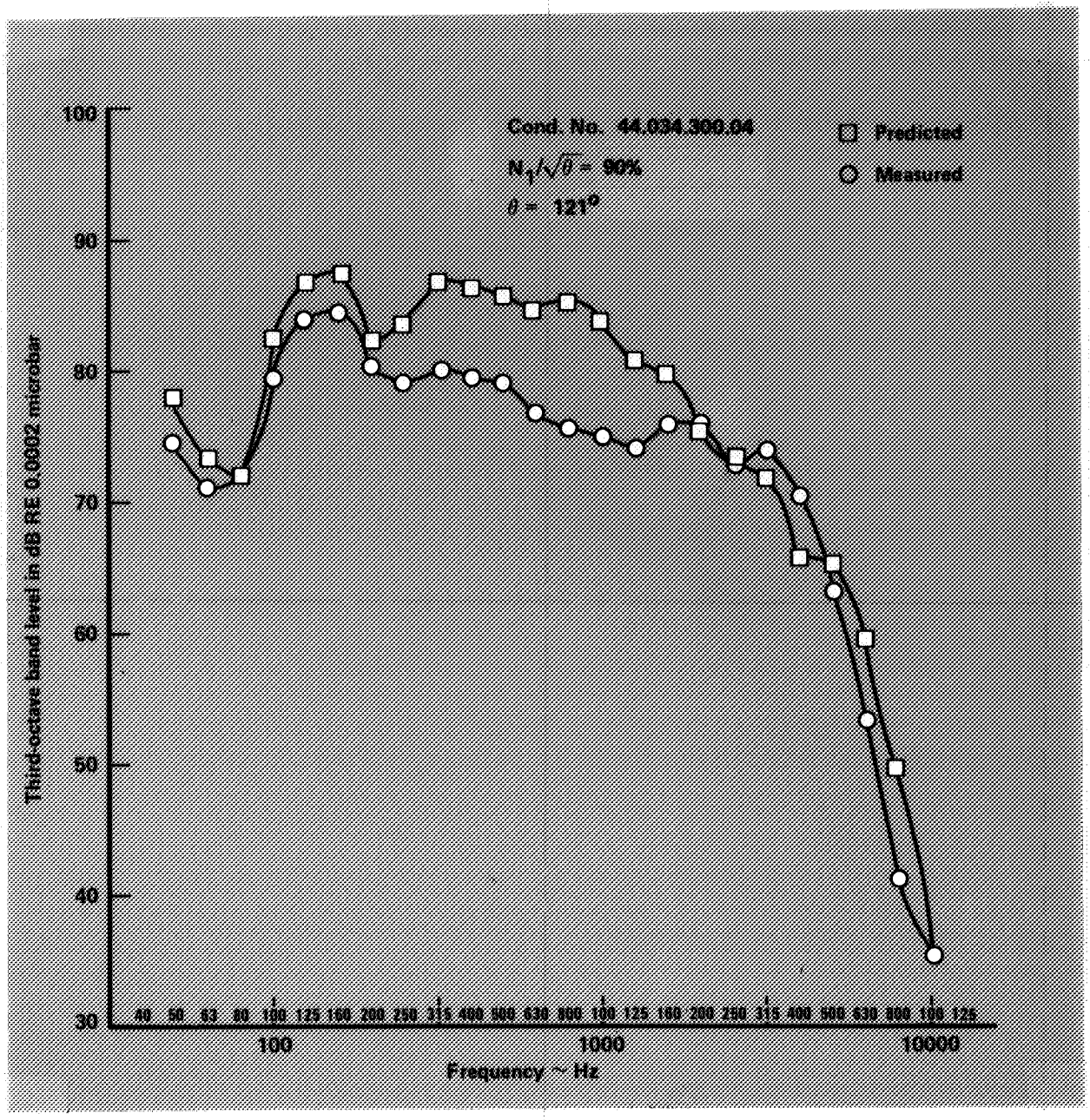

Figure 50. - Comparison of component spectra, condition no. 44.034.300.04, $\theta = 121^{o}$.

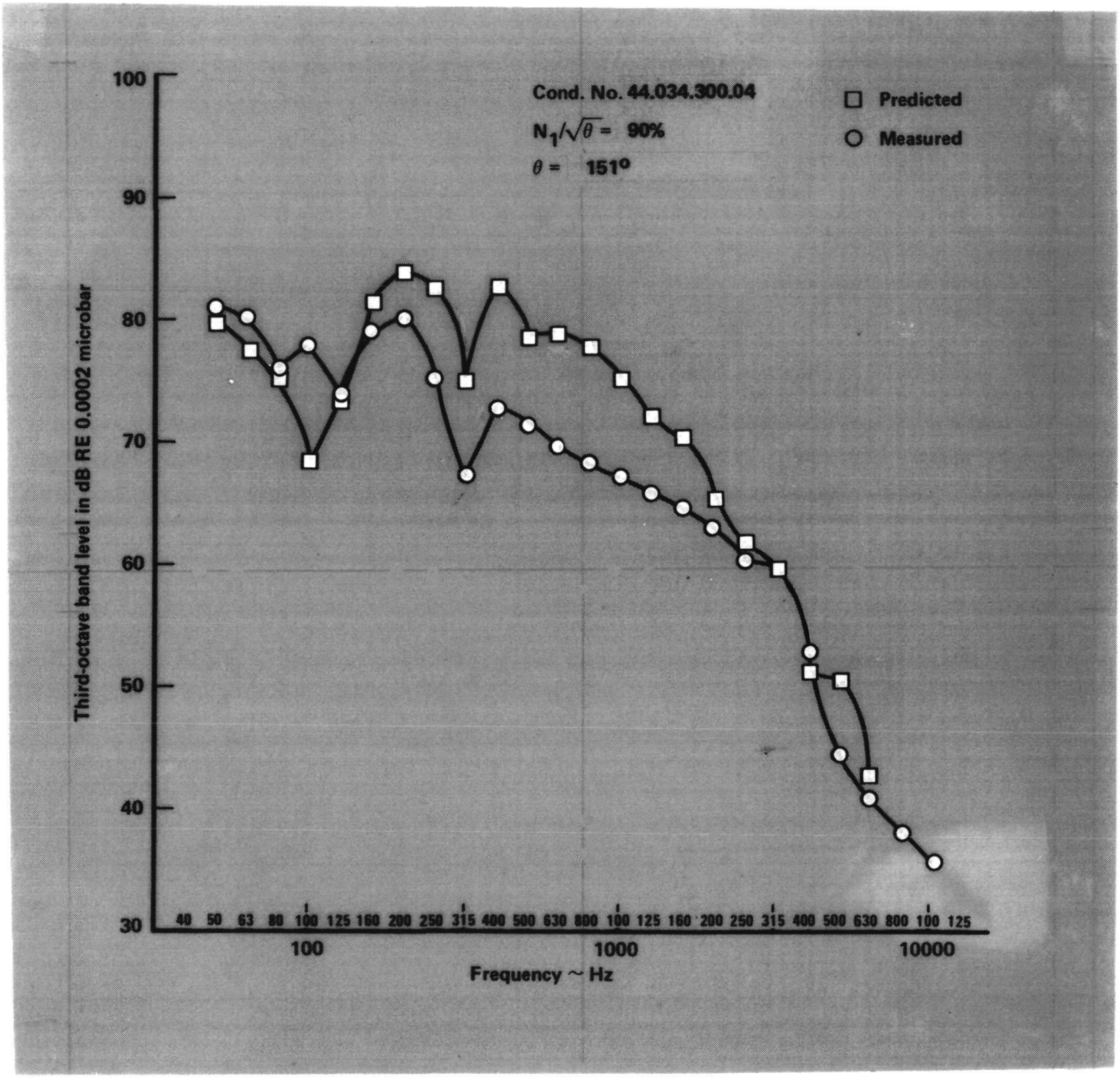

Figure 51. - Comparison of component spectra, condition no. 44.034.300.04, $\theta = 151^{\circ}$.

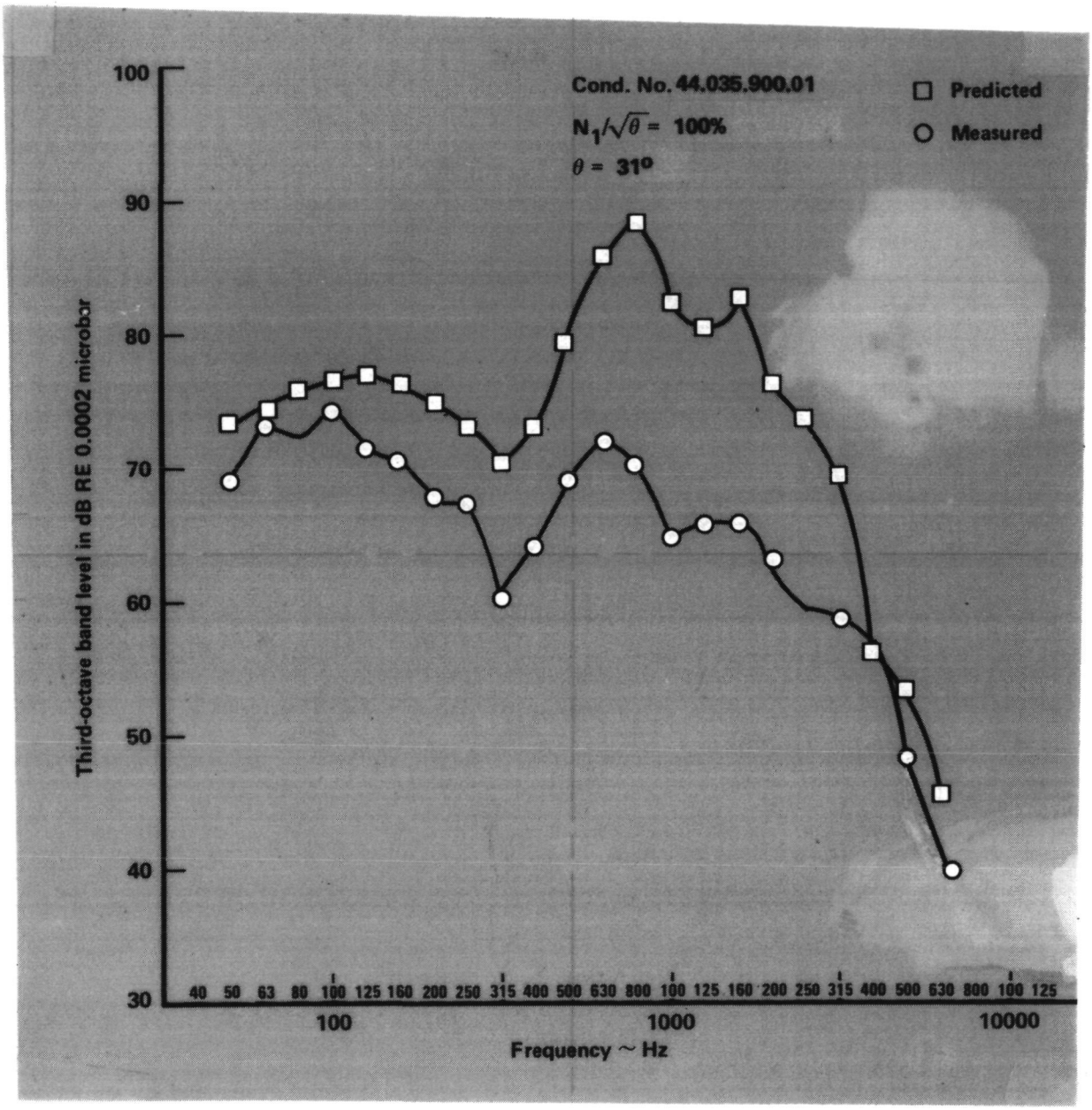

Figure 52. - Comparison of component spectra, condition no. 44.035.900.01, $\theta = 31^{\circ}$.

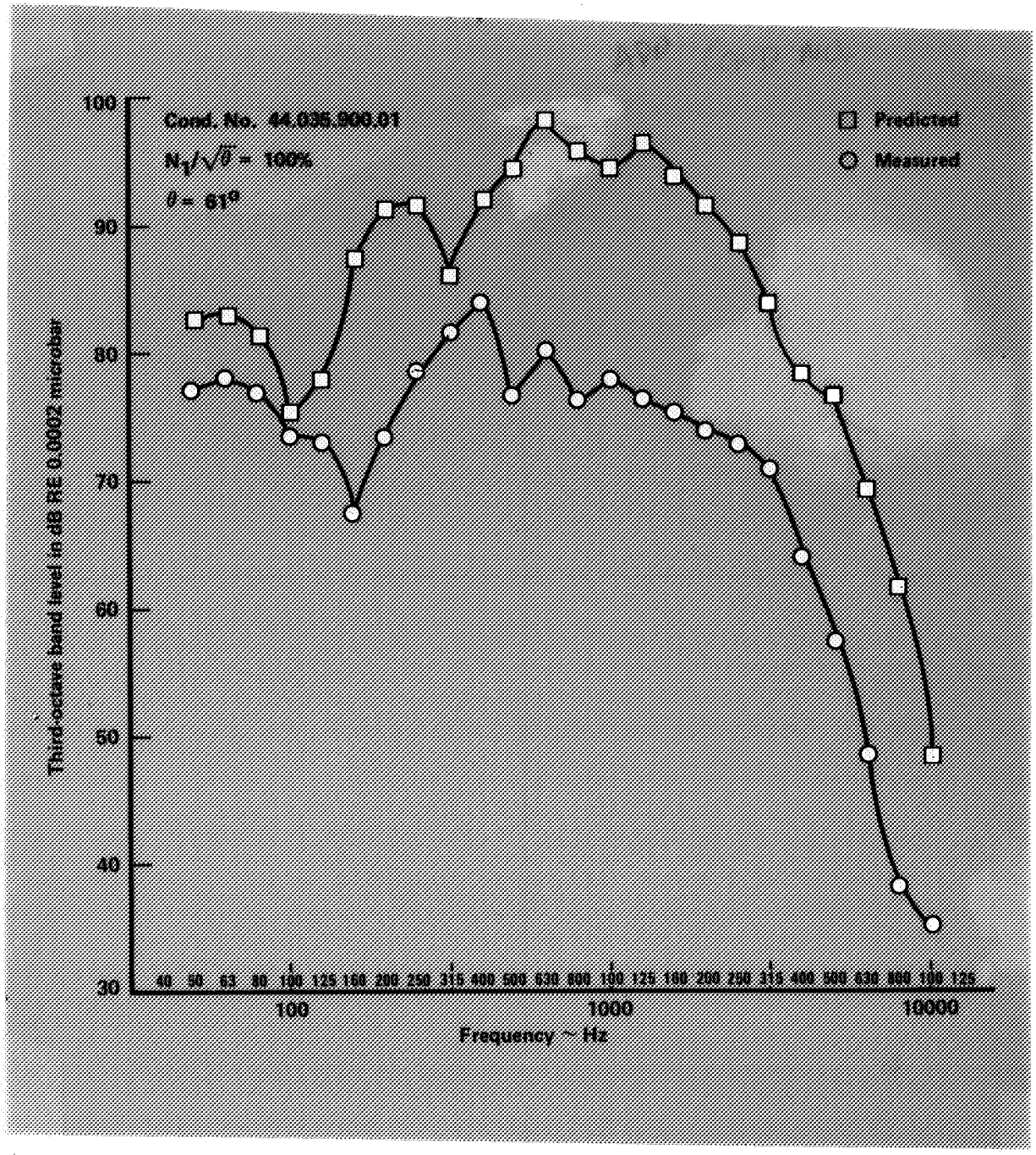

Figure 53. - Comparison of component spectra, condition no. 44.035.900.01, $\theta = 61^{\circ}$.

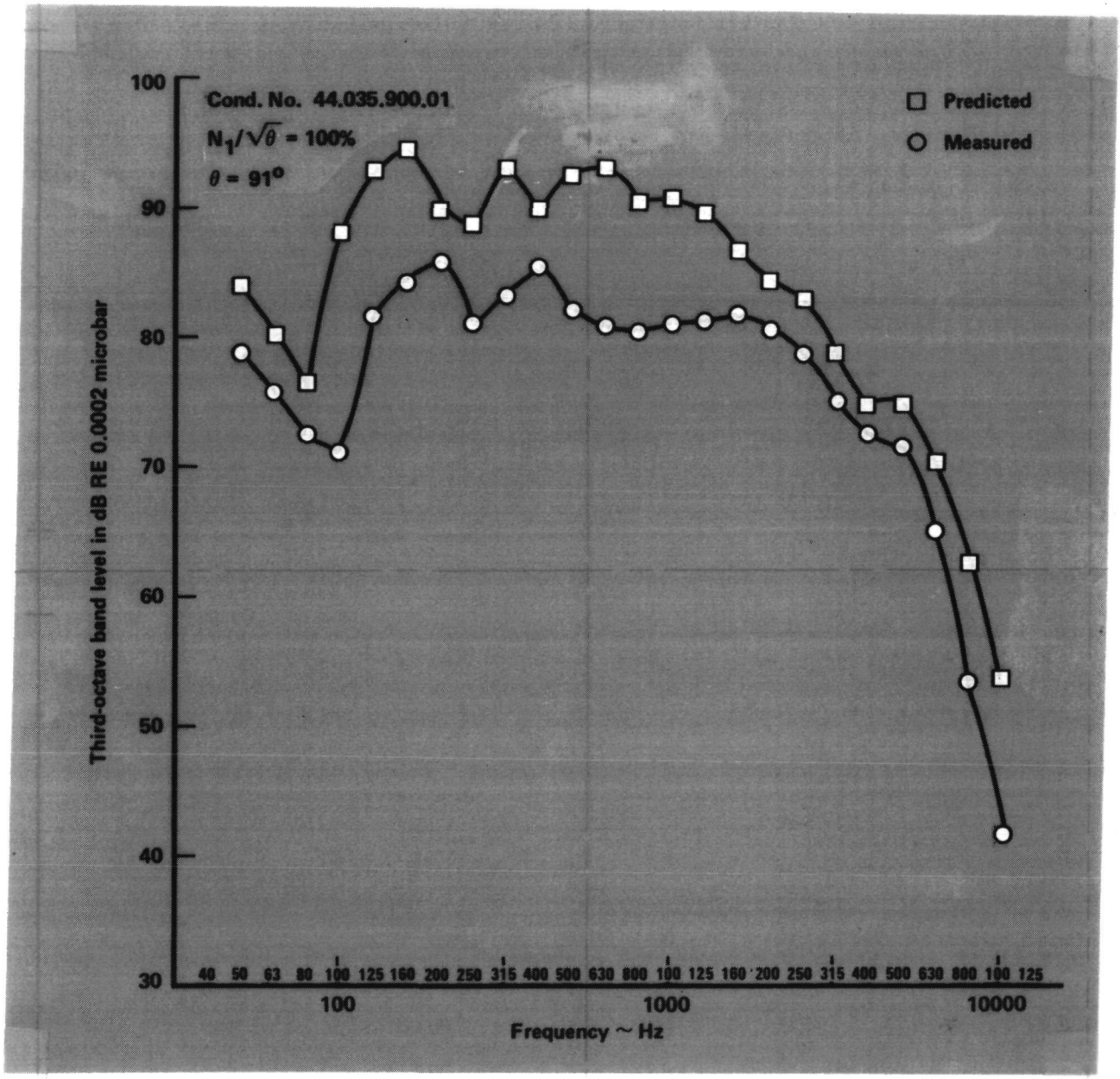

Figure 54. - Comparison of component spectra, condition no. 44.035.900.01, $\theta = 91^{o}$.

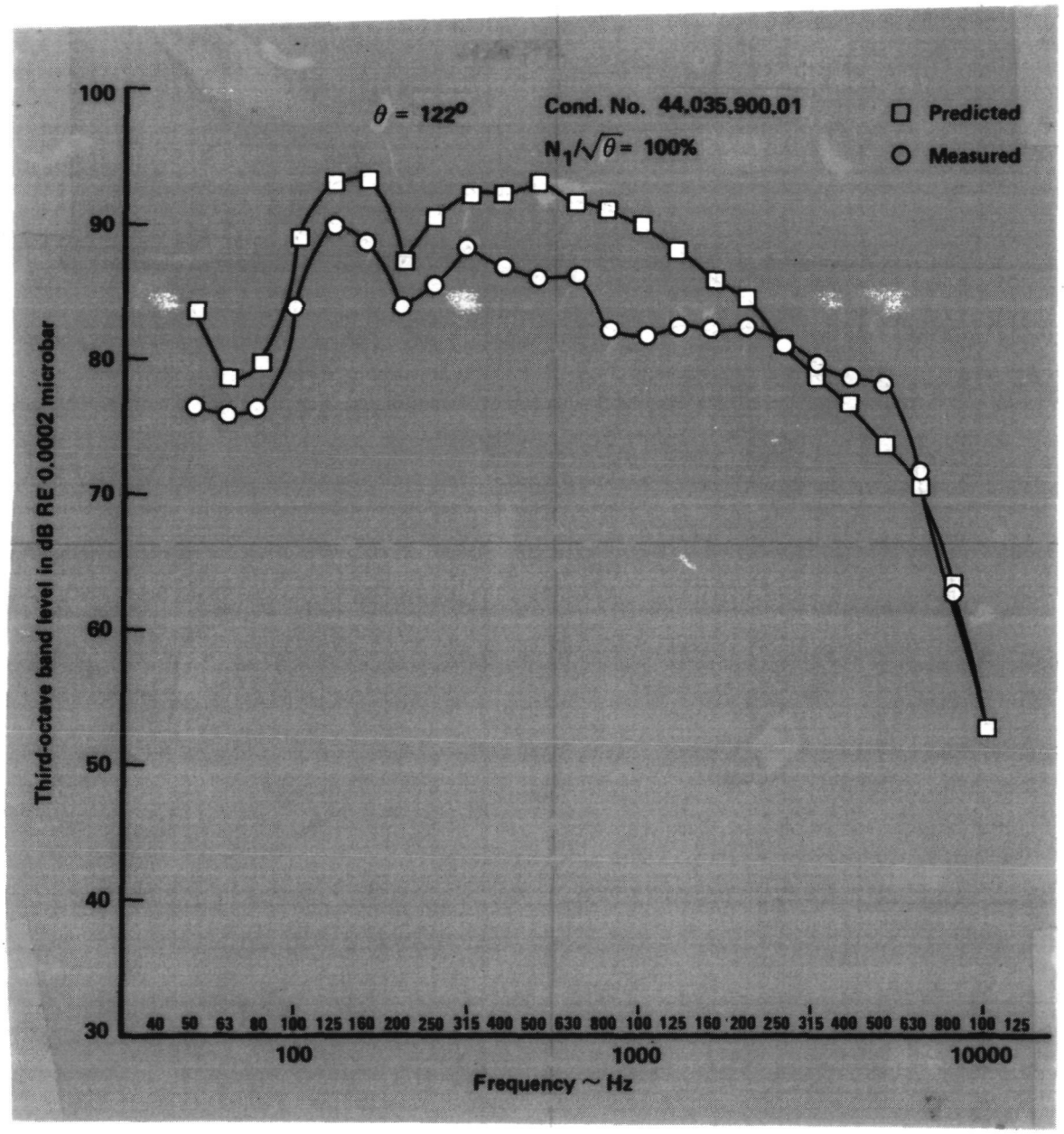

Figure 55. - Comparison of component spectra, condition no. 44.035.900.01, $\theta = 122^{o}$.

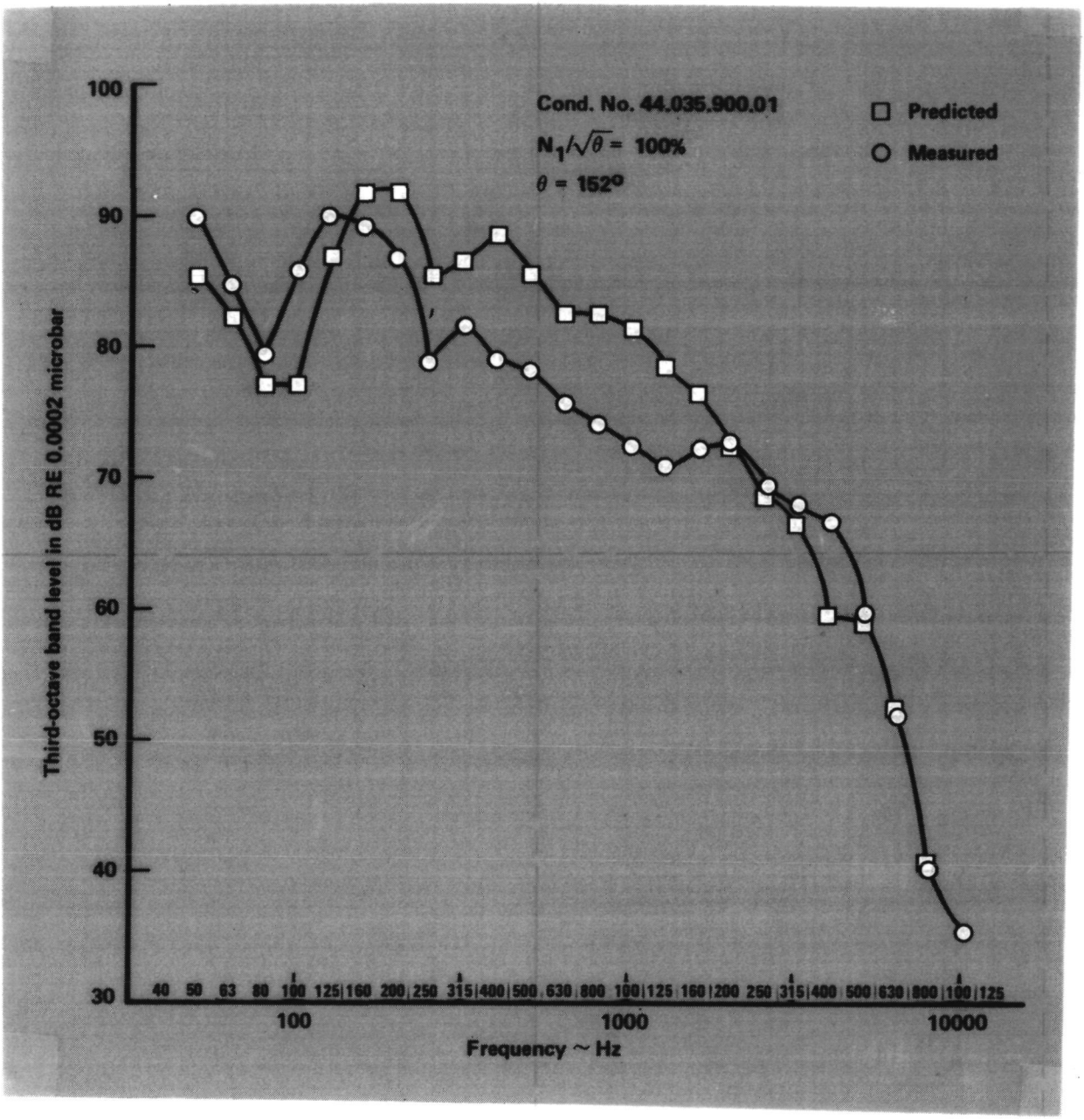

Figure 56. - Comparison of component spectra, condition no. 44.035.900.01, $\theta = 152^{\circ}$.

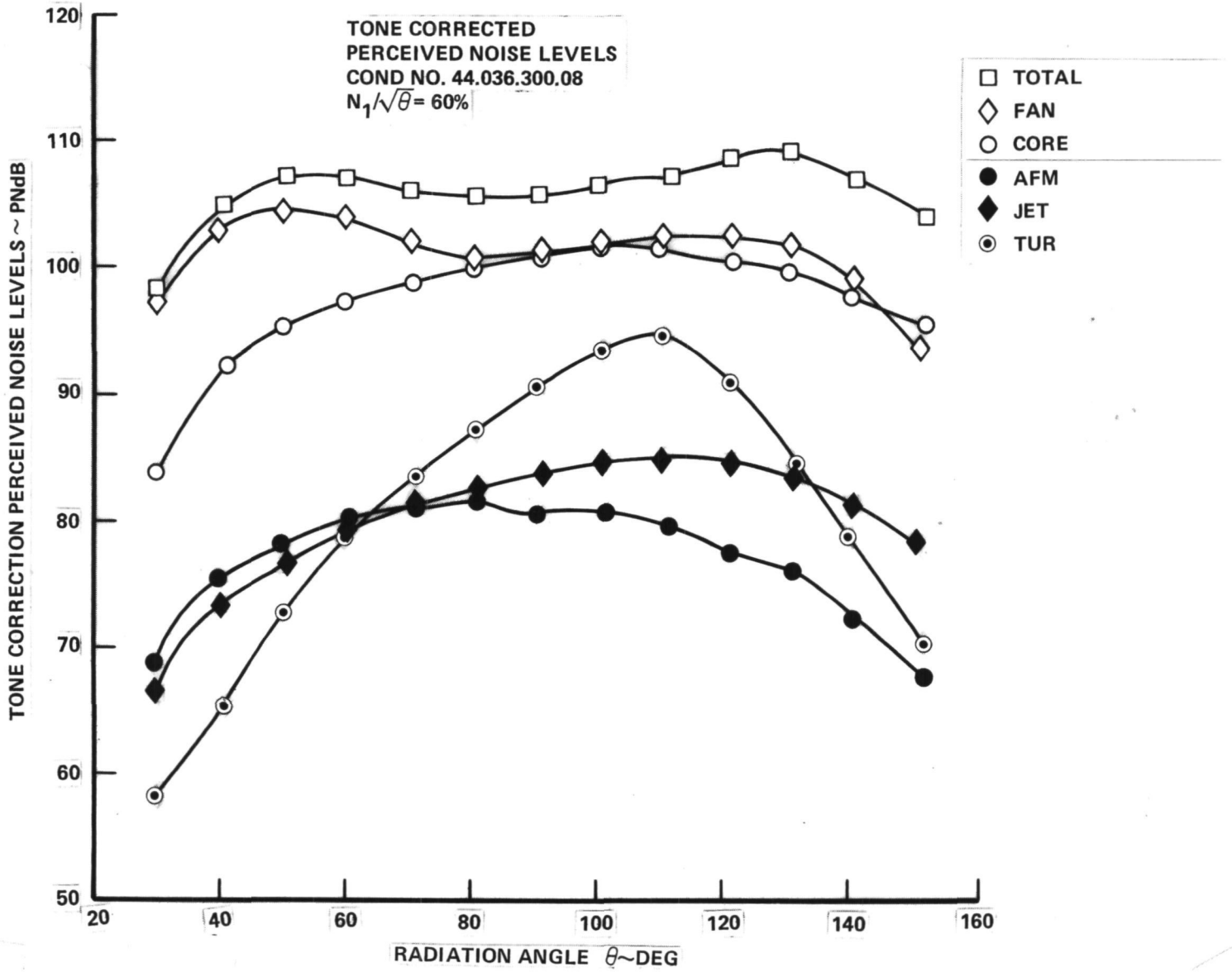

Figure 57. - Component field shape, condition no. 44.036.300.08, $N_1/\sqrt{\theta}$ = 60%.

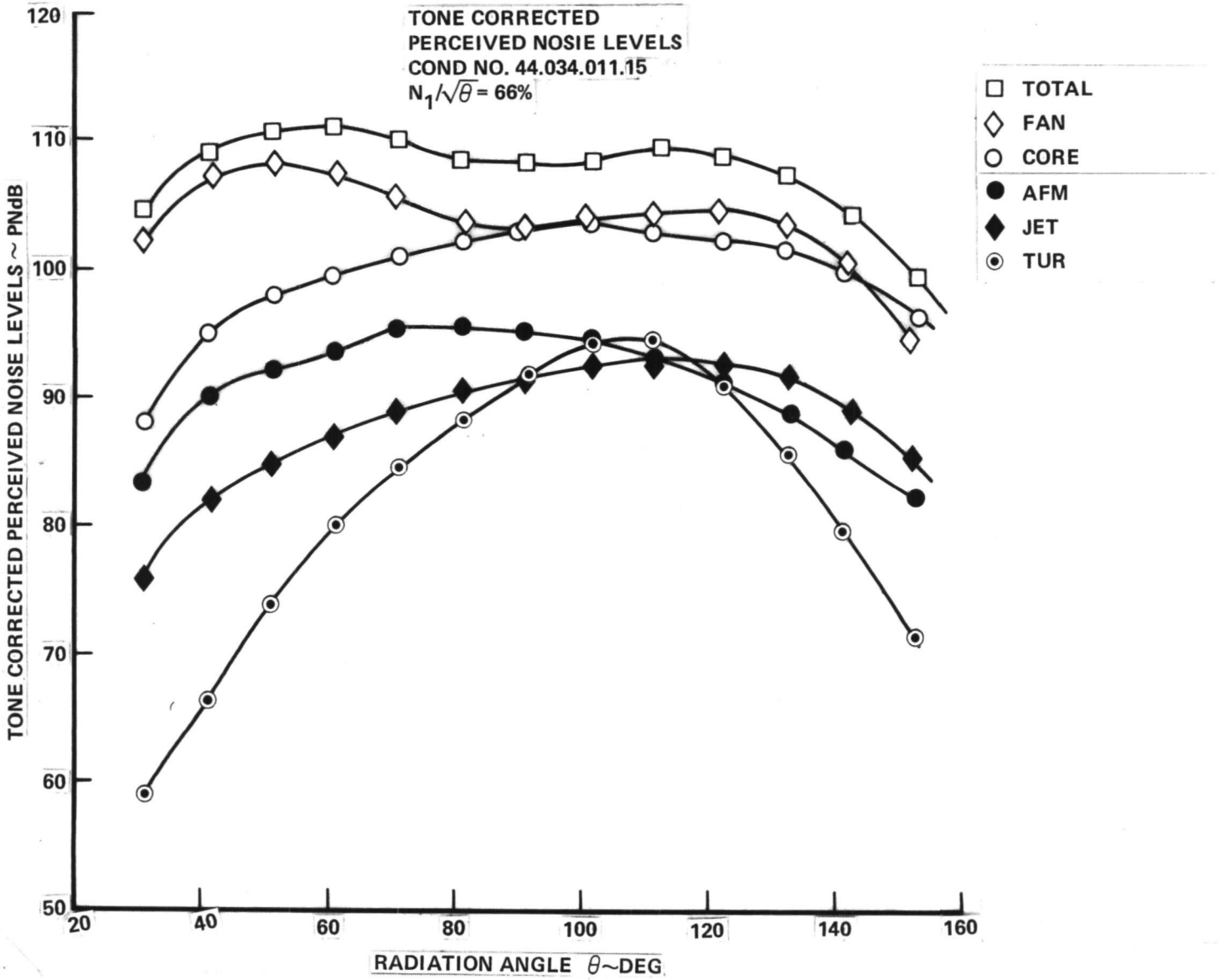

Figure 58. - Component field shape, condition no. 44.034.011.15, $N_1/\sqrt{\theta}$ = 66%.

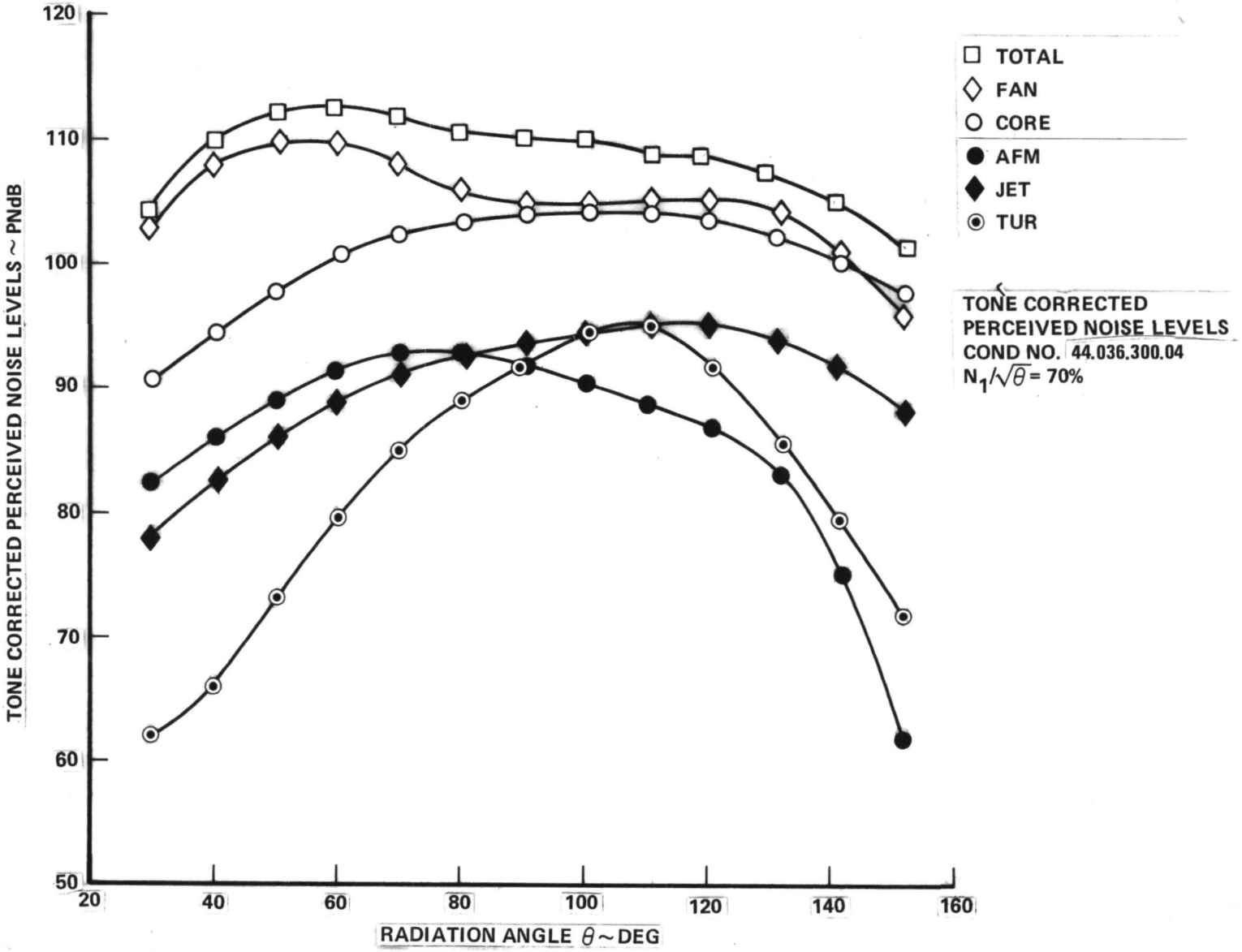

Figure 59. - Component field shape, condition no. 44.036.300.04, $N_1/\sqrt{\theta}$ = 70%.

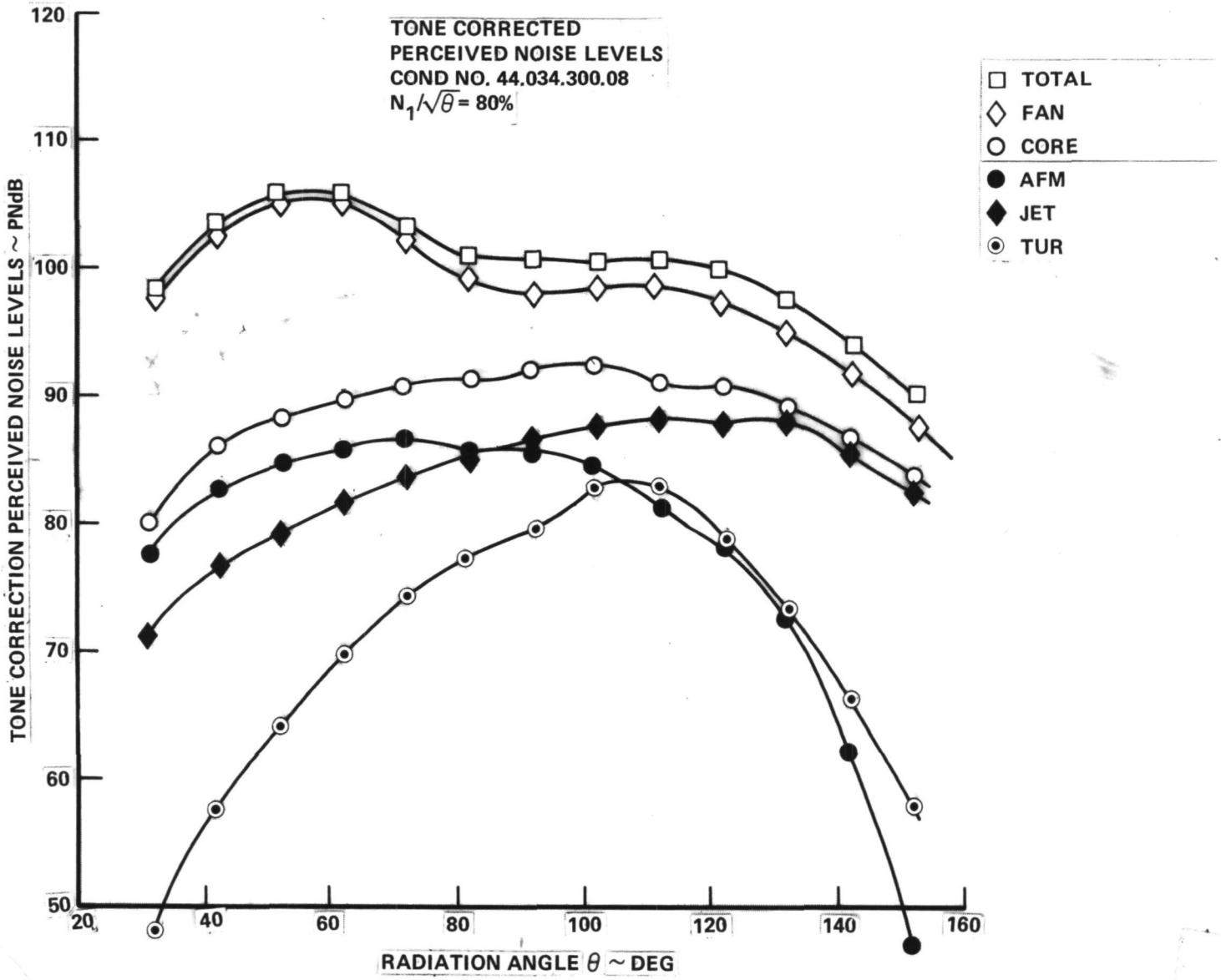

Figure 60. Component field shape, condition no. 44.034.300.08, $N_1/\sqrt{\theta}$ = 80%.

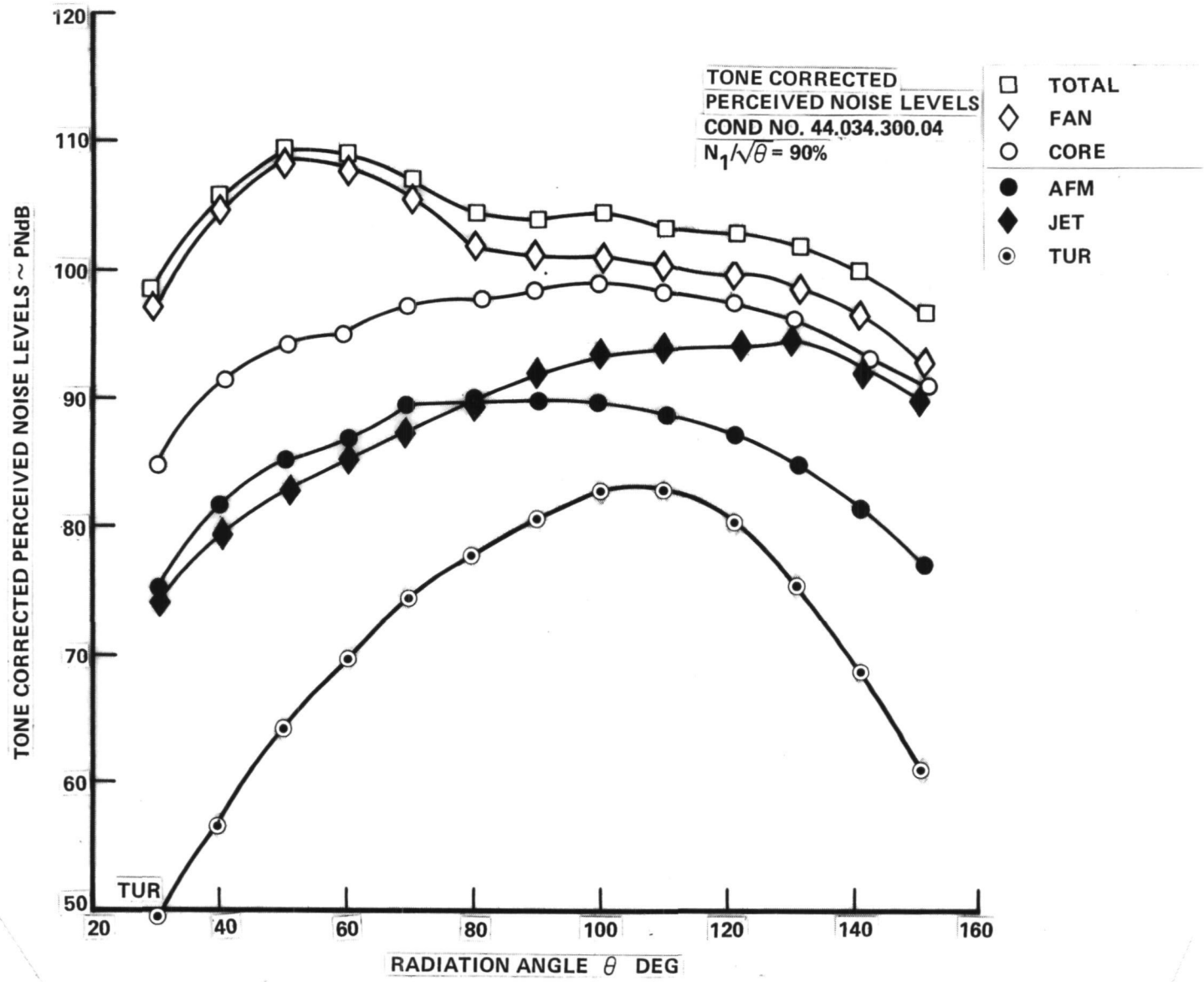

Figure 61. - Component field shape, condition no. 44.034.300.04, $N_1/\sqrt{\theta}$ = 90%.

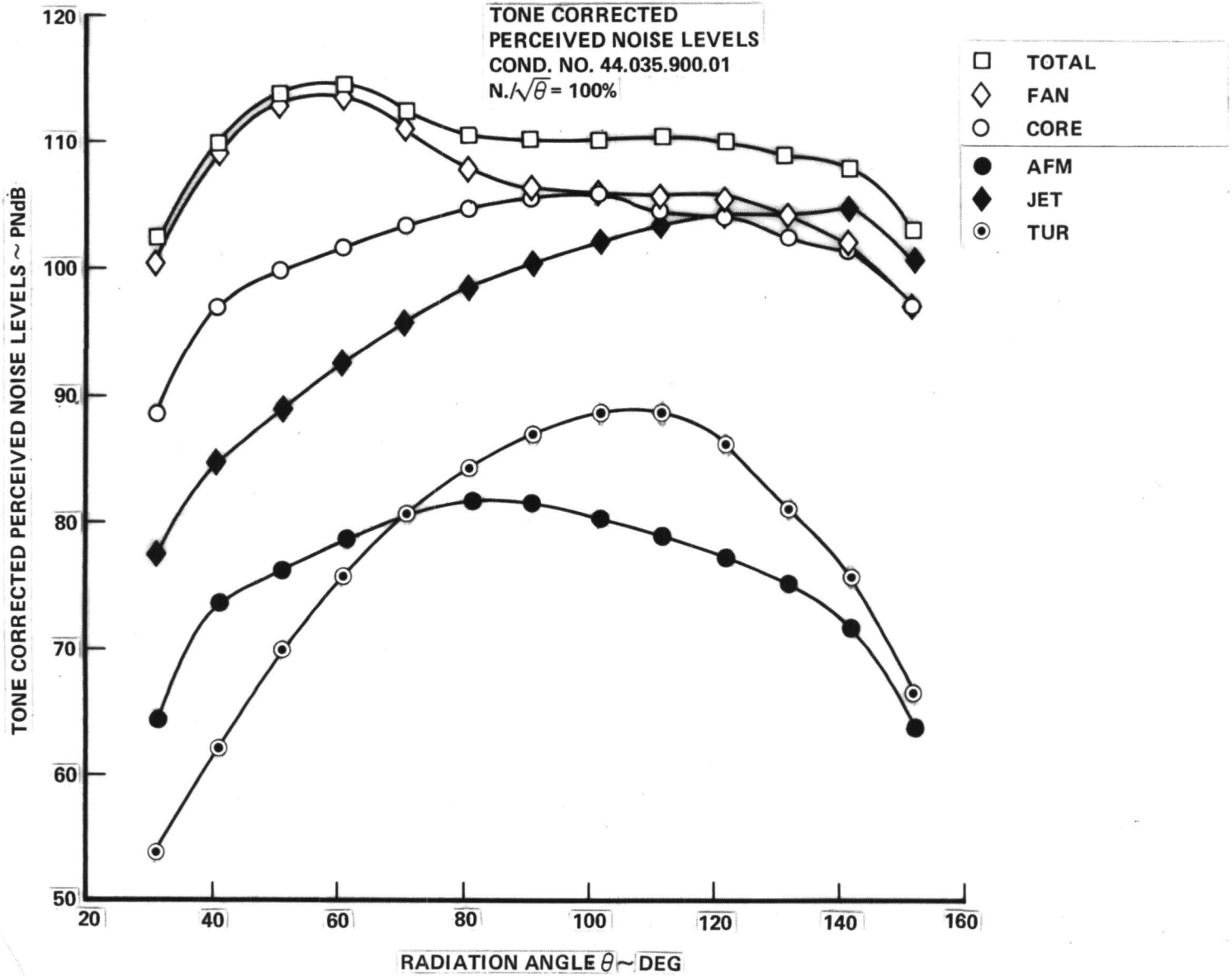

Figure 62. - Component field shape, condition no. 44.035.900.01, $N_1/\sqrt{\theta}$ = 100%.

TABLE 17. - RANKING OF NOISE SOURCES FROM FIELD SHAPES

$N_1/\sqrt{\theta} \sim$ %	60	66	70	80	90	100
Source						
Fan	1	1	1	1	1	1
Core	2	2	2	2	2	2
Jet	4	4	3	3	3	3
Airframe	3	5	5	5	5	4
Turbine	5	3	4	4	4	5

4.1.2 Third-octave band sound pressure levels. - Plots were made from third-octave band sound pressure levels of each noise component output from ANOPP. These spectra are shown in figures 63 through 92.

4.2 Correction of Predicted Noise Levels to Measured Noise Levels

4.2.1 Perceived noise levels. - Differences between predicted and measured tone corrected perceived noise levels are plotted as a function of radiation angle in figures 93 and 94. These are grouped together for the low and for the high power settings with an average curve computed for each. By applying the average curve that lies in the appropriate power settings range, ANOPP can only be corrected to agree with measured data within a 3 PNdB difference in most cases. Therefore, it is necessary to select a difference curve for each specific condition. Linear interpolations for other power settings can be made.

To obtain PNLT component noise it is necessary to assume that the directivity and relative magnitude of the various sources are correctly predicted by ANOPP. Then, applying the previously cited difference curves to each noise source, the flight corrected PNLT component noise is known. This procedure need only be done for the dominant noise sources of the test condition.

4.2.2 Third octave band sound pressure levels. - Corrections have been computed to adjust predicted source sound pressure levels to measured values. For the engine conditions and noise source components shown in table 18 the frequency range of these corrections is specified. The SPL corrections are presented in tables 19 through 24 for each $N_1/\sqrt{\theta}$ as a function of radiation angle and frequency. To adjust the predicted spectra, the ΔdB SPL is then subtracted from each component sources SPL in its frequency range. Where the frequencies overlap, corrections should be applied to each of the components.

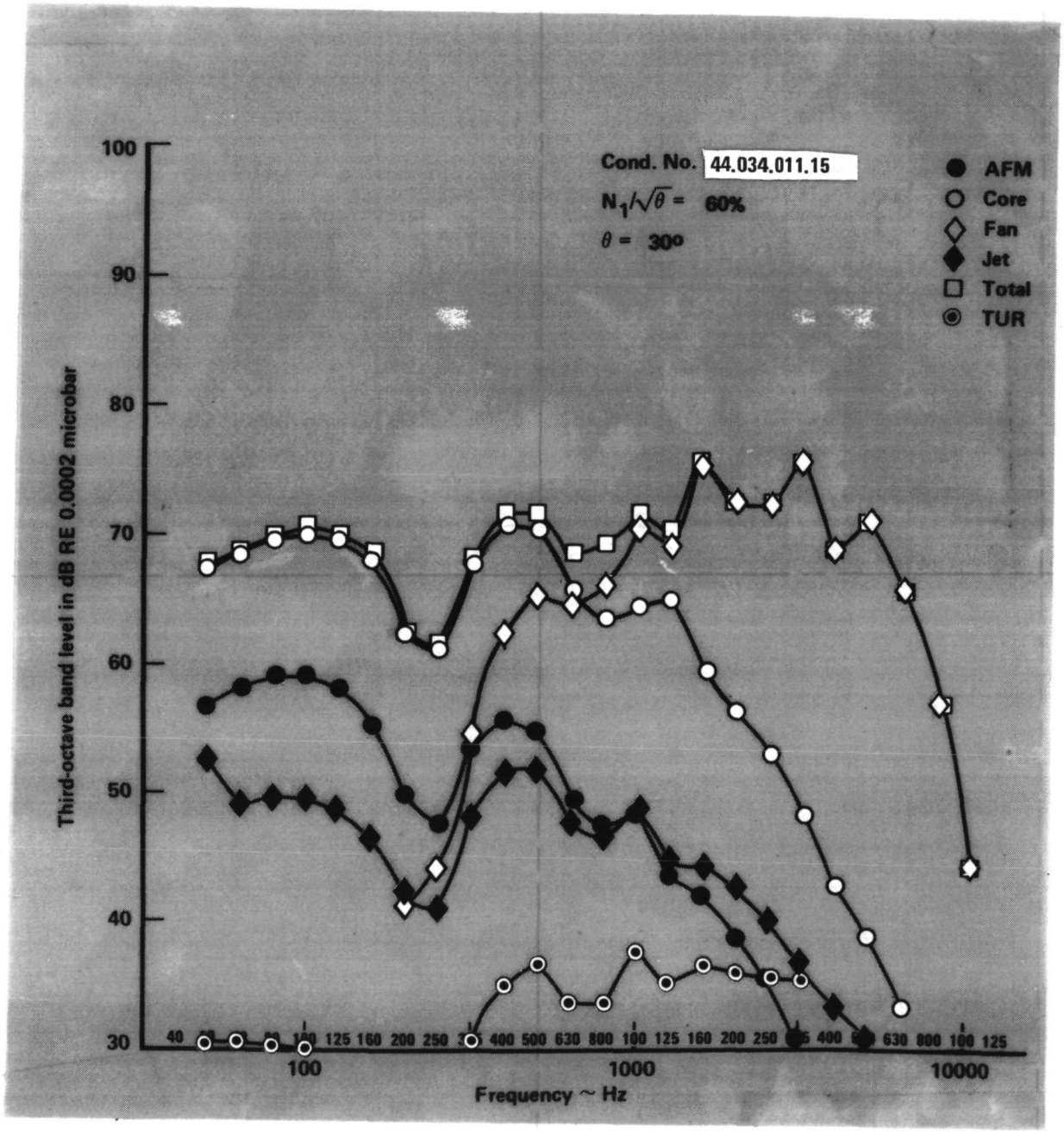

Figure 63. - Component spectra, condition no. 44.034.011.15, $\theta = 30^{\circ}$.

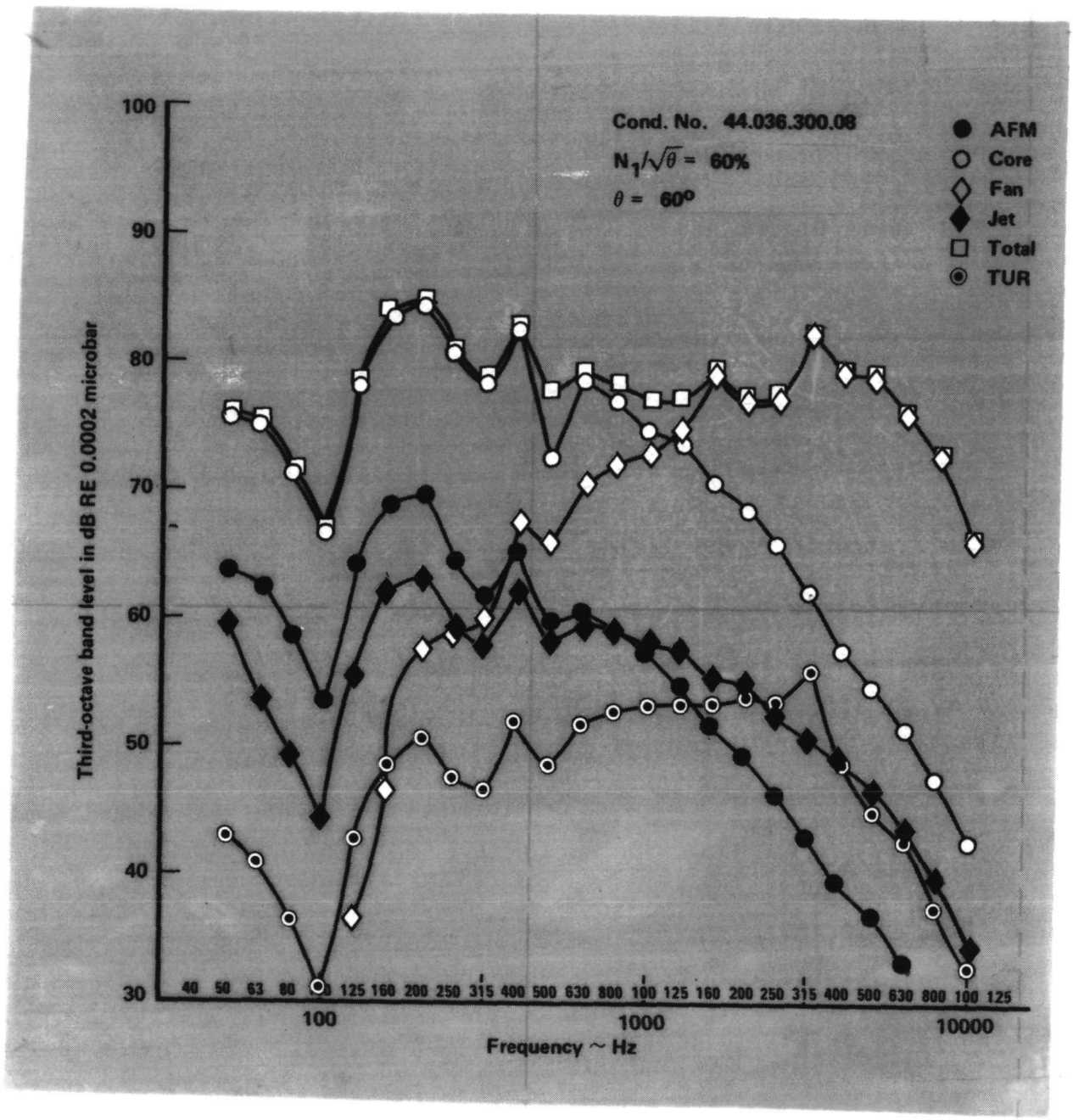

Figure 64. - Component spectra, condition no. 44.036.300.08, θ = 60°.

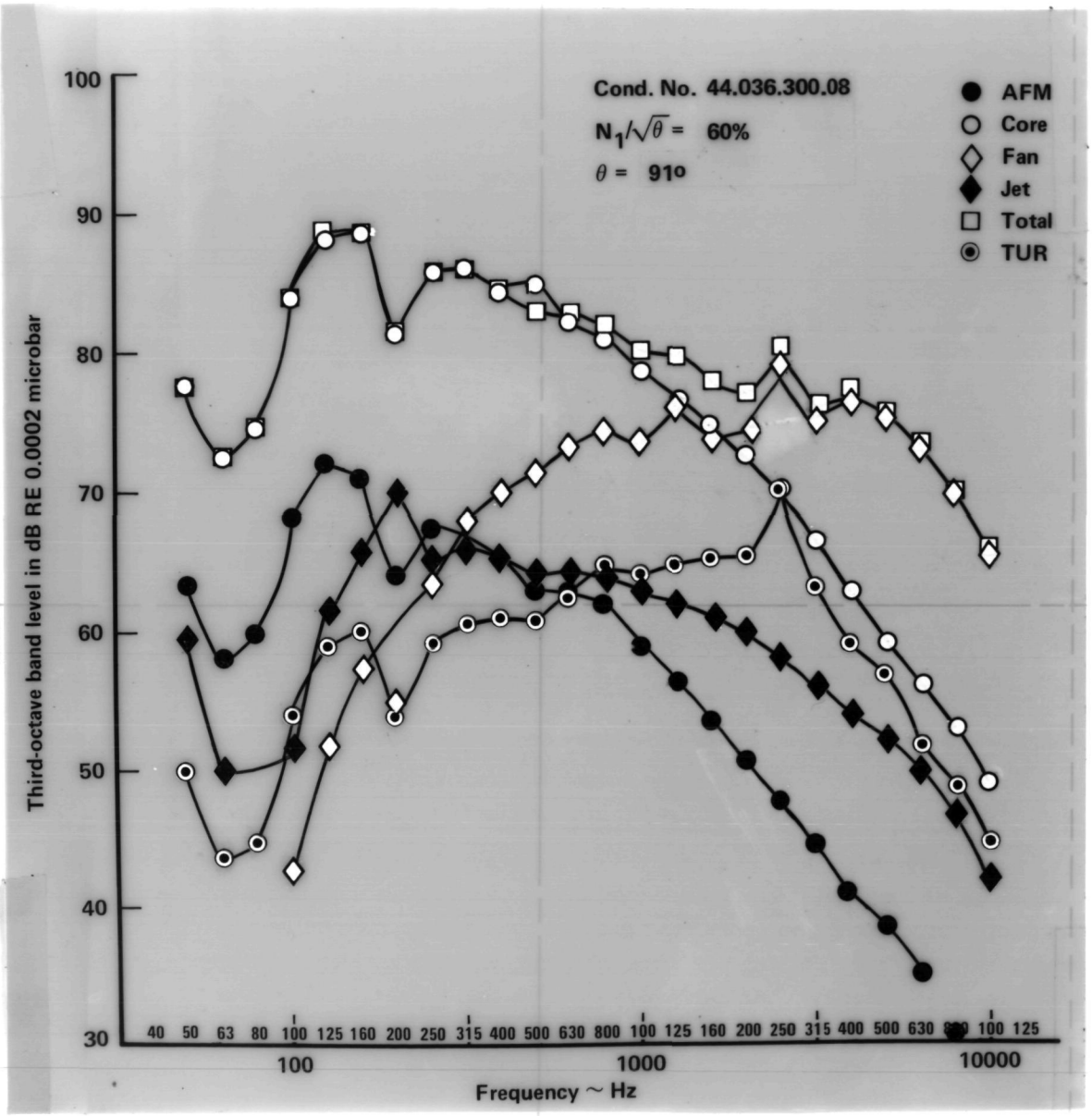

Figure 65. - Component spectra, condition no. 44.036.300.08, $\theta = 91^{\circ}$.

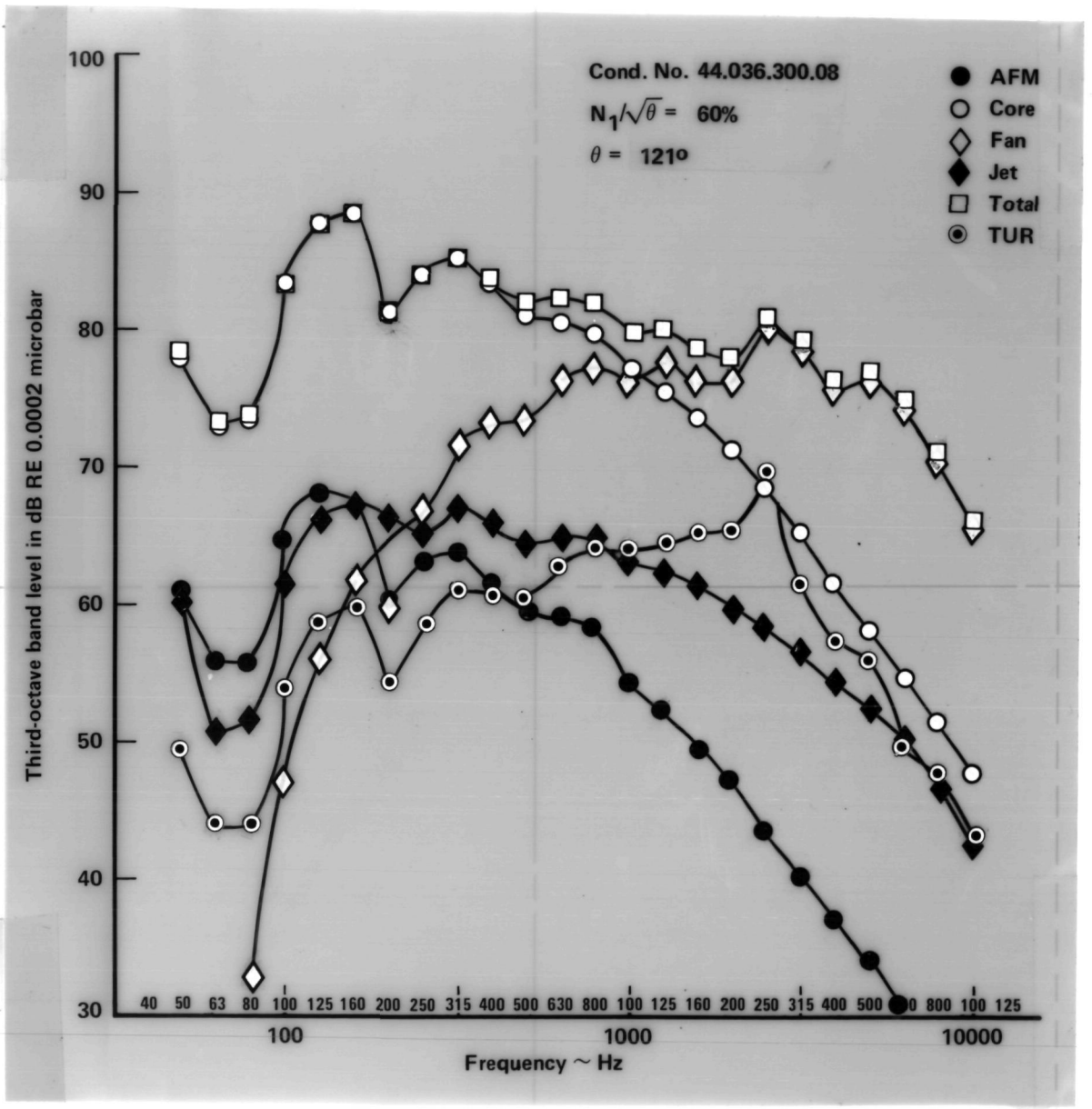

Figure 66. - Component spectra, condition no. 44.036.300.08, θ = 121°.

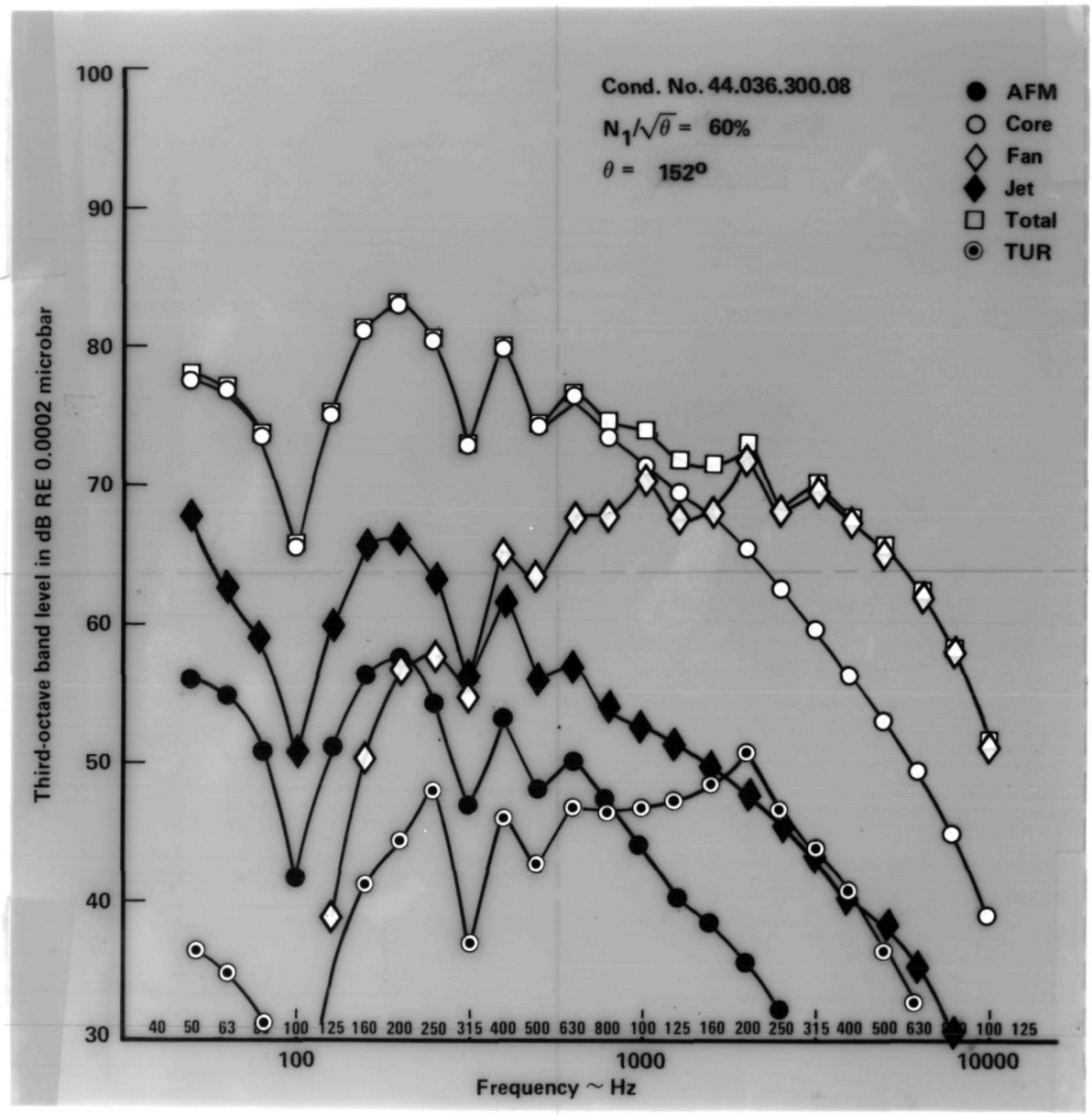

Figure 67. - Component spectra, condition no. 44.036.300.08, θ = 152°.

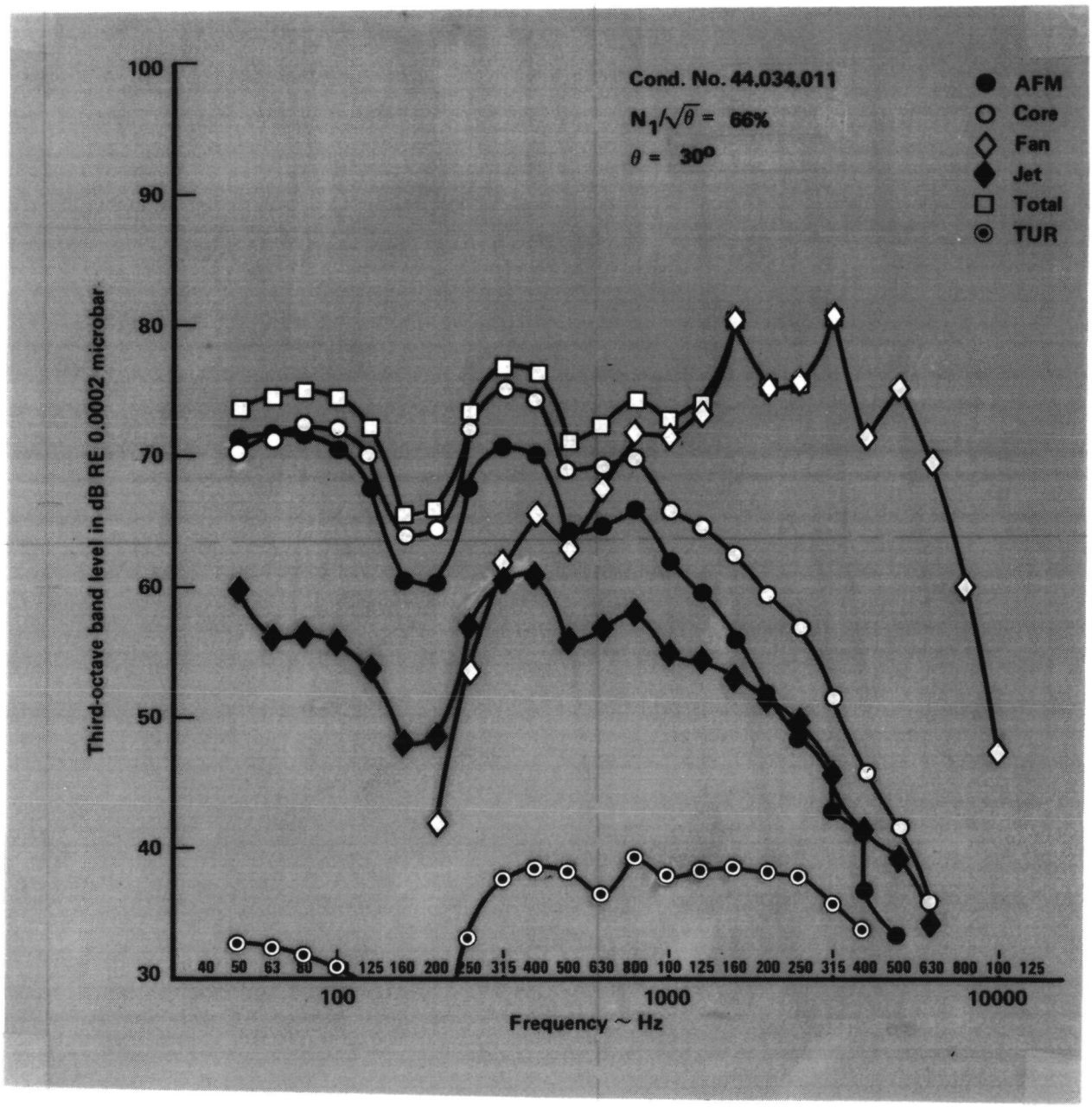

Figure 68. - Component spectra, condition no. 44.034.011.15, $\theta = 30^{\circ}$.

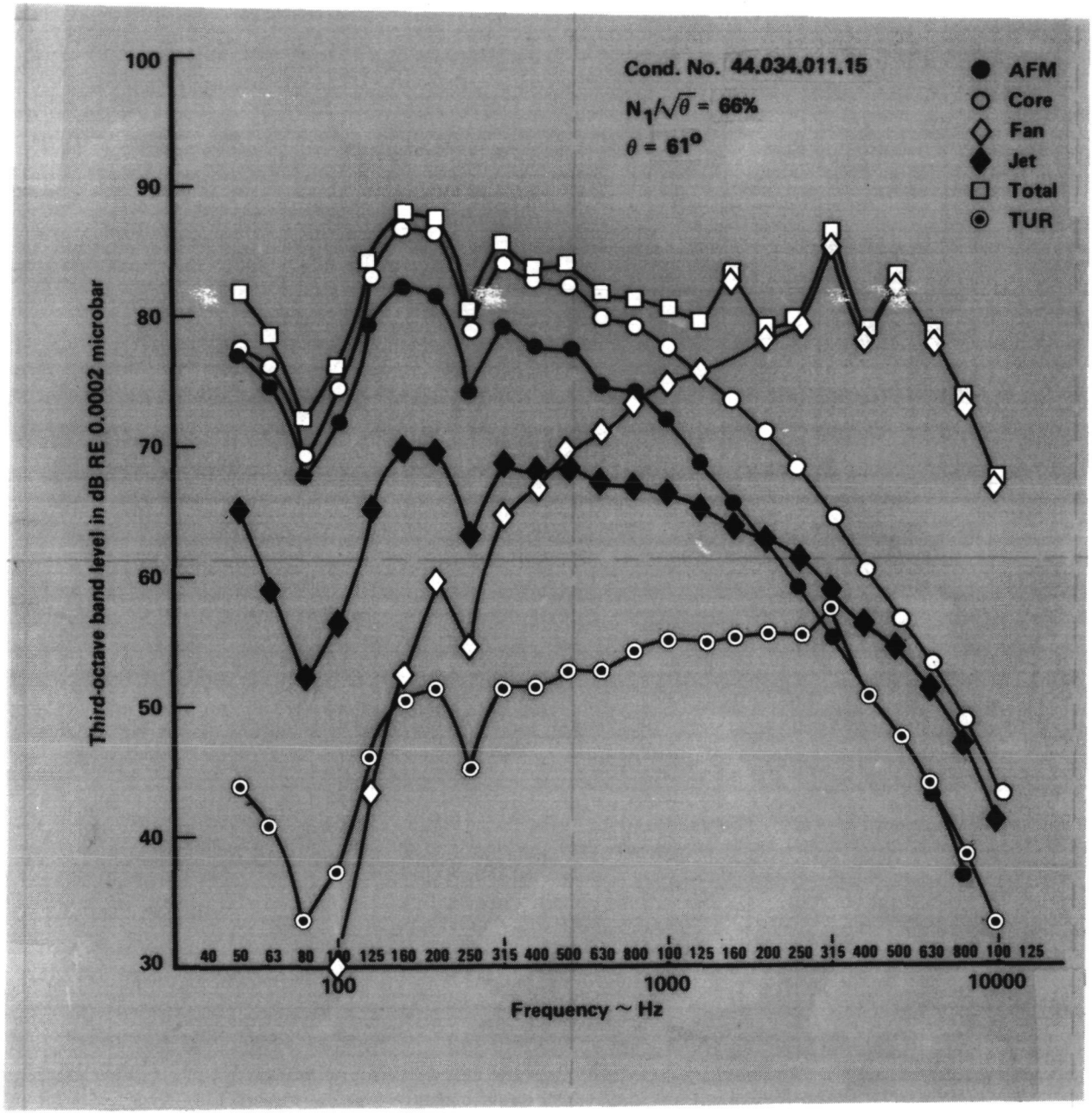

Figure 69. - Component spectra, condition no. 44.034.011.15, θ = 61°.

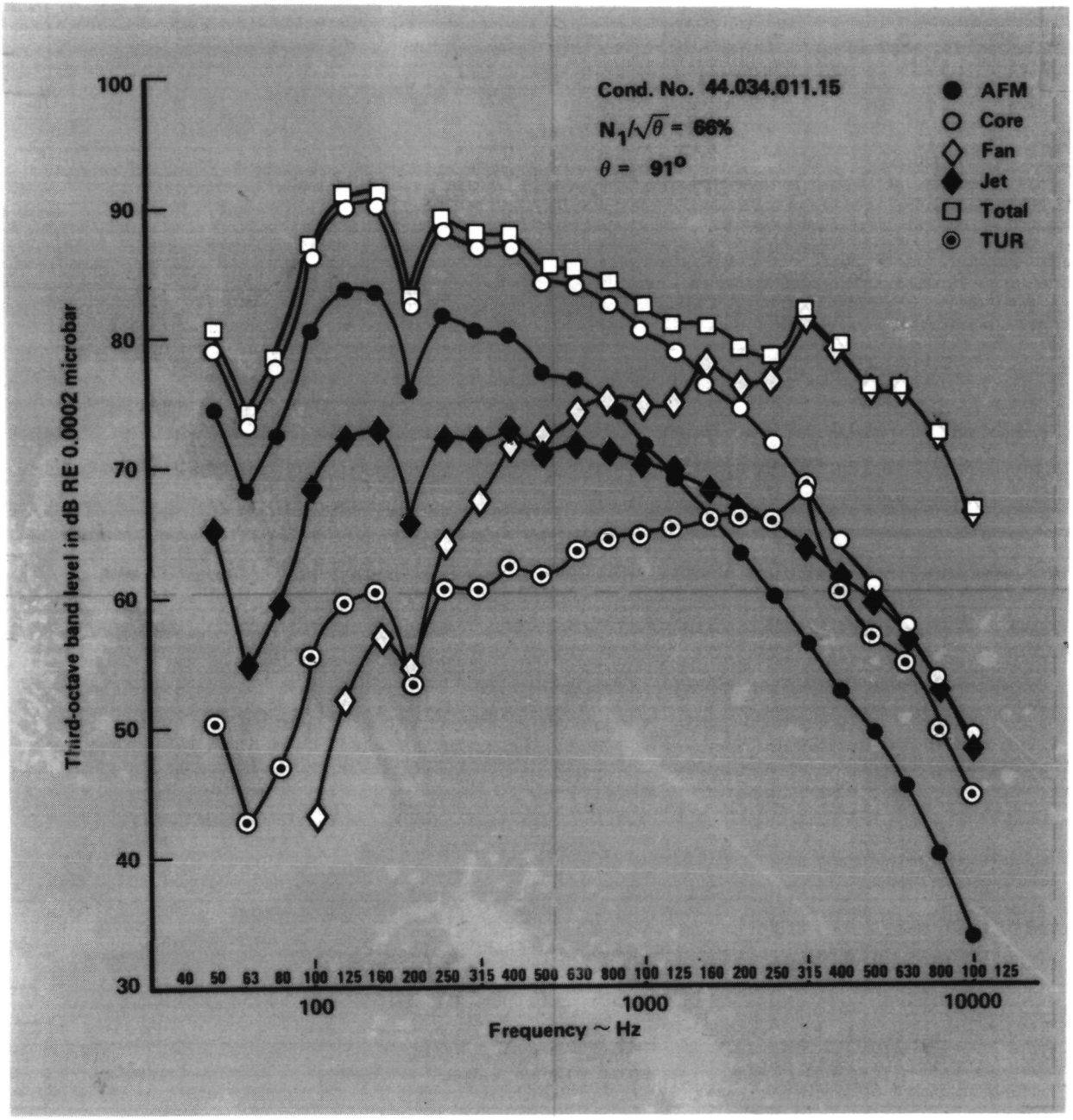

Figure 70. - Component spectra, condition no. 44.034.011.15, θ = 91°.

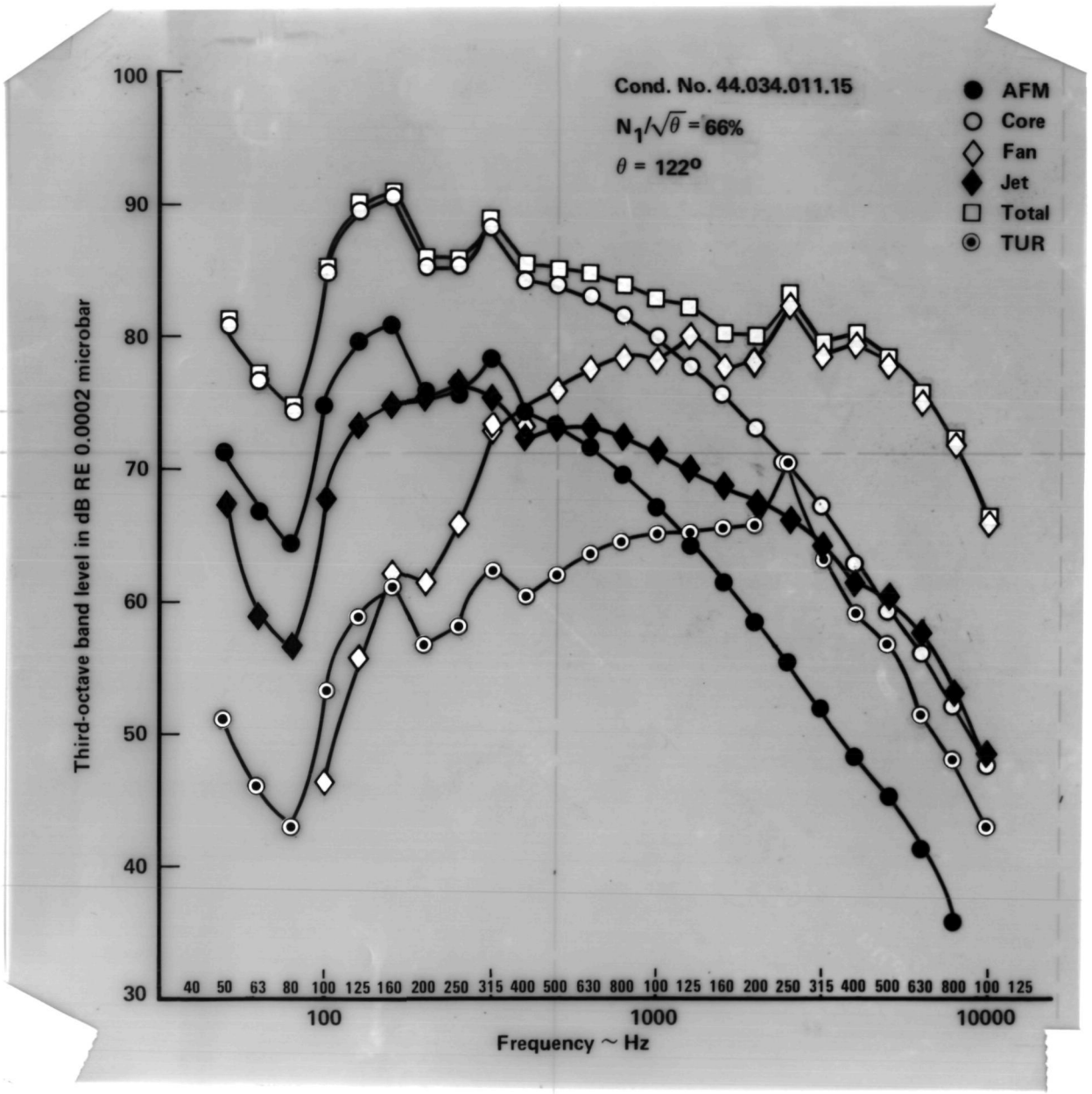

Figure 71. - Component spectra, condition no. 44.034.011.15, = 122°.

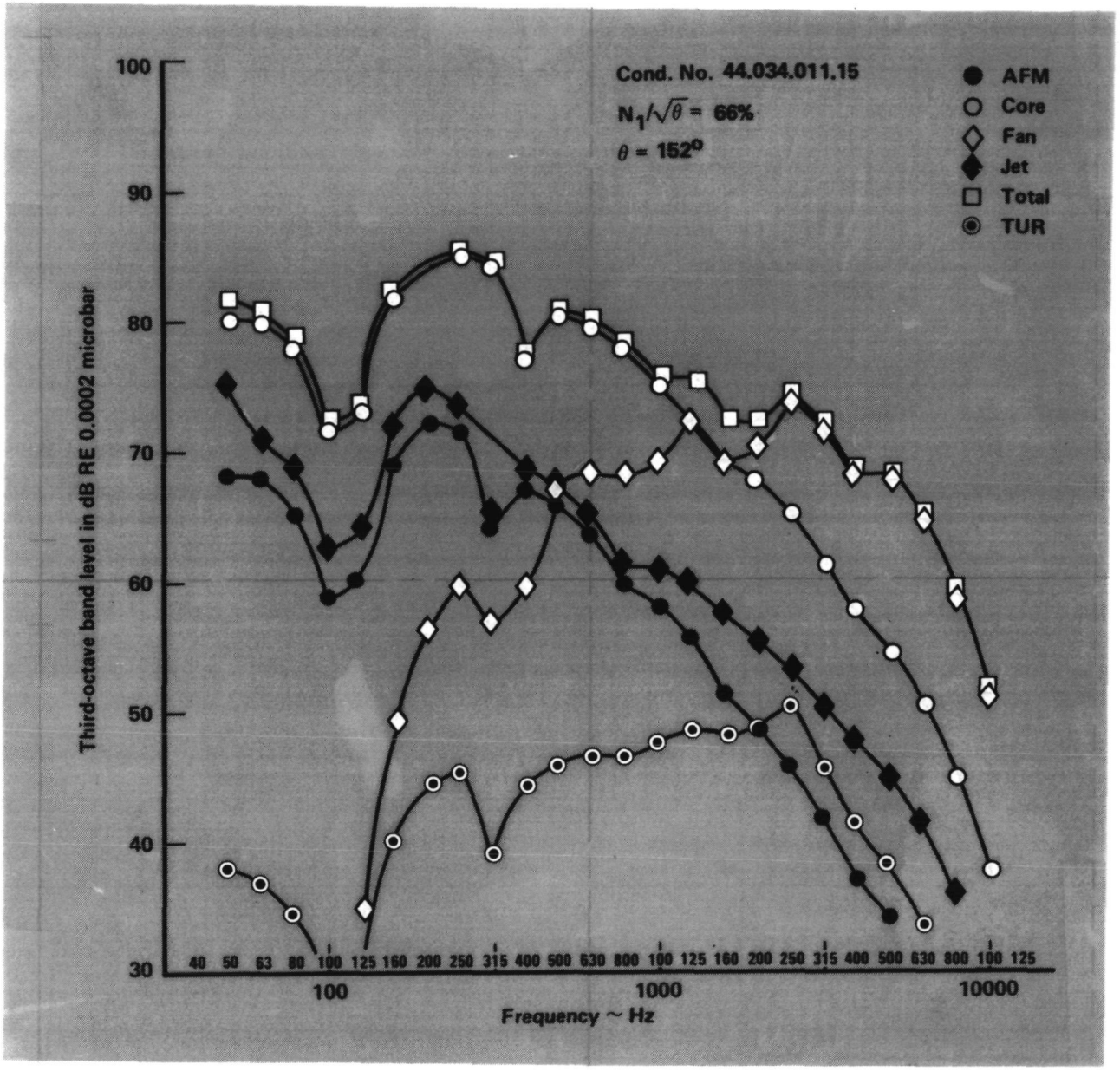

Figure 72. - Component spectra, condition no. 44.034.011.15, θ = 152°.

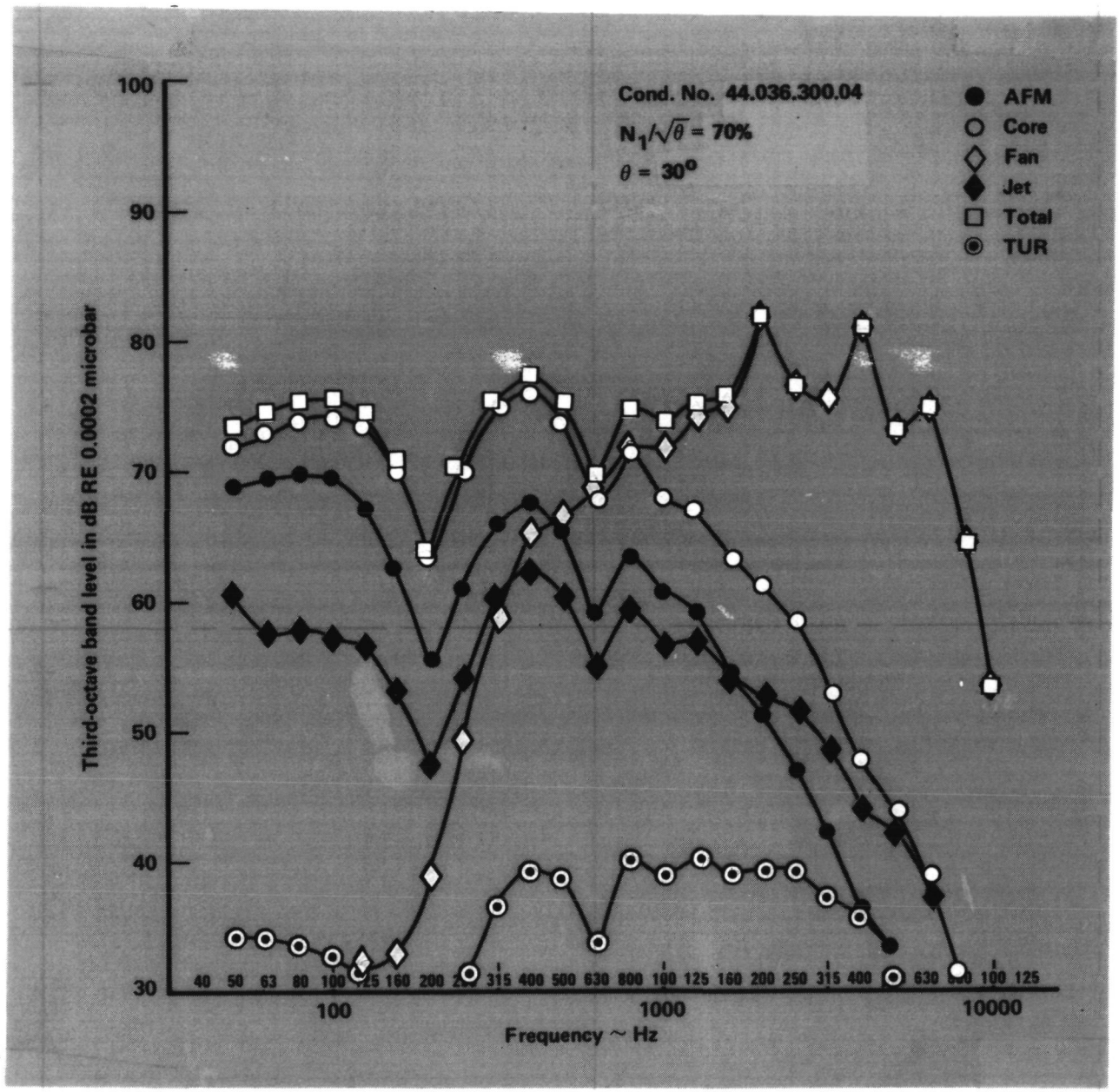

Figure 73. - Component spectra, condition no. 44.036.300.04, $\theta = 30^{\circ}$.

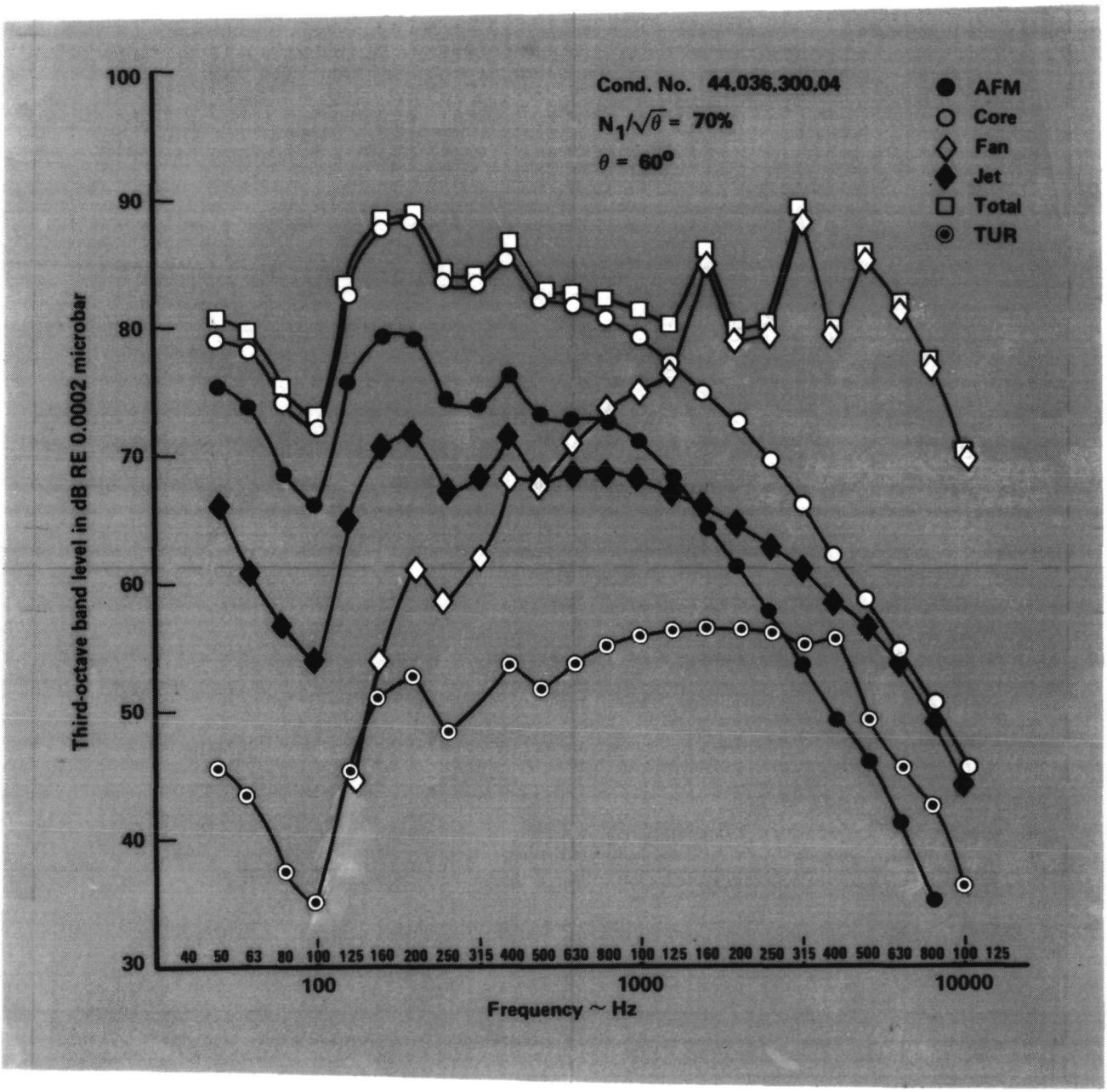

Figure 74. - Component spectra, condition no. 44.036.300.04, $\theta = 60^{\circ}$.

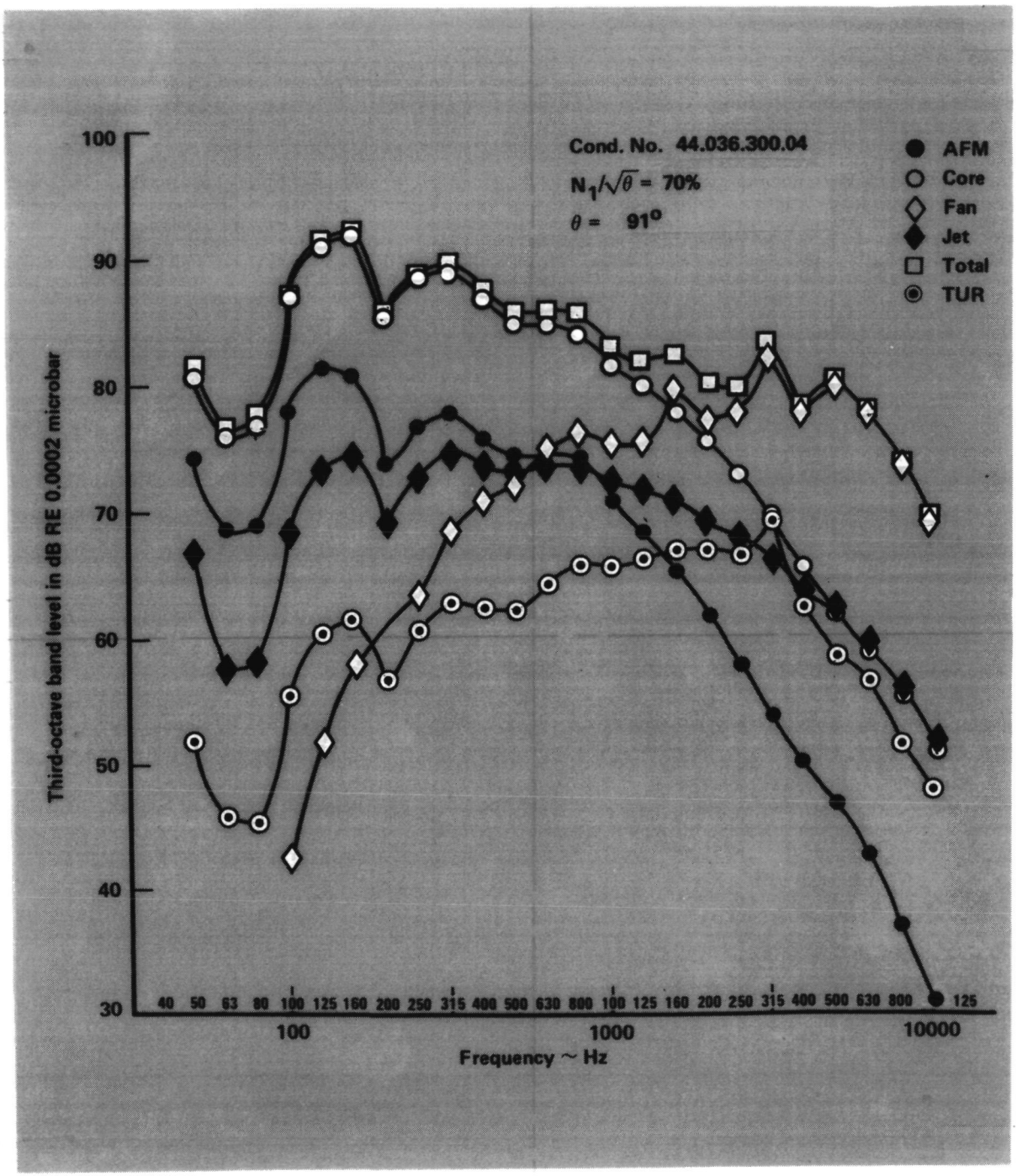

Figure 75. - Component spectra, condition no. 44.036.300.04, $\theta = 91^{\circ}$.

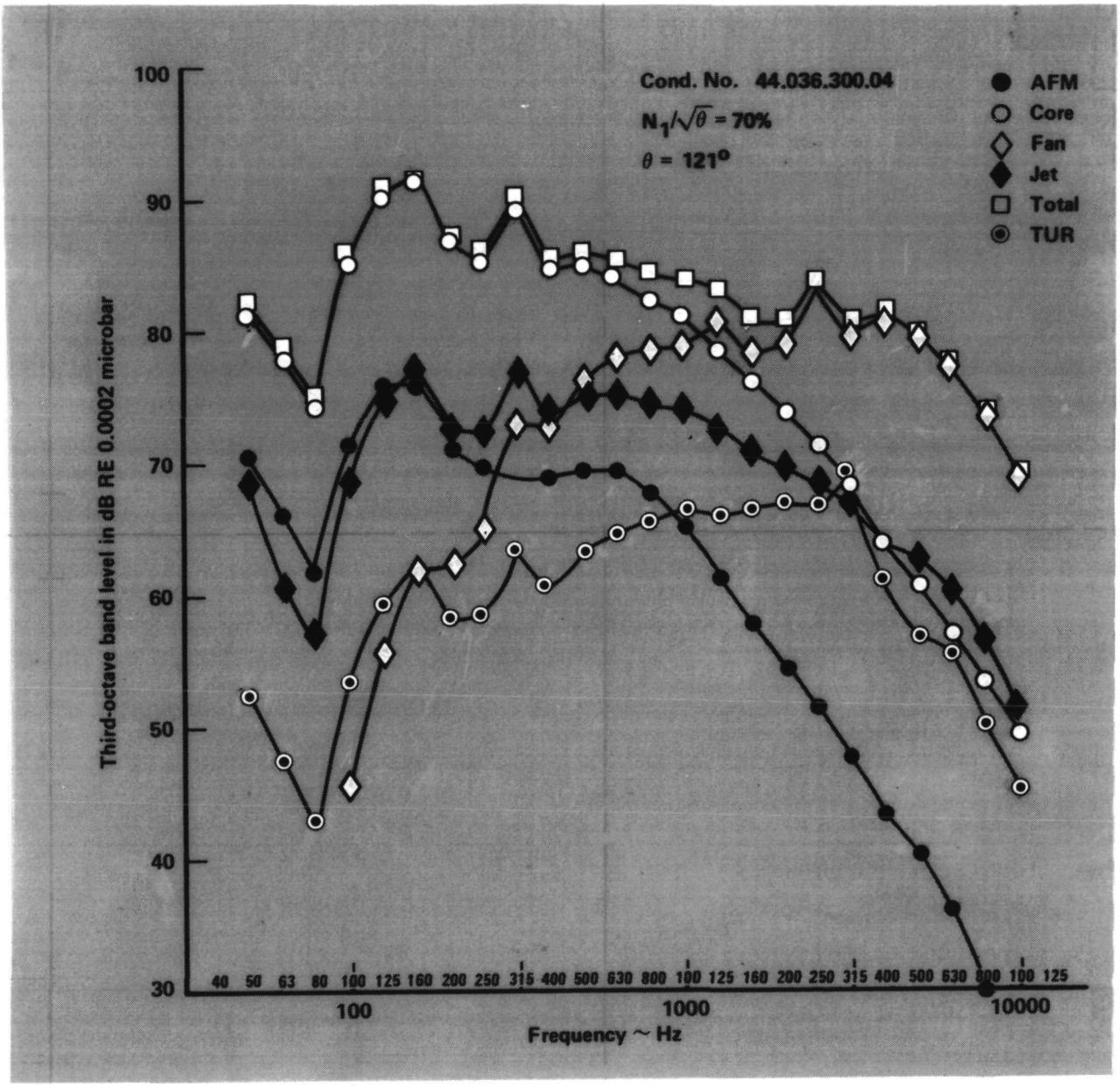

Figure 76. - Component spectra, condition no. 44.036.300.04, θ = 121°.

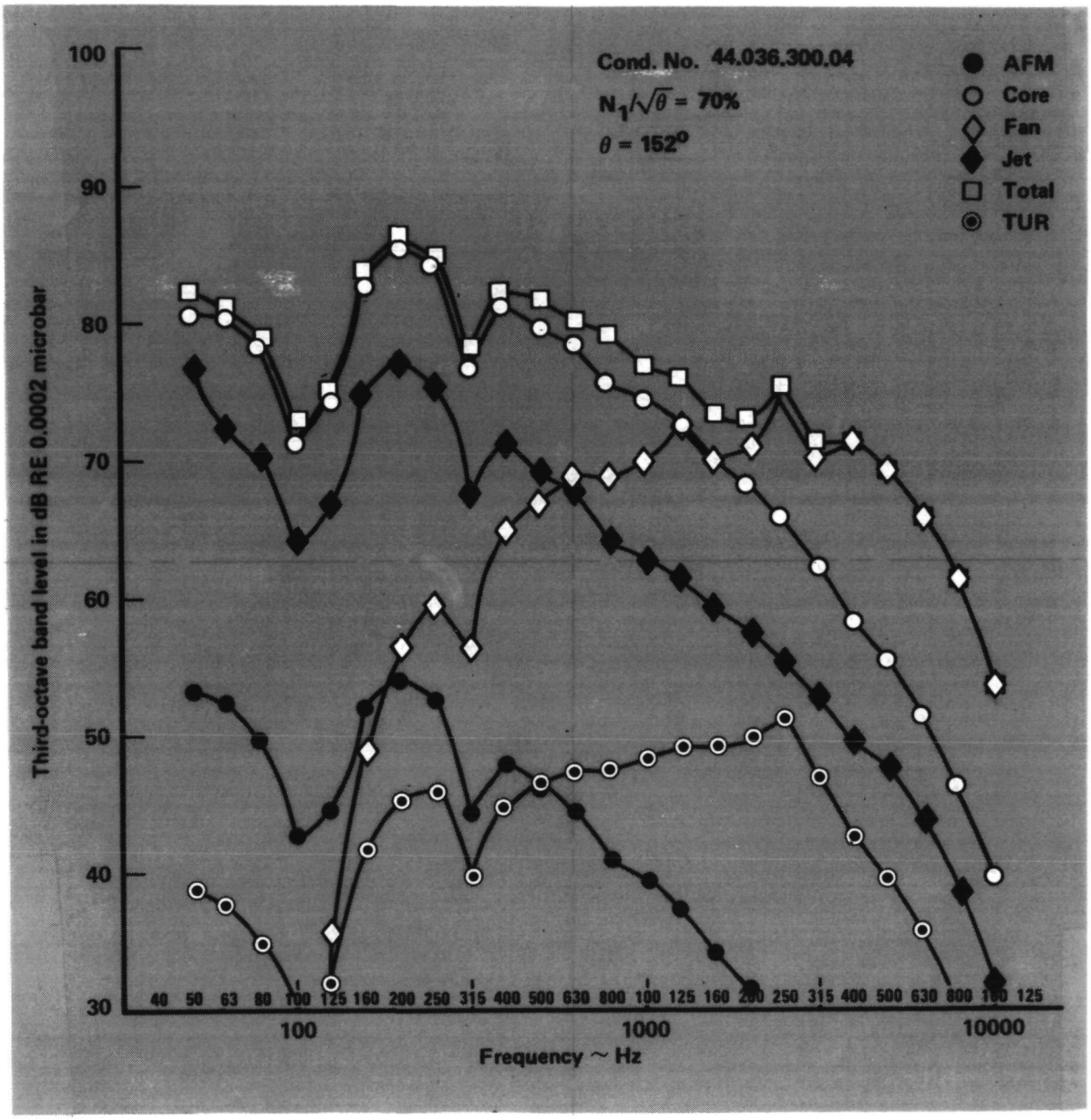

Figure 77. - Component spectra, condition no. 44.036.300.04, $\theta = 152^{\circ}$.

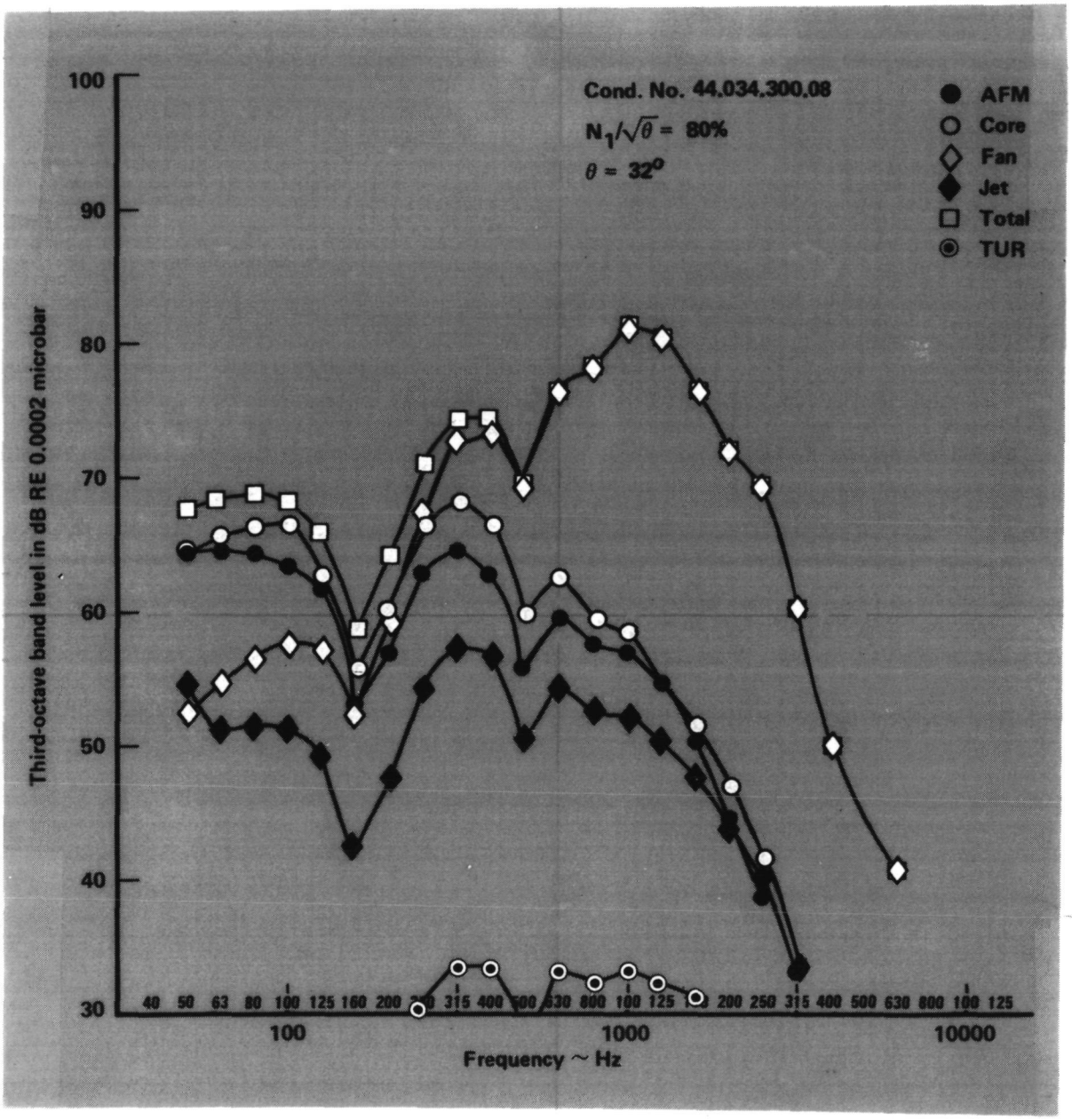

Figure 78. - Component spectra, condition no. 44.034.300.08, θ = 32°.

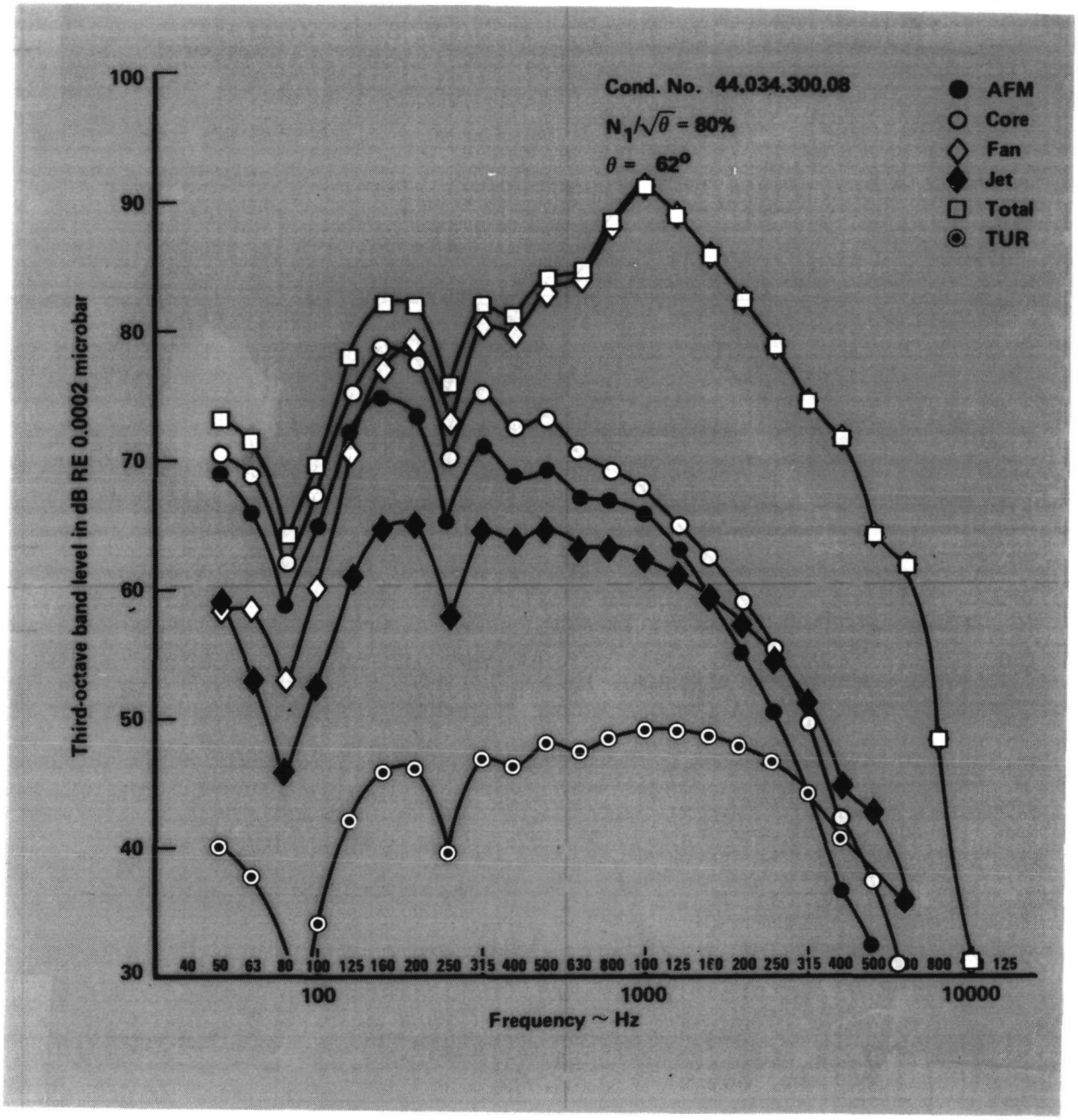

Figure 79. - Component spectra, condition no. 44.034.300.08, θ = 62°.

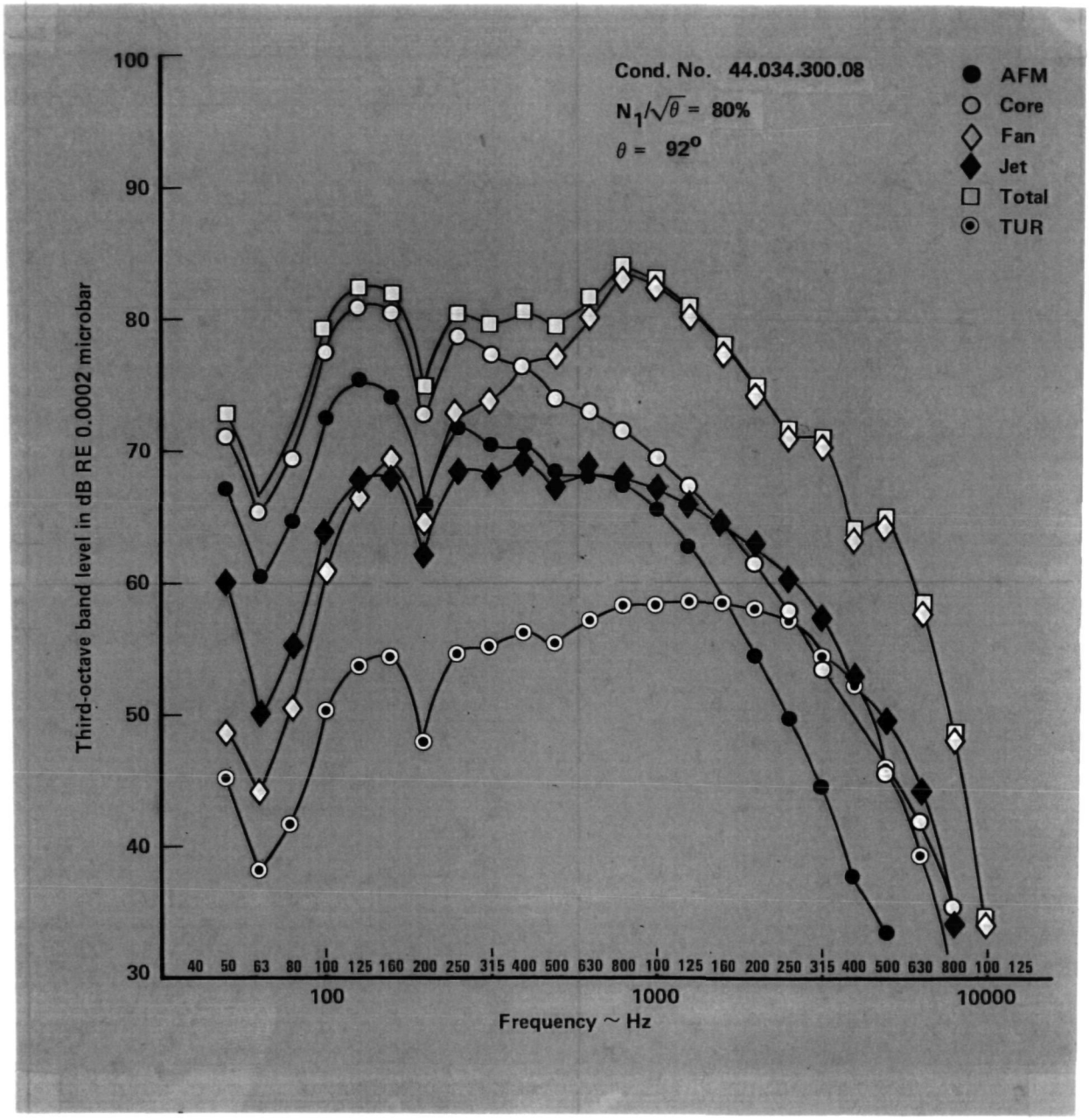

Figure 80. - Component spectra, condition no. 44.034.300.08, $\theta = 92^{\circ}$.

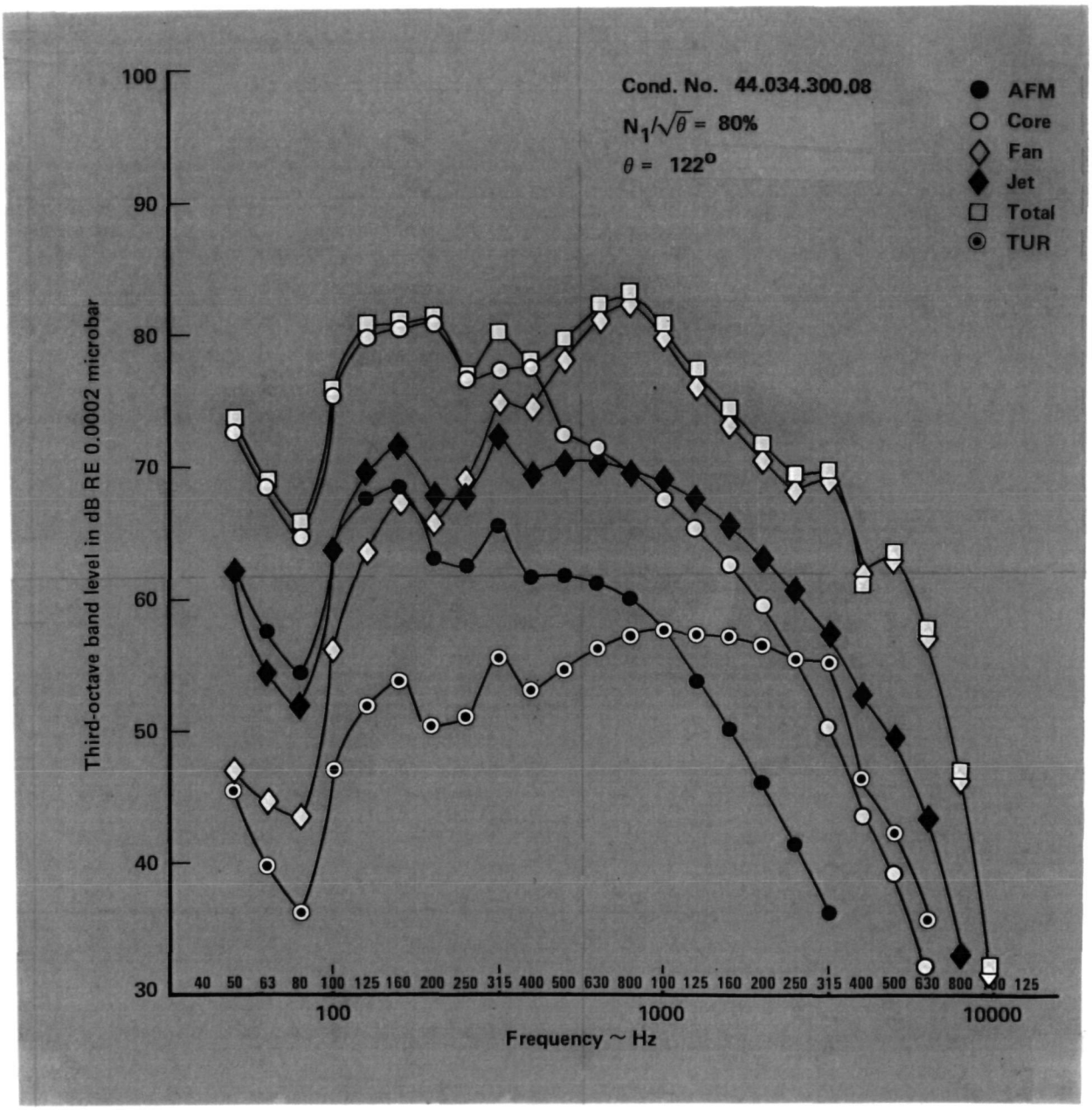

Figure 81. - Component spectra, condition no. 44.034.300.08, θ = 122°.

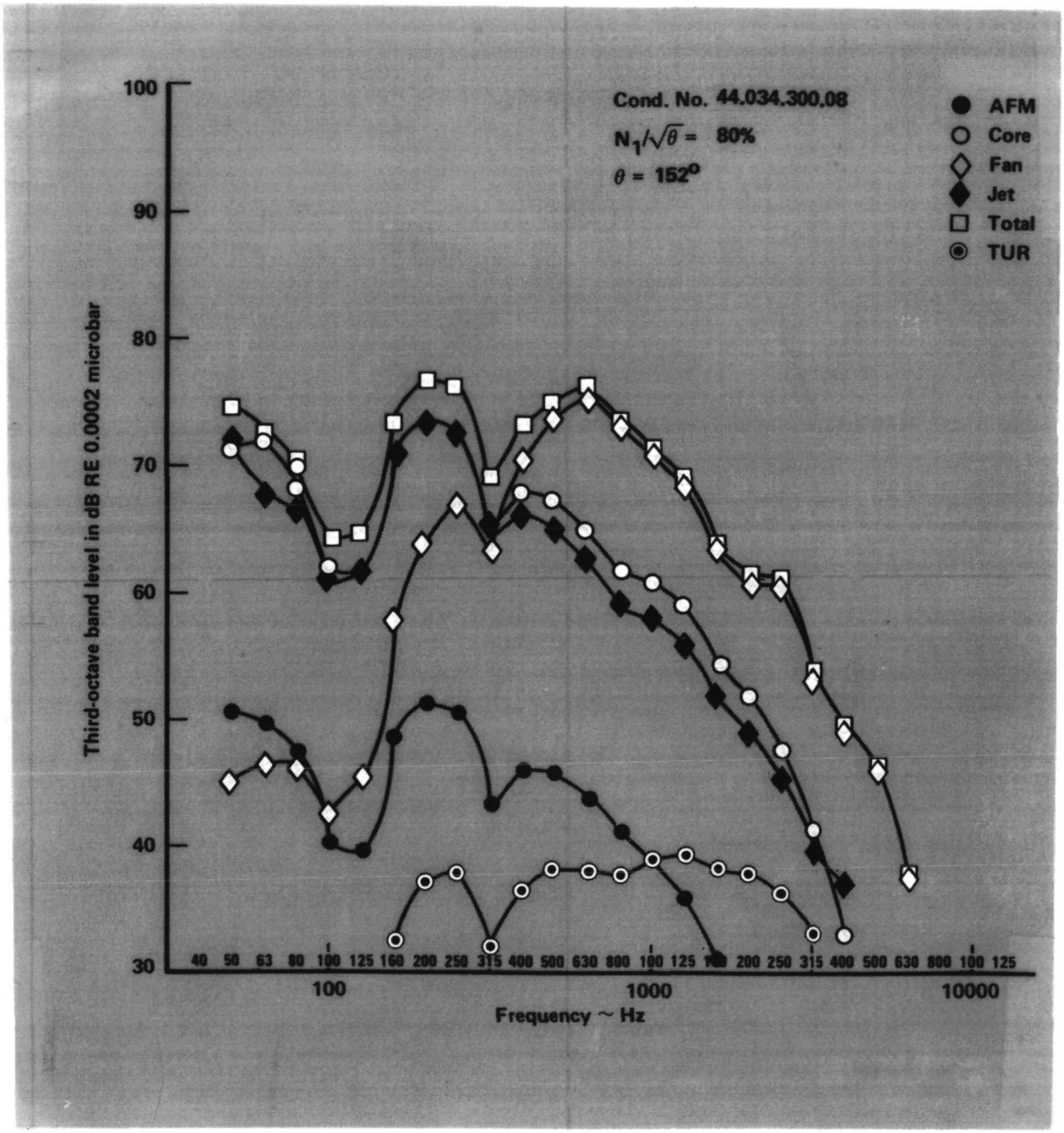

Figure 82. - Component spectra, condition no. 44.034.300.08, θ = 152°.

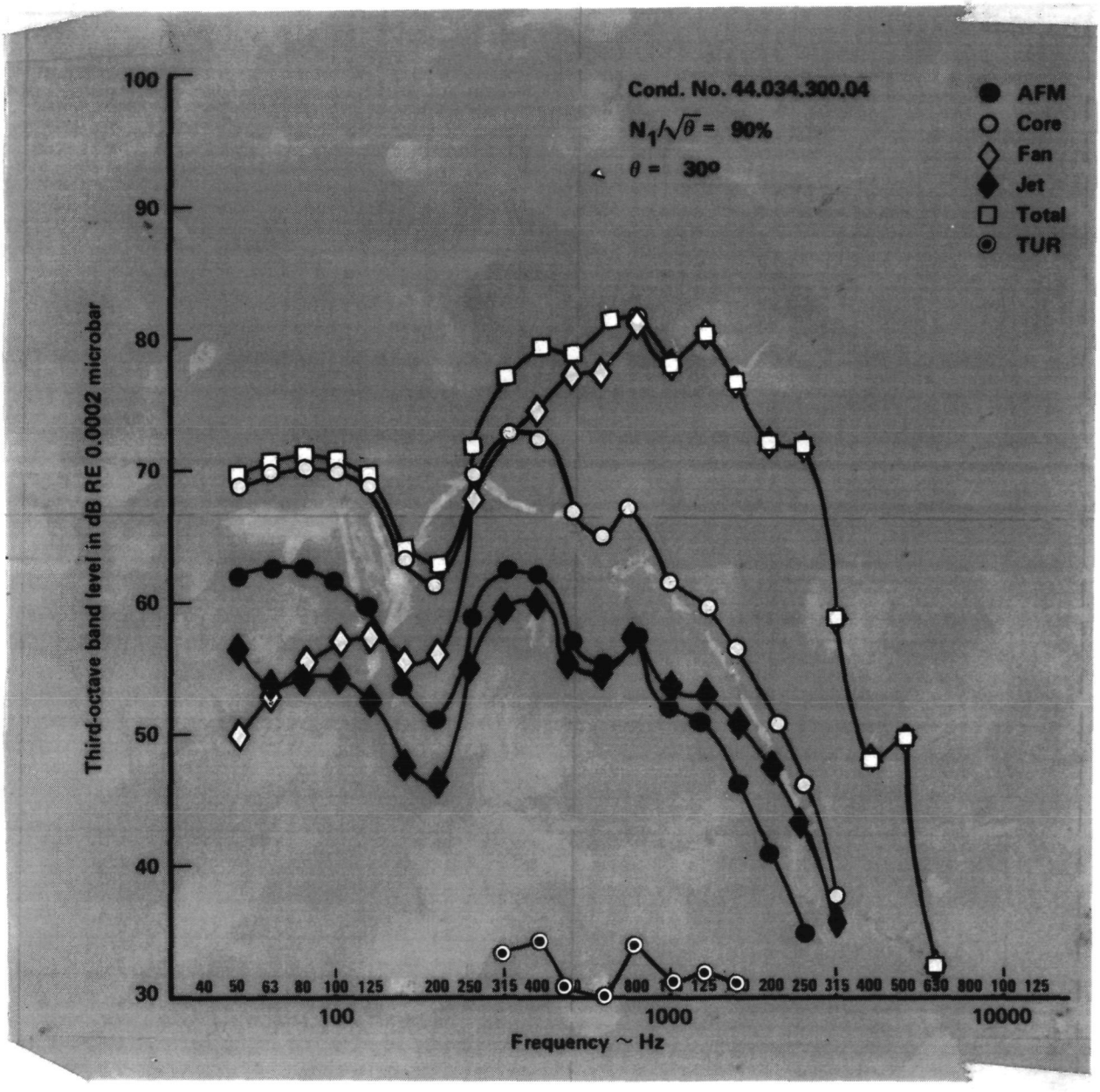

Figure 83. - Component spectra, condition no. 44.034.300.04, = 30°.

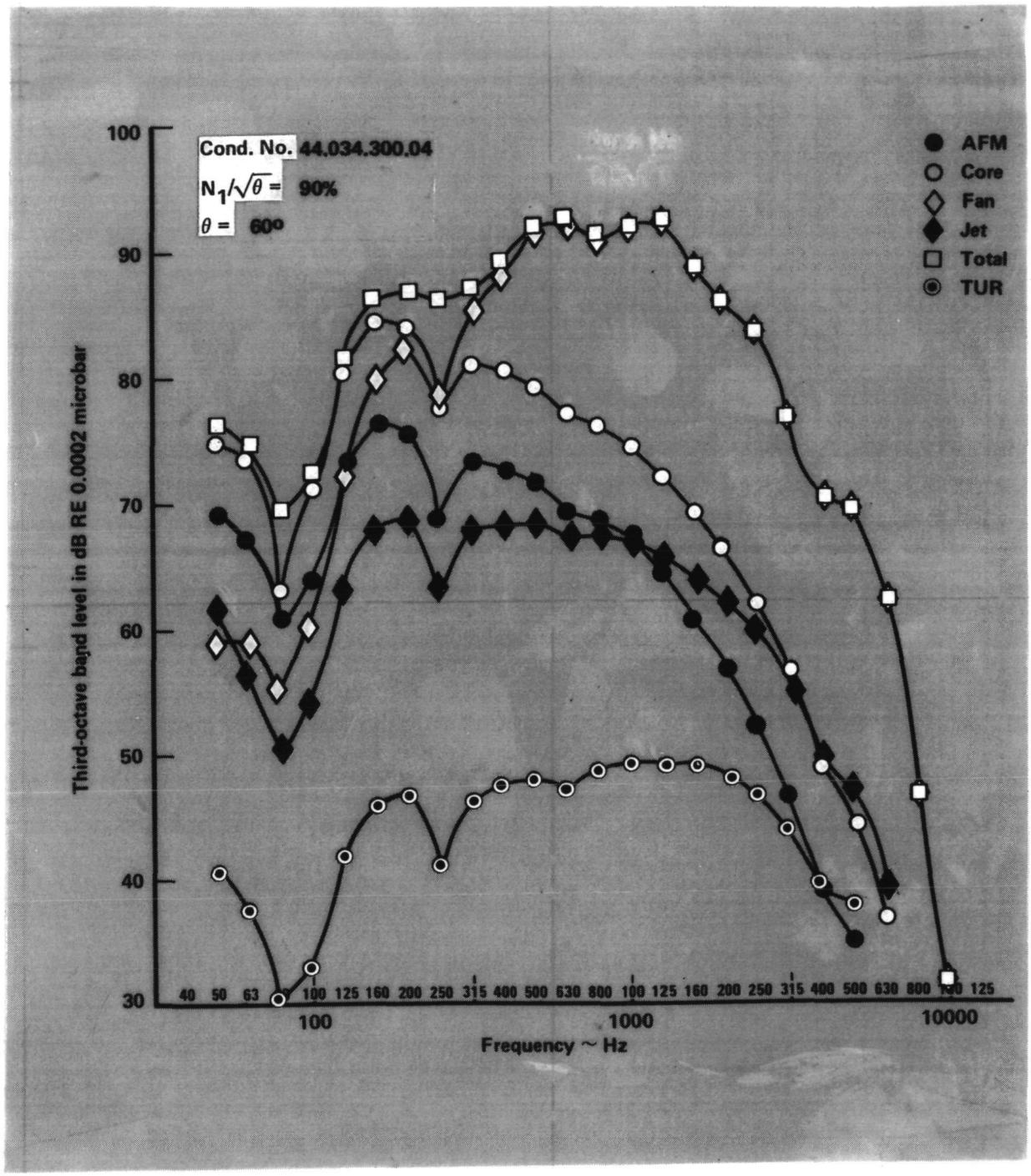

Figure 84. - Component spectra, condition no. 44.034.300.04, $\theta = 60^{\circ}$.

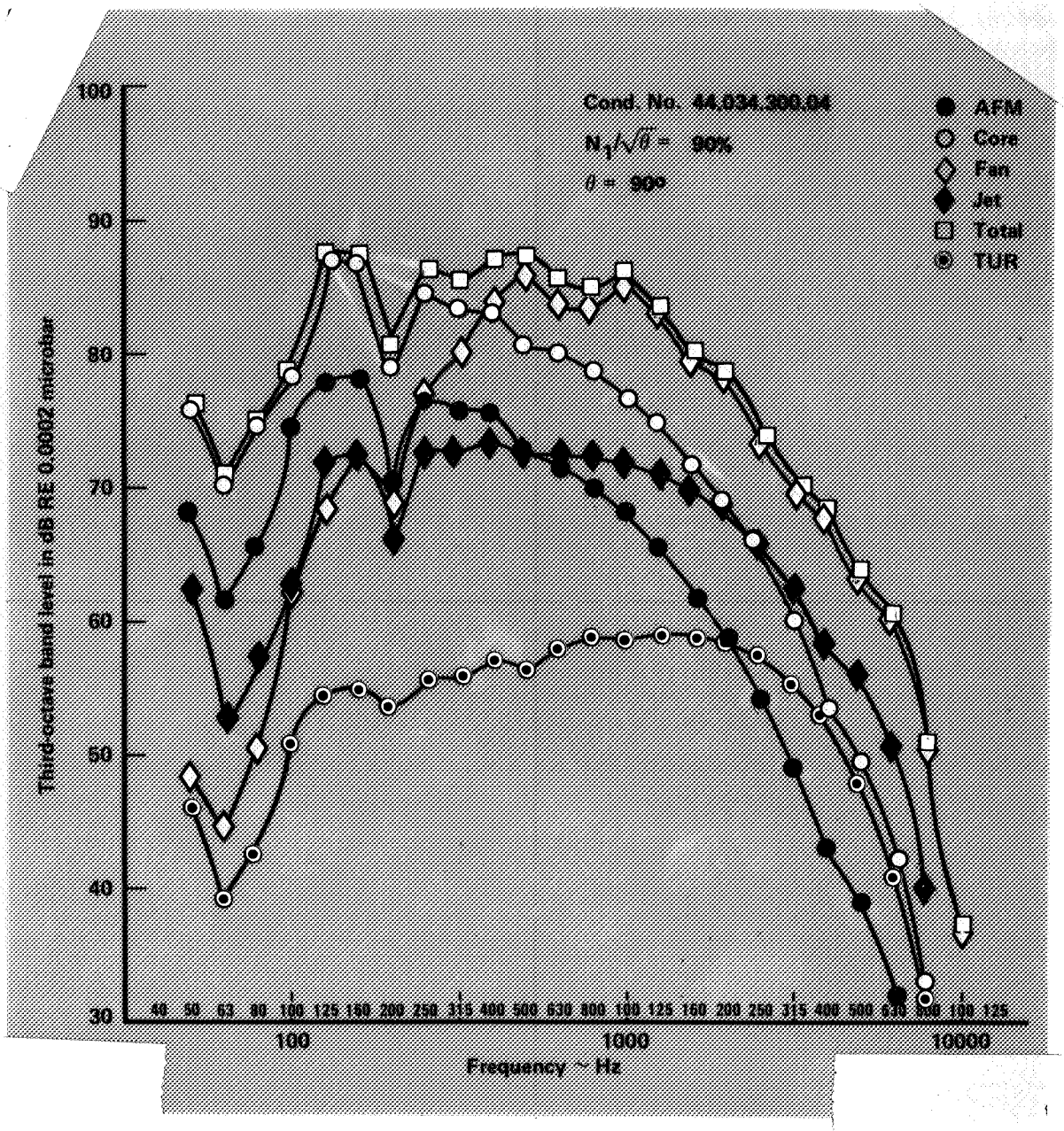

Figure 85. - Component spectra, condition no. 44.034.300.04, $\theta = 90^{o}$.

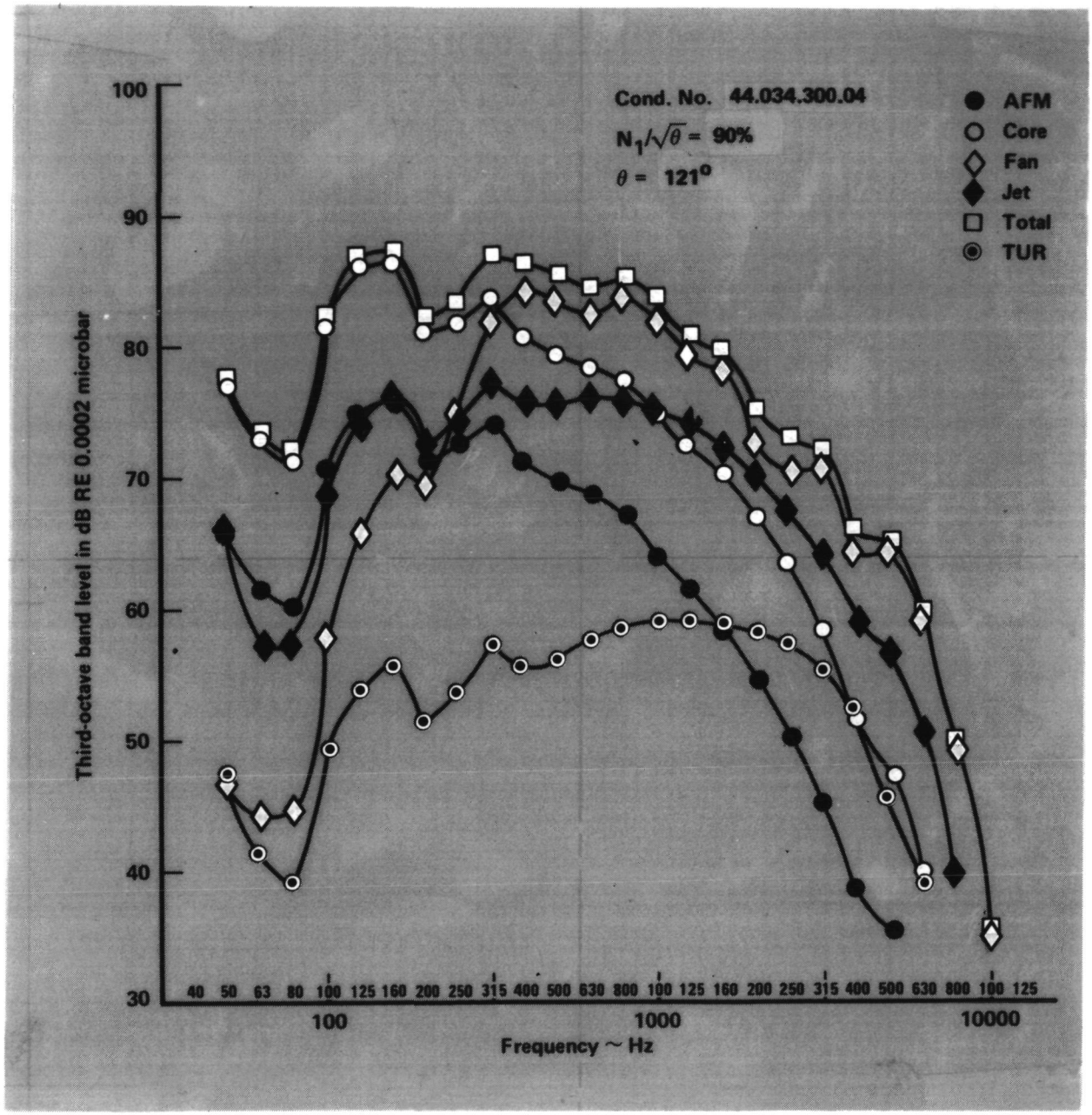

Figure 86. - Component spectra, condition no. 44.034.300.04, θ = 121°.

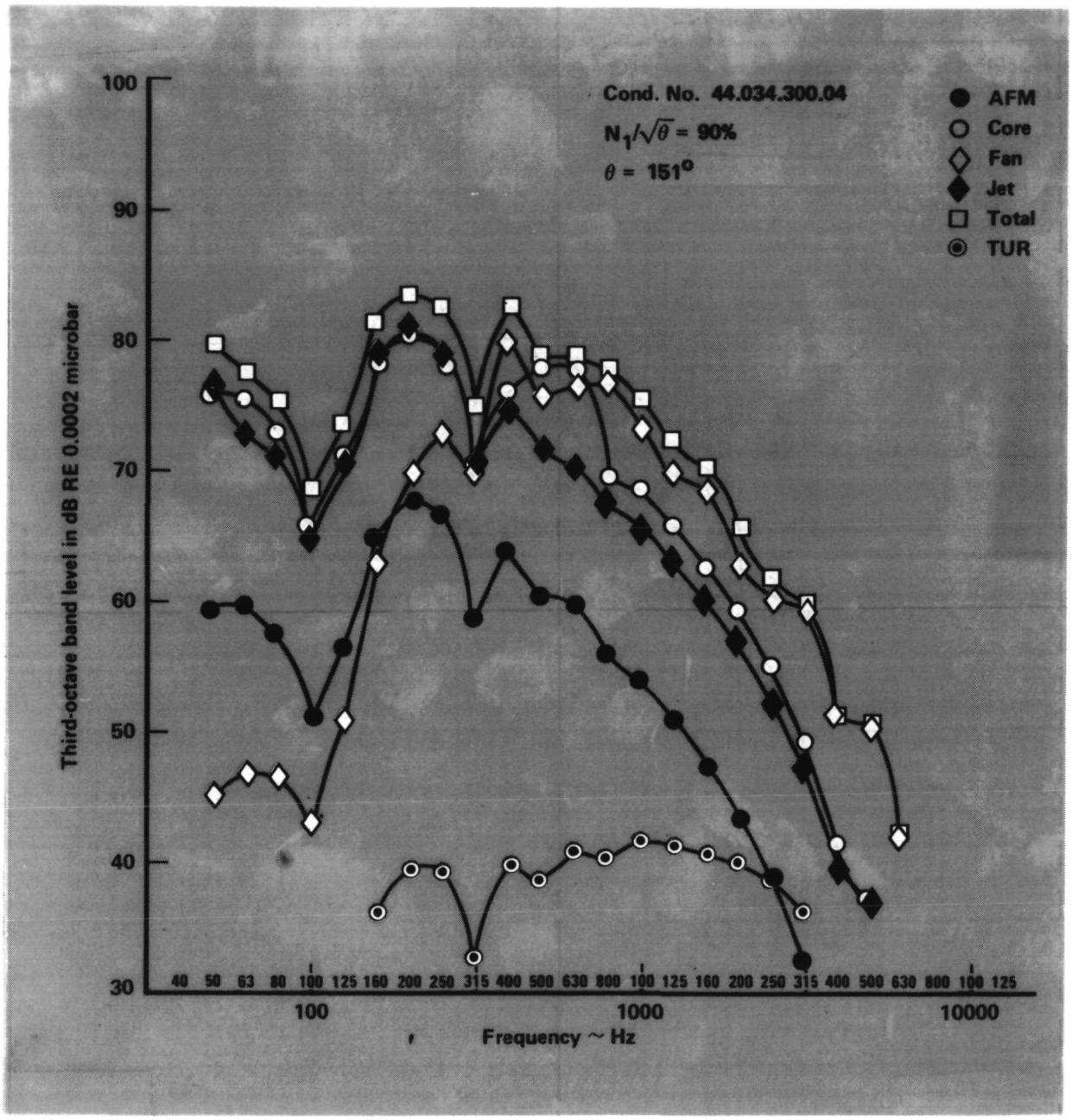

Figure 87. - Component spectra, condition no. 44.034.300.04, θ = 151°.

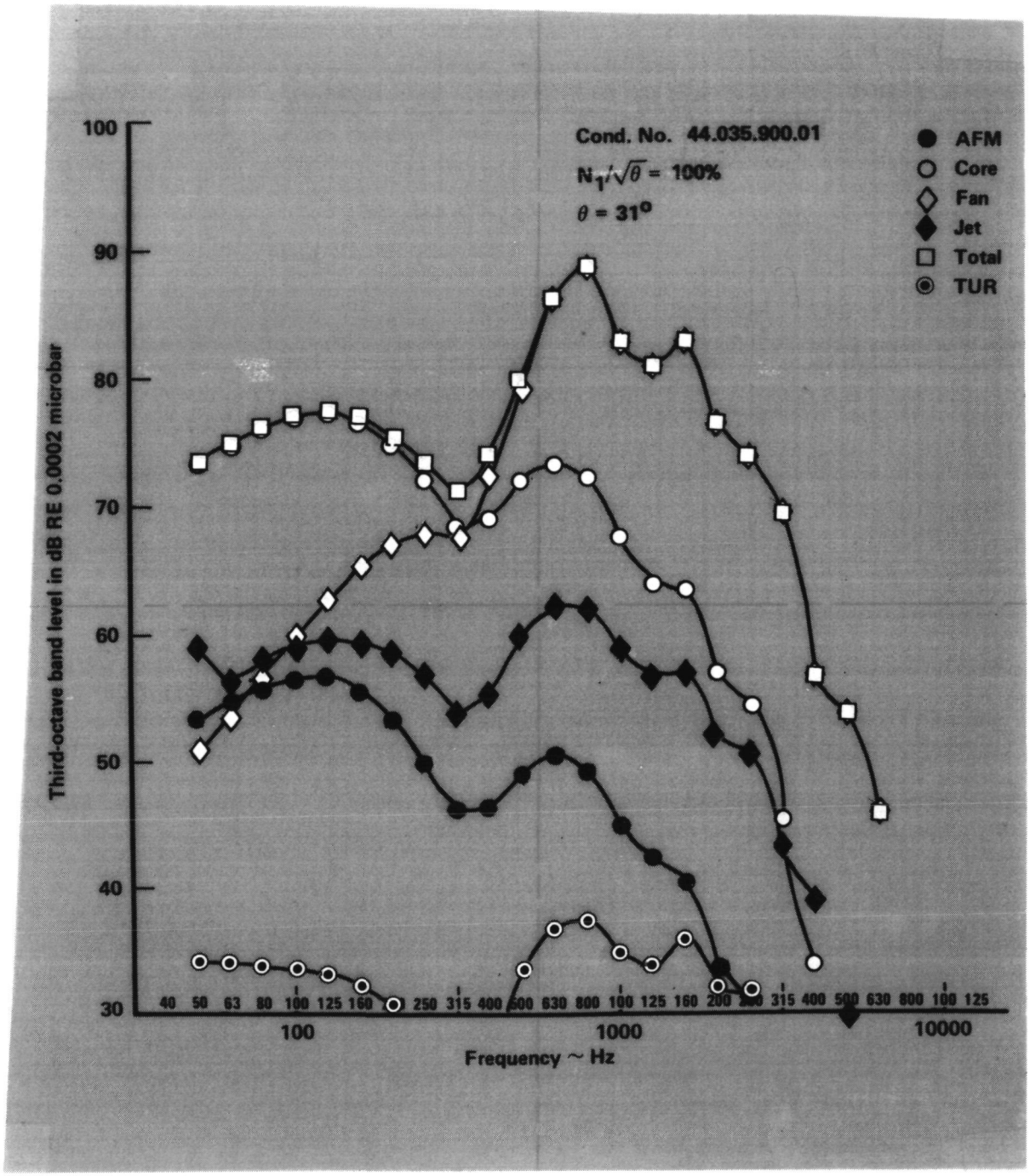

Figure 88. - Component spectra, condition no. 44.035.900.01, θ = 31°.

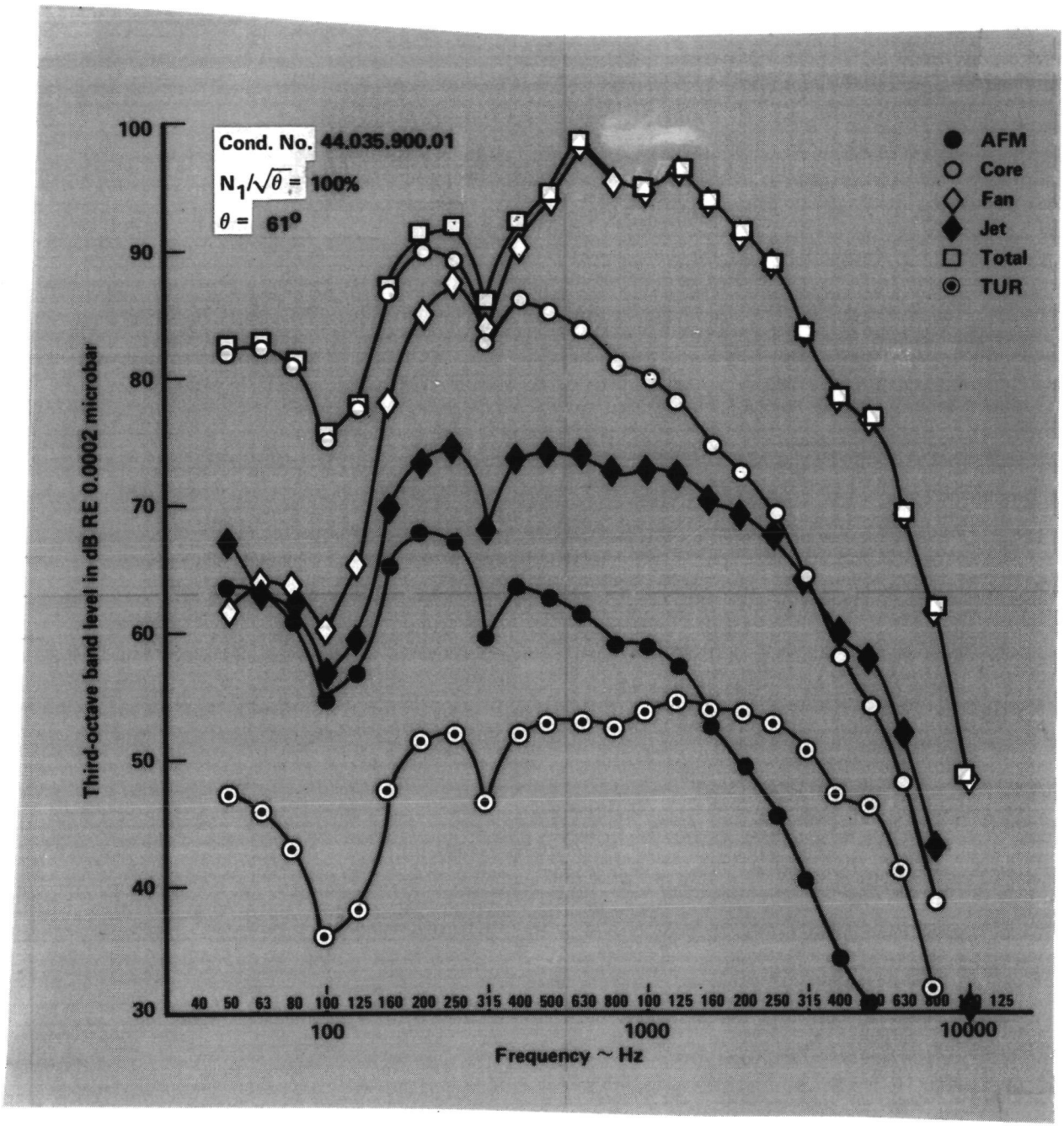

Figure 89. - Component spectra, condition no. 44.035.900.01, $\theta = 61^{\circ}$.

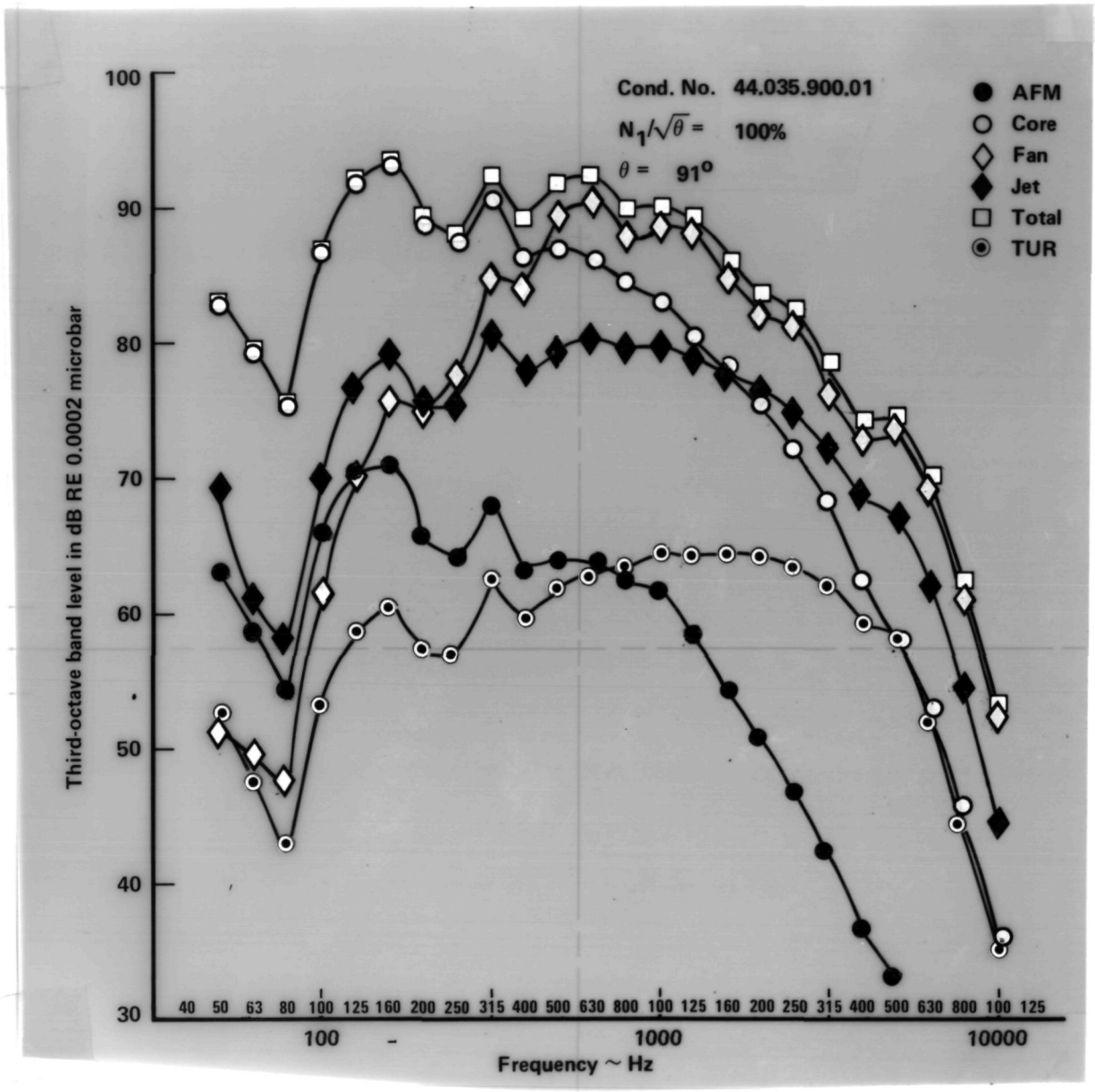

Figure 90. - Component spectra, condition no. 44.035.900.01, θ = 91°.

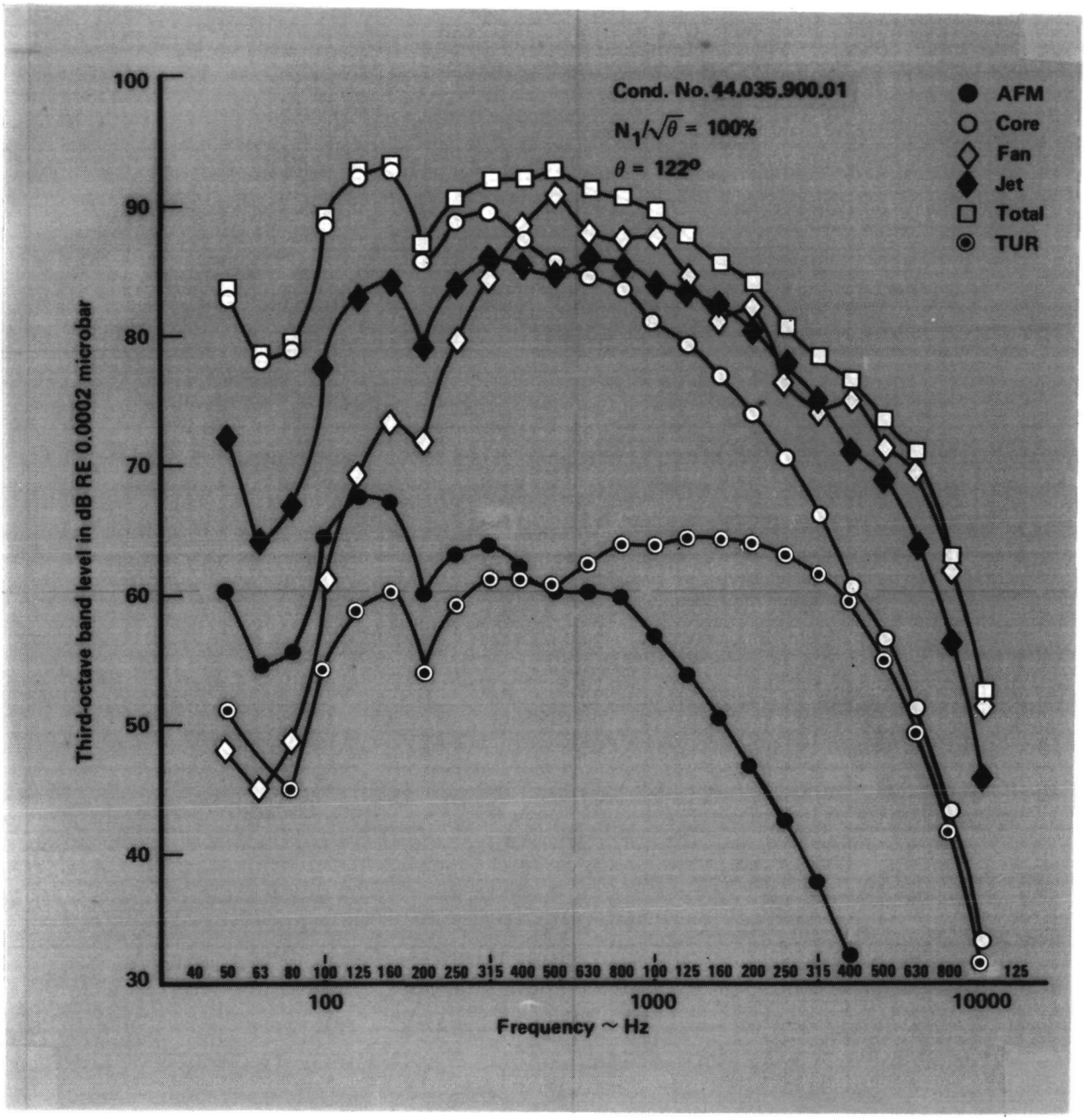

Figure 91. - Component spectra, condition no. 44.035.900.01, θ = 122°.

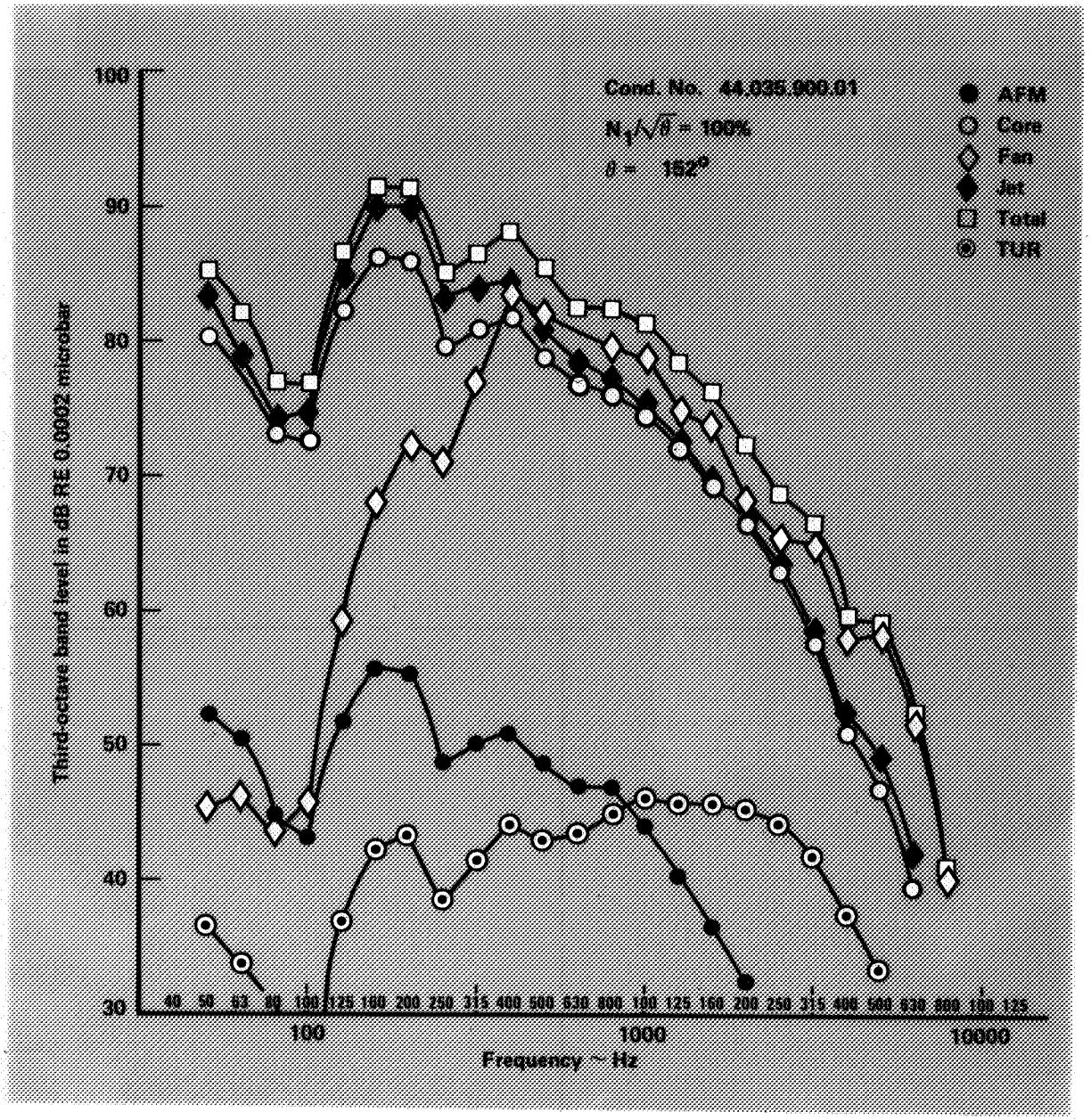

Figure 92. - Component spectra, condition no. 44.035.900.01, $\theta = 152^{\circ}$.

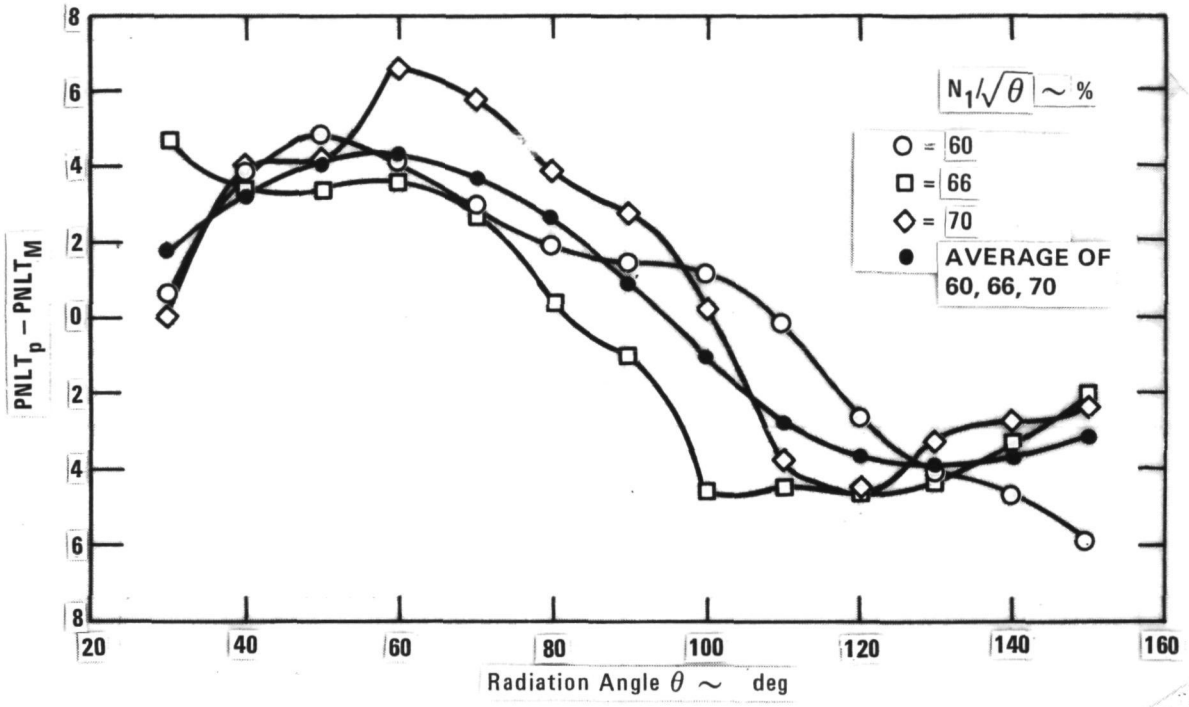

Preceding Page Blank

Figure 93. - Average difference between predicted and measured tone corrected perceived noise levels, 60%, 66%, and 70%.

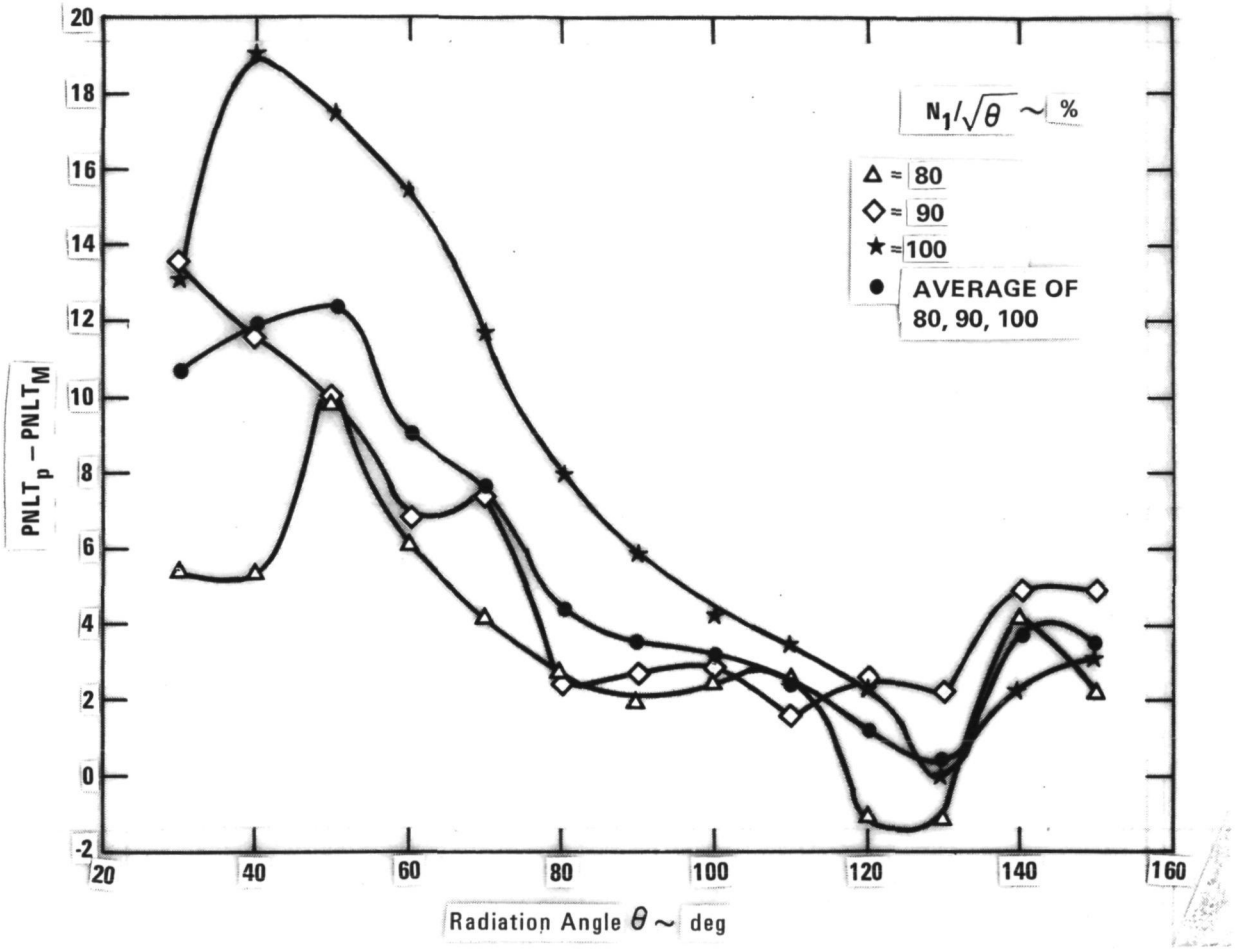

Figure 94. - Average difference between predicted and measured tone corrected perceived noise levels, 80%, 90%, and 100%.

TABLE 18. - FREQUENCY RANGE FOR ΔdB CORRECTIONS

$N_1/\sqrt{\theta}$	Frequency	
69% - 70%	Fan	315 - 10000 Hz
	Core	50 - 3150 Hz
80% - 90%	Forward Quadrant	
	Fan	160 - 10000 Hz
	Core	50 - 1000 Hz
	Aft Quadrant	
	Fan	200 - 1000 Hz
	Core	50 - 10000 Hz
	Jet	50 - 10000 Hz
100%	Forward Quadrant	
	Fan	160 - 10000 Hz
	Core	50 - 1000 Hz
	Jet	500 - 10000 Hz
	Aft Quadrant	
	Fan	160 - 10000 Hz
	Core	50 - 10000 Hz
	Jet	50 - 10000 Hz

5. CONCLUSIONS AND RECOMMENDATIONS

There is little doubt that the general acoustical character of the L-1011 aircraft with the RB.211-524B engine is that of a fan-dominated far-field noise source. Peak noise levels of the fan occur at blade passage frequency (1,200 Hz to 2,200 Hz) and its second and third harmonics in both aft and forward quadrants. At $N_1/\sqrt{\theta}$ of 80% or greater, the fan tip Mach becomes supersonic and fan buzz-saw tones are produced in the frequency range of 500 Hz to 1,000 Hz. The only other source tone that is identifiable in the measured spectra appears to be either jet or core noise at 250 Hz to 400 Hz.

Since the accuracy of the total noise prediction for this aircraft is almost entirely dependent on the fan source, it is necessary that the fan functional module be scrutinized carefully. The predicted fan tones (buzz-saw, BPF, and harmonics) are significantly higher than measurement indicates. This problem is further compounded by the perceived noise level weighting at these frequencies and tone corrections added to these increased noise levels.

TABLE 19. - Δ dB SPL CORRECTIONS CONDITION
No. 44.036.08 $N_1/\sqrt{\theta}$ = 60%

f \ θ	30	60	90	120	150
50	-2.3	-0.6	1.5	3.7	0.8
63	-0.4	2.2	0.	6.2	5.3
80	2.1	3.4	5.9	2.5	6.7
100	0.5	-3.1	5.0	2.9	-8.7
125	-1.5	1.1	5.8	4.5	-5.5
160	0.2	4.3	6.5	5.3	-1.5
200	-2.6	4.2	3.8	3.7	3.1
250	-4.4	4.4	6.8	2.3	4.7
315	0.7	1.6	2.7	1.9	-7.3
400	1.2	1.8	2.2	-2.0	1.7
500	-0.2	-0.8	-1.4	-2.4	-3.5
630	-0.5	0.6	0.7	-2.3	0.1
800	-1.5	1.7	2.3	-0.1	-0.9
1000	-1.8	0.6	1.0	0	-1.5
1250	-3.9	-0.2	1.2	0.3	-3.9
1600	-0.1	3.1	0.6	-1.0	-3.9
2000	-4.2	0.7	0.4	-1.4	-4.7
2500	-3.0	0.5	2.5	-2.4	-10.8
3150	-0.9	5.6	-2.4	-4.5	-9.1
4000	-3.9	2.8	0.7	-6.3	-11.2
5000	3.3	3.2	-1.2	-6.5	-11.0
6300	5.7	2.7	-3.6	-7.1	-11.2
8000	7.1	4.6	-2.2	-9.4	-12.9
10000	-1.9	4.6	-1.2	-6.3	-11.8

TABLE 20. - Δ dB SPL CORRECTIONS CONDITIONS
No. 44.034.011.15 $N_1/\sqrt{\theta}$ = 66%

f \ θ	30	60	90	120	150
50	-4.4	-0.2	-2.4	-0.2	-3.1
63	-2.0	-1.0	-1.6	3.7	-2.4
80	-2.7	-2.6	4.6	-1.2	1.0
100	-1.1	2.2	5.4	1.3	1.9
125	-1.6	2.5	4.2	1.3	-2.1
160	-3.4	3.3	1.9	0.1	1.2
200	0.1	1.3	-2.2	2.2	4.0
250	3.9	-2.5	6.0	0.1	4.6
315	2.1	3.1	-0.1	-0.5	0.4
400	-2.2	-1.1	2.1	-1.5	1.9
500	-7.0	2.3	-0.9	-2.8	2.4
630	0.8	0.1	0.5	-2.5	0.3
800	-0.4	1.0	0.5	-1.8	0.4
1000	-1.4	0	0.7	-1.1	-0.1
1250	-2.2	-2.3	-1.3	-2.1	0.8
1600	3.7	1.4	-0.8	-3.1	-1.3
2000	-1.7	-1.7	-2.2	-4.7	-2.3
2500	-0.1	-1.7	-3.4	-3.5	-2.5
3150	5.0	3.4	-2.5	-10.1	-5.0
4000	-3.0	-3.1	-2.6	-7.0	-6.9
5000	8.9	3.0	-4.8	-7.6	-4.9
6300	11.5	2.6	-3.9	-8.3	-4.1
8000	11.0	2.4	-2.7	-8.1	-5.7
10000	1.7	3.5	-3.0	-8.4	-5.0

TABLE 21. - Δ dB SPL CORRECTIONS CONDITIONS
No. 44.036.300.04 $N_1/\sqrt{\theta}$ = 70%

f \ θ	30	60	90	120	150
50	0.5	4.2	1.1	3.1	6.2
63	1.7	3.6	2.0	7.9	5.1
80	3.2	3.7	7.7	-0.4	7.9
100	1.9	3.3	7.9	1.5	1.5
125	5.3	7.6	7.9	3.7	-3.3
160	4.2	7.8	6.6	6.5	0.8
200	-1.6	7.4	4.5	7.1	5.1
250	-0.3	4.9	9.3	0.9	10.1
315	0	0.5	3.3	2.8	-0.6
400	-0.9	2.3	3.7	-0.9	1.8
500	1.7	2.6	2.1	-0.3	2.7
630	-4.6	2.8	3.2	-0.6	1.7
800	-2.2	2.6	3.0	-0.2	1.6
1000	-3.1	1.8	2.3	1.2	1.2
1250	-3.6	0	1.3	0.7	1.0
1600	-4.7	3.9	2.2	-1.9	-1.5
2000	0.8	-3.1	0.7	-3.1	-3.9
2500	-2.8	-0.3	-0.2	-3.5	-4.8
3150	-3.2	7.5	1.7	-10.5	-9.0
4000	0	-2.5	-2.6	-6.4	-6.5
5000	1.1	6.0	1.1	-6.4	-5.9
6300	9.3	5.3	-0.5	-7.4	-5.8
8000	9.3	4.7	-0.7	-7.2	-6.3
10000	6.8	5.9	1.6	-6.5	-6.1

TABLE 22. - Δ dB SPL CORRECTIONS CONDITION
No. 44.034.300.08 $N_1/\sqrt{\theta}$ = 80%

f \ θ	30	60	90	120	150
50	-4.1	1.0	1.0	2.1	-2.8
63	-1.3	-0.9	-3.2	-0.9	-1.2
80	-0.3	0.3	-5.1	-6.0	-0.4
100	0	0	1.0	1.6	-0.2
125	-0.9	1.3	3.4	0.3	-3.4
160	60.6	1.7	1.6	0.5	-3.7
200	2.9	3.3	0.3	0.3	0.3
250	2.9	5.7	3.6	0.9	5.1
315	4.6	6.2	-0.6	0.7	5.1
400	1.3	5.0	-0.4	2.4	4.6
500	3.2	9.1	1.3	4.0	8.7
630	8.3	11.7	3.4	7.9	9.4
800	11.6	16.7	8.2	10.8	9.1
1000	15.1	19.7	9.9	9.5	6.9
1250	14.7	17.9	6.4	4.8	5.2
1600	11.8	14.9	3.9	1.3	2.7
2000	5.3	5.7	1.6	-1.7	1.9
2500	0.5	10.5	1.7	-5.6	1.3
3150	6.1	10.3	2.2	-6.4	-3.8
4000	6.7	7.9	-5.5	-6.2	1.0
5000	18.5	10.1	3.8	-3.1	6.4
6300	9.5	17.5	6.4	3.8	6.2
8000	-16.3	18.6	8.0	5.2	-6.8
10000	-43.7	3.5	6.0	2.5	-27.1

TABLE 23. - Δ dB SPL CORRECTIONS CONDITION
No. 44.034.300.04 $N_1/\sqrt{\theta}$ = 90%

f \ θ	30	60	90	120	150
50	-0.3	2.1	-0.3	3.2	-1.4
63	-2.2	-0.2	-0.8	2.3	-2.6
80	-0.7	-0.6	6.1	-0.1	-0.8
100	1.3	-0.4	4.2	2.7	-4.6
125	-0.9	4.2	5.3	2.8	-0.5
160	-1.4	5.1	4.6	2.8	2.4
200	-1.2	6.2	2.9	1.9	3.8
250	9.7	7.9	6.0	4.4	7.3
315	13.9	8.4	3.7	3.7	7.9
400	12.2	10.6	6.7	6.9	10.0
500	13.2	15.2	7.8	6.4	7.1
630	22.6	16.7	5.7	7.8	9.0
800	20.1	15.0	5.7	9.6	9.5
1000	18.8	15.9	8.3	8.5	8.0
1250	20.8	17.2	7.0	6.5	6.0
1600	20.9	14.6	4.2	3.4	5.6
2000	18.6	10.7	2.2	-0.7	2.2
2500	13.7	4.6	1.8	0.4	1.5
3150	10.2	9.5	0.3	-2.4	-0.2
4000	1.9	8.2	-1.7	-5.0	-1.8
5000	6.0	13.1	-4.1	2.0	6.3
6300	-8.7	18.2	7.8	5.8	1.4
8000	-27.9	8.6	11.0	8.2	-10.7
10000	-62.6	-4.0	1.3	-0.6	-29.1

TABLE 24. - Δ dB SPL CORRECTIONS CONDITION
No. 44.035.900.01 $N_1/\sqrt{\theta}$ = 100%

f \ θ	30	60	90	120	150
50	3.8	5.4	4.8	6.6	-4.3
63	0.8	4.7	4.2	2.1	-2.5
80	3.2	4.5	3.6	3.0	-2.4
100	2.1	1.8	16.2	4.8	-8.8
125	5.5	4.6	10.7	3.2	-3.0
160	5.9	20.0	9.6	4.8	2.6
200	7.5	17.9	3.5	3.0	4.9
250	5.5	13.2	6.8	5.3	6.4
315	10.3	4.3	9.4	3.7	4.9
400	9.3	13.0	3.6	5.3	9.5
500	9.8	18.2	9.8	6.9	7.5
630	13.6	18.1	11.5	4.7	7.0
800	17.8	19.4	9.5	8.3	8.5
1000	17.3	16.9	9.0	8.3	9.2
1250	14.5	19.9	8.4	5.4	7.2
1600	16.8	18.5	5.8	3.6	4.0
2000	12.9	17.2	3.4	2.3	-0.7
2500	14.1	15.7	4.0	-0.5	-0.8
3150	10.7	13.0	3.1	-1.4	-1.4
4000	9.2	14.2	1.9	-2.1	-0.7
5000	9.8	19.3	3.2	-4.9	-0.9
6300	5.1	20.9	5.0	-1.0	-0.4
8000	-16.4	23.5	8.4	0.7	0.2
10000	-42.5	13.2	11.5	-0.2	-11.3

The accuracy of the prediction in the forward quadrant seems to depend on the propagation distance. It can be noted that half of the flight test cases have minimum propagation distances of approximately 90 m (295 ft) while the remainder have 335 m (1100 ft). Those comparisons of measured and predicted noise that have larger propagation distances show larger differences in noise levels.

It is important to notice that frequency for a predicted and a corresponding measured tone differ sometimes by a third-octave. This can be attributed to doppler frequency shift change caused either by a tone occurring at the frequency limits of a third-octave filter band or a basic error in correlating measured and predicted data at the same radiation angle. Further, a difference in tone amplitudes can be explained in terms of an aircraft velocity effect that seems to be most significant in the forward quadrant as seen in earlier cited data. This flight effect can be traced to a direct result of empirical fan source noise prediction or acoustic liner insertion losses based on static engine data.

Another factor that would particularly increase predicted forward inlet radiated noise relative to measured is structural shielding. The L-1011 center engine inlet is most likely shielded by the fuselage during overhead flyover measurements. Possibly, a better method to compute noise would include using two inlets and three exhaust flows rather than assuming three of each.

Accuracy of the prediction of the ground reflection phenomenon is very good. Upon examining the spectral plots comparing measured and predicted data, the cancellation and reinforcement effects from an above ground microphone match very closely. In fact, a good procedure for determining the difference in radiation angles of measured and predicted data could lie in the location of the first null from a ground reflection.

Particular significance is placed on the capability of predicting peak aircraft flyover noise in the aft quadrant. This is demonstrated reasonably well by ANOPP.

ANOPP improvements that would be helpful to a user would include:

- more detailed documentation on technical content of prediction methods
- general procedure or guidelines for constructing a run deck applied to a particular type airplane or specified testing requirements
- capability of generating aircraft community noise characteristics
  - noise versus distance curves
  - noise contours.

Even with the brevity of the existing ANOPP documentation it is possible for someone with rudimentary knowledge of computer programming to successfully use ANOPP within a few weeks. Once it is realized there is nothing mysteriously or technically prohibitive about ANOPP, then it is merely a task of becoming familiar with the program structure and format.

ANOPP would be useful in performing noise trade-off studies. By adjusting aircraft/engine operating parameters flyover noise could be minimized at particular location(s) on the ground. Criteria of performance and economics would be used to determine optimum flyover noise level. Another utility of ANOPP would be in preliminary design studies where aircraft/engine design parameters are varied to produce a minimum noise airplane. In most cases the absolute magnitude of noise levels is not a critical factor. The goal of trade-off and preliminary design studies is very often to permit identification of trends reducing or increasing aircraft noise.

REFERENCES

1. Anon., "Noise Standards: Aircraft Type Certification", Part 36 of the Federal Aviation Regulations, FAA/DOT, Washington, D.C., December 1969.

2. Bushell, Ken and Tomlinson, David, Rolls Royce, Private Communication to Larry Golby, May, 1979.

3. Gillian, R.E., Wilkins, D.J. and Baucom, P.H., ANOPP User's Manual, NASA, July, 1978.

1. REPORT NO.	2. GOVERNMENT ACCESSION NO.	3. RECIPIENT'S CATALOG NO.
NASA ER-159138		

4. TITLE AND SUBTITLE	5. REPORT DATE
ANOPP Validation Study - Lockheed L-1011	October 1979
	6. PERFORMING ORG CODE

7. AUTHOR(S)	8. PERFORMING ORG REPORT NO.
L.A. Godby	LR 29177
	10. WORK UNIT NO.

9. PERFORMING ORGANIZATION NAME AND ADDRESS	11. CONTRACT OR GRANT NO.
LOCKHEED-CALIFORNIA COMPANY P.O. BOX 551 BURBANK, CALIFORNIA 91520	NASA1-15651
	13. TYPE OF REPORT AND PERIOD COVERED CONTRACTOR REPORT

12. SPONSORING AGENCY NAME AND ADDRESS	14. SPONSORING AGENCY CODE
National Aeronautics & Space Administration Washington, DC 20546	

15. SUPPLEMENTARY NOTES

LANGLEY TECHNICAL MONITOR: DR. WILLIAM E. ZORUMSKI

16. ABSTRACT

This report describes the work completed by Lockheed to verify the Aircraft Noise Prediction Program (ANOPP) developed by NASA Langley Research Center. In this study, ANOPP was used to predict the far-field noise characteristics of an L-1011 aircraft equipped with RB.211-524B engines.

A comparison was made with actual flight noise with noise predicted for the same operating and weather conditions. Correlation of predicted and measured results was very good in the aft quadrant of radiated noise. Predicted noise levels were significantly different from measured values in the forward quadrant because fan noise was predicted high.

Since the major noise sources were fan and core, corrections are supplied to adjust ANOPP fan and core noise components so that the total predicted noise matches the measured L-1011 noise levels.

17. KEY WORDS (SUGGESTED BY AUTHOR(S))	18. DISTRIBUTION STATEMENT
Acoustics Aircraft Noise Prediction Aircraft Noise Measurements	UNCLASSIFIED - UNLIMITED

19. SECURITY CLASSIF. (OF THIS REPORT)	20. SECURITY CLASSIF. (OF THIS PAGE)	21. NO. OF PAGES	22. PRICE*
Unclassified	Unclassified		